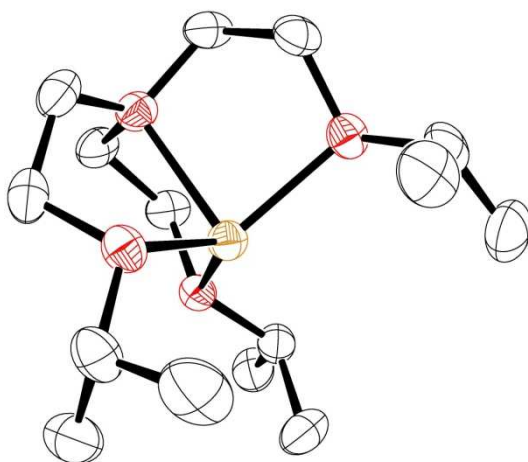




Justus-Liebig-Universität Gießen
Fachbereich Biologie und Chemie
Institut für Anorganische und Analytische Chemie

Synthetic and mechanistic investigations of copper and iron complexes with 'small' tripodal, aliphatic N-donor ligands and their reactivity towards dioxygen



Inaugural-Dissertation
zur Erlangung des Doktorgrades der Naturwissenschaften

vorgelegt von Janine Will aus Gießen im Jahre 2021

Acknowledgements

The results described in this doctoral thesis have been obtained between November 2009 and November 2019 at the Institute of Inorganic and Analytical Chemistry of the Justus Liebig University Gießen under the supervision of Prof. Dr. Siegfried Schindler.

I would like to thank my supervisor Prof. Dr. Siegfried Schindler for his support, his guidance and especially his patience during all those years.

Furthermore, I wish to thank my dear and former colleagues and lab mates Dr. Anja Henss, Dr. Sabrina Turba, Dr. Sandra Kisslinger, Dr. Alexander Beitat, Dr. Thomas Nebe, Dr. Christian Würtele, Dr. Tobias Hoppe, Dr. Lars Valentin, Dr. Ildikó Kerezsi, Dr. Jennifer Blank, Dr. Melanie Jopp, Dr. Sabrina Handeck, Natascha Kempf, Jun. Prof. Dr. Sabine Becker, Dr. Jonathan Becker, Dr. Cornelius Brombach, and Stefan Schaub for their friendship, encouragement and thoroughly enjoyable lab atmosphere.

I would like to express my gratitude to Dr. A. Beitat, Dr. C. Würtele, Dr. O. Walter and Dr. M. Serafin, Dr. Jonathan Becker and Jun. Prof. Dr. Sabine Becker for their kind support with the X-ray crystallographic studies found in this thesis. Dr. Jörg Glatthaar I want to thank for his valuable support in carrying out low-temperature IR measurements. MSc Lars Schneider needs to be thanked for his kind support in checking experimental results concerning the synthesis of the imine ligand and for his most valuable contributions in general.

Moreover, I would like to thank the people of the Institute of Inorganic and Analytic Chemistry, and the people of the Institute of Organic Chemistry at the Justus Liebig University Gießen for their support of my work.

However, my biggest thanks are deserved by my friends and colleagues in our research group. You certainly did make life in the laboratory more than just a work space.

Of course, I would also like to thank my close friends outside university, especially those who took care of Emma while I was working on this thesis.

Finally, and most importantly, I want to thank my entire family for their support during all these years. Without your patience and moral support this would have never been possible. This is also for you guys.

If you don't know where you are going, any road will get you there.

Lewis Carroll

For my family.

*For Martijn,
without whom this would have never been possible.*

*For Emma,
who is luckily turning out just as bullheaded as me.*

Kurzzusammenfassung

Die vorliegende Arbeit befasst sich mit der Modellierung von Ligandensystemen, welche sodann mit Kupfer- bzw. Eisensalzen unter Sauerstoffausschluss zu niedrig oxidierten Precursor-Komplexen umgesetzt wurden, um bei einer anschließenden Oxidation mit Sauerstoff eine mögliche Formation von intermediären Sauerstoff-Addukt-Komplexen zu beobachten, zu untersuchen und näher zu charakterisieren.

Sauerstoff-Addukt-Komplexe sind in der Natur als reaktive Zwischenspezies bei oxidativen Vorgängen in vivo von großer Bedeutung und dienen als Vorbild für Modellkomplexe, welche im Labor dazu dienen sollen, Oxidationen unter milden Bedingungen durchzuführen. Um ein besseres Verständnis über jene oxidativen Vorgänge im Labor zu erhalten, wurden bereits in der Vergangenheit viele unterschiedliche kupfer- und eisenbasierte Modellkomplexe, welche die Reaktivität der entsprechenden Sauerstoff-Addukt-Komplexe näher beleuchten, von unterschiedlichen Arbeitsgruppen dargestellt und charakterisiert.

Die vorliegende Arbeit leistet einen Beitrag zum besseren Verständnis und zu einem umfassenderen Bild von Kupfer- bzw. Eisen-Sauerstoff-Addukt-Komplexen und deren Eigenschaften. Ausgehend von dem Ligandengerüst *tren* wurden in dieser Arbeit weitere ‚einfache‘ tripodale Liganden (*Me₃tren*, *Isoprop₃tren*, *Me₃isoprop₃tren* und *Imine₃tren*) zum Teil neu synthetisiert und charakterisiert und anschließend mit Kupfer- bzw. Eisensalzen zu niedrig oxidierten Precursor-Komplexen unter Sauerstoffausschluss umgesetzt. Die erhaltenen Komplexe wurden umfassend spektroskopisch und, wann immer möglich, kristallografisch charakterisiert und danach, im Falle der Kupferkomplexe, bei sehr tiefen Temperaturen mit Sauerstoff zur Reaktion gebracht. Jene Reaktionen wurden mit Hilfe von unterschiedlichen Messverfahren (z.B. Tieftemperatur-Stopped Flow, Cyclovoltammetrie) untersucht, die Ergebnisse interpretiert und mit bereits vorhandener Literatur verglichen.

Die hierzu erhaltenen Ergebnisse wurden in den Jahren 2019 und 2020 in Fachzeitschriften veröffentlicht.

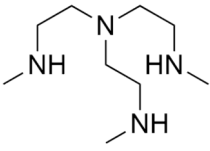

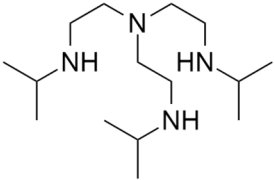

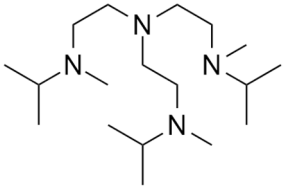

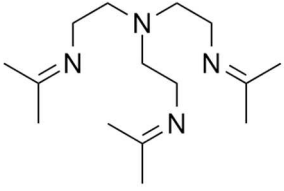
Table of Contents

Kurzzusammenfassung	I
Table of Contents	III
Ligands and Complexes Used.....	VI
Abbreviations	VII
1. Introduction	1
1.1 Copper	1
1.1.1 Copper in Biology	2
1.1.2 Metalloproteins Containing Copper.....	4
1.1.3 Types and Roles of Copper Proteins	4
1.2 Iron.....	7
1.2.1 Iron in Biology.....	9
1.2.2 Metalloproteins Containing Iron.....	11
1.2.3 Types and Roles of Iron Proteins.....	12
1.3 Copper and Iron Dioxygen Complexes in Nature	17
1.4 Model Compounds for Copper and Iron Proteins.....	22
1.5 Tripodal, Tetradentate Ligands of the Tren Family	27
1.6 Research Goals	32
1.6.1 Project One: Ligand Synthesis	33
1.6.2 Project Two: Formation of Copper(I) and (II) Complexes and Formation of an Iron(Imine ₃ tren) Complex	34
1.6.3 Project Three: Formation of Copper Dioxygen Complexes and Formation of an Iron(Imine ₃ tren) Oxygen Adduct Complex.....	35
2 Copper Complexes – Experiments and Results.....	36
2.1 Synthesis, crystal structures and reactivity towards dioxygen of copper(I) complexes with tripodal aliphatic amine ligands	36
2.1.1 Abstract	36
2.1.2 Introduction.....	36
2.1.3 Experimental Section	38
2.1.3.1 Materials and Physical Measurements.....	38
2.1.3.2 X-ray Crystallography.....	39
2.1.3.3 Stopped-Flow Instruments, Software and Handling	39

2.1.3.4	Synthesis and Characterization of Ligands	39
2.1.3.5	Synthesis of Copper(I) Complexes	40
2.1.3.6	Synthesis of Copper(II) Complexes	42
2.1.4	Results and Discussion	43
2.1.4.1	Synthesis and General Characterizations	43
2.1.4.2	Bench Top Experiments of the Reaction of Copper(I) Complexes with Dioxygen	47
2.1.4.3	Low Temperature Stopped-Flow Measurements.....	49
2.1.5	Conclusions and Outlook.....	53
2.2	Supporting Information	54
2.2.1	Selected Crystallographic Data	54
2.3	Additional Material and Unpublished Results.....	58
2.3.1	Synthesis of Ligands	58
2.3.2	Synthesis of [Cu(L)]BF ₄	58
2.3.3	Bench Top Experiments.....	59
2.3.4	Low Temperature Stopped Flow Measurements of [Cu(Me ₃ tren)]ClO ₄ in EtCN...	61
2.3.5	Low Temperature Stopped Flow Measurements of [Cu(Isoprop ₃ tren)]SbF ₆ in EtCN	62
2.3.6	UV-vis Measurements of Copper(II) Complexes	64
3	Iron Complexes – Experiments and Results.....	65
3.1	Synthesis and Reactivity of Iron(II) Complexes with a New Tripodal Imine Ligand ..	65
3.1.1	Abstract	65
3.1.2	Introduction.....	65
3.1.3	Results and Discussion	67
3.1.3.1	Synthesis and crystallographic characterization of iron complexes.....	67
3.1.3.2	Reactivity of the iron(II) complexes 1 and 3 towards dioxygen, peroxides and ozone...	73
3.1.4	Summary	73
3.1.5	Experimental	74
3.1.5.1	General	74
3.1.5.2	Crystallographic Characterization.....	74
3.1.5.3	Synthesis of [Fe(Imine ₃ tren)(OAc) ₂] (1)	74
3.1.5.4	Synthesis of [Fe(Imine ₃ tren)(OAc)]OTf (2).....	74
3.1.5.5	Synthesis of [(Fe(Imine ₃ tren)) ₂ (F) ₂](SbF ₆) ₂ (4).....	75
3.2	Supporting Information & Additional Material	75

3.2.1	Synthesis of Iron Complexes	75
3.2.1.1	Synthesis of $[\text{Fe}(\text{Imine}_3\text{tren})(\text{OAc})]\text{BPh}_4$ (3)	75
3.2.1.2	Synthesis of $[\text{Fe}_2(\text{tren})_2(\text{Oxido})_2](\text{OTf})_2$ (5)	75
3.2.1.3	Synthesis of $[\text{Fe}(\text{ClEt})_2(\text{H}_2\text{O})(\text{OAc})](\text{OAc})$ (6)	75
3.2.1.4	Synthesis of $[\text{Fe}(\text{Imine}_1\text{amine}_1\text{aldol}_1\text{tren})(\text{OH}_2)](\text{NTf}_2)_2$ (7)	76
3.2.1.5	Synthesis of $[\text{Fe}(\text{Imine}_1\text{amine}_1\text{aldol}_1\text{tren})(\text{OH}_2)](\text{PF}_6)_2$ (8)	76
3.2.1.6	Synthesis of $2 [\text{Fe}(\text{tren})](\text{MeCN})_2^{2+} + [\text{Fe}((\text{CF}_3)_2\text{C}(\text{OH})(\text{O}))_4]^{2-} +$ $[\text{Fe}((\text{CF}_3)_2\text{C}(\text{OH})(\text{O}))_4(\text{MeCN})]^{2-}$ (9)	76
3.2.1.7	Synthesis of $[(\text{Fe}(\text{Imine}_3\text{tren}))_2(\text{F})_2](\text{BPh}_4)_2$ (10)	76
3.2.2	Electrochemical Measurements	77
3.2.3	IR Measurements	78
3.2.4	UV-vis Measurements	79
3.2.5	Low Temperature Stopped Flow Measurements	80
3.2.6	Details of X-ray Crystal Structure Determination	81
3.2.6.1	Selected Crystallographic Data	82
4	Additional Procedures	103
4.1	UV-vis Measurements	103
4.2	IR Measurements	103
5	Summary	104
5.1	Synthetic and Mechanistic Investigations of Copper Complexes	104
5.2	Synthetic and Mechanistic Investigations of Iron Complexes	107
	Curriculum Vitae	111
	Sources & References	112
	List of Figures	118
	List of Schemes	121
	List of Tables	122
	Erklärung	124

Ligands and Complexes Used

Structure	Formula	Photo	Name / Molar Mass
 <p>Me₃tren</p>	C ₉ H ₂₄ N ₄		tris-[(2-methyl-amino)ethyl]amine 188,27 g/mol
 <p>Isoprop₃tren</p>	C ₁₅ H ₃₆ N ₄		tris[2-(isopropyl-amino)ethyl]amine 272,33 g/mol
 <p>Me₃isoprop₃tren</p>	C ₁₈ H ₄₂ N ₄		tris[2-(isopropyl-methylamino)ethyl]amine 317,33 g/mol
 <p>Imine₃tren</p>	C ₁₅ H ₃₀ N ₄	n.a.	tris-[2-(propan-2-ylidene-amino)ethyl]amine 266 g/mol

Abbreviations

Bz ₃ tren	tris-(N-benzyl-N-methylaminoethyl)amine
cf.	compare (Latin: confer)
ch.	chapter
CH ₂ Cl ₂	dichloromethane
d	doublet (NMR)
D-Pen	D-penicillamine
δ	chemical shift in ppm (NMR)
e. g.	for example (<i>Latin: exempli gratia</i>)
EtCN	propionitrile
Et ₂ O	diethyl ether
EtOH	ethanol
HB(3,5-iPrpz) ₃	tris-(3,5-diisopropyl-1H-pyrazol-1-yl)hydroborate
HB(3-tBu-5-iPrpz) ₃	tris-(3-tert-butyl-5-isopropyl-1H-pyrazol-1-yl)hydroborate
Imine ₃ tren	tris-[2-(propan-2-ylideneamino)ethyl]amine
Isoprop ₃ tren	tris[2-(isopropylamino)ethyl]amine
IR	infrared
m	multiplet
Me ₂ uns-penp	2-dimethyl-(aminoethyl)-bis-(2-methylpyridyl)amine
Me ₃ isoprop ₃ tren	tris[2-(isopropylmethylamino)ethyl]amine
Me ₃ TACN	1,4,7-trimethyl-1,4,7-triazacyclononane
Me ₃ tren	tris-[(2-methylamino)ethyl]amine
Me ₆ tren	tris-[(2-dimethylamino)ethyl]amine
Me ₄ apme	bis-(2-dimethyl-aminoethyl)(2-methylpyridyl)amine
MeCN	acetonitrile
MeOH	methanol
n.a.	not available
NEt ₃	triethylamine
NMR	nuclear magnetic resonance

OAc	acetate
PPA	phenylacetic acid
RT	room temperature
s	singlet (NMR)
t	triplet (NMR)
TMG ₃ tren	tris-(tetramethylguanidino)tren
Tp ^{iPr2}	tris(3,5-diisopropyl-1-pyrazolyl)borate
UV-vis	ultraviolet-visible

1. Introduction

1.1 Copper

Elemental copper has already been known to mankind for about 5000 years. In the Neolithic era, elemental copper was used in manufacturing due to its characteristic physical properties just like the noble metals gold and silver.^[1] The element's name derives from the Mediterranean island of Cyprus where high amounts of copper could be found in Roman times. Therefore, the Romans named the reddish and soft metal *aes cyprum* (ore from Cyprus), a name which later on evolved into the name *cuprum* and is the basis for today's symbol *Cu* in the periodic table of elements.^[2,3]

Table 1.1: Some general, physical and chemical properties of elemental copper.^[1]

Appearance	Reddish, metallic
Atomic Number	29
Weight Per Cent in Geosphere	0.01 %
Density	8.92 g/cm ³
Melting Point	1084.4 °C
Boiling Point	2567 °C
Thermal Conductivity	401 W/(m · K)
Electrical Conductivity	65 · 10 ⁶ Ω ⁻¹ m ⁻¹ at 0°C
Magnetism	Diamagnetic
Oxidation States	+ I, + II (+ III and + IV are known, but very rare)
Electron Configuration	[Ar] 4s ¹ 3d ¹⁰

As shown in Table 1.1, elemental copper is nowadays mostly used because of its high electric and thermal conductivity. Thus, copper is used for electric wiring, cables and components as well as heat sinks. Because of the element's resistance to oxidation, it is also used as a mintage metal and roofing material. Contact with the air's oxygen merely leads to the formation of an oxide coating which protects the metal from further corrosion.

Wearing a copper skin, American landmark, the Statue of Liberty (installed in 1886) was the largest use of copper in a single structure at that time containing about 31 tons of the metal. The only part of the statue restored until today is the torch which was covered in 24K gold in 1984.^[4]

Copper is also the basis for alloys like bronze or brass which have already been known in ancient Greece. Today, the alloy *constantan* consisting of 55% copper and 45% nickel is of high interest to the metal processing industry, as it is widely used for the production of high-precision resistors.^[1,3]

However, not only is copper a very important element, many of its compounds also bear important properties in nature and copper is also an important trace element in the human body.^[1,5]

1.1.1 Copper in Biology

As demonstrated in chapter 1.1, copper is a most versatile element. Not only does it play an important role in its solid state, but it also occurs as an essential metal ion in bacteria, fungi, mammals and plants. Because of its redox properties, namely the easy transition between Cu(I) and Cu(II) oxidation states, copper is essential for a number of enzymes, e.g. dopamine β -hydroxylase (D β H) and acts as a cofactor in fundamental processes like respiration in cells, e.g. cytochrome c oxidase, or photosynthesis, e.g. plastocyanin.^[6]

However, those very properties make it also extremely poisonous for living organisms when present in excess. Copper in a higher concentration, e.g. taken in through contaminated water, can lead to symptoms such as nausea, diarrhea, and can also result in tissue injury and eventually in disease.

Wilson's disease is a hereditary disease which produces an excess level of copper in the person affected. Due to the mutation of genes which are responsible for producing ATP7B that absorbs and transports copper in the living organism, the copper metabolism in the body is disrupted and copper accumulates.^[7] If untreated the disorder leads to the patient's death. The toxicity of copper is based on the generation of reactive oxygen species through Fenton-like reactions and the fact that most metalloproteins prefer binding copper over other bivalent metals following the Irving-Williams series.^[8] Wilson's disease cannot be cured yet, but it is possible to remove excess copper which accumulates in the liver and eventually in the brain and which is clearly visible by the formation of a so-called Kayser-Fleischer ring, a rusty brown ring formed around the eyes' iris of affected patients.^[6,9-12] Using chelation therapy, the amino acid D-penicillamine is administered to bind, transport and excrete excess copper probably forming the mixed-valent complex $[\text{Cu}^{\text{II}}_6\text{Cu}^{\text{I}}_8(\text{D-Pen})_{12}\text{Cl}]^{5-}$ which can be detected in vitro.^[12,13] The structure of D-penicillamine is depicted in Fig. 1.2. D-Pen reduces the copper level in plasma, because it binds and transports the metal across the kidney membrane. Subsequent excretion through urine gets rid of the metal. Also, the drug reduces Cu(II) to Cu(I) which weakens its binding ability to other proteins, because the square planar layout is destroyed when a reduction to Cu(I) takes place.^[12]

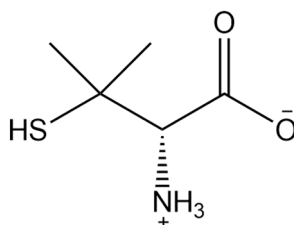


Figure 1.1: The copper scavenging amino acid D-Pen depicted in its ionic form as a zwitterion. The compound is protonated in water.

On the other hand, a lack of copper in humans can also lead to serious health issues, like fatigue, weakness and in more severe cases even in tissue injury and disease. As copper is also essential for absorbing iron in the body, copper deficiency consequently also leads to iron deficiency. This means that in case of copper/iron deficiency the body is unable to transport enough oxygen through its tissues which eventually results in severe tissue injury.

Menkes syndrome is a rare hereditary disease which is linked to the X-chromosome in humans and therefore mostly affects the male sex. The liver of affected patients cannot absorb copper which is needed in the body to survive and therefore the disease is already lethal in early childhood.^[10,11,14,15] The protein ATP7A which is supposed to transport copper from the gastrointestinal tract to the liver does not function properly and because of that the metal ion never arrives in the liver. Subsequently, the transport of copper through the blood/brain barrier cannot take place. So far, treatment can only prolong a patient's life, but the disease itself has remained incurable.^[7,11]

In order to stabilize the amount of copper in the body, healthy living organisms have developed homeostatic mechanisms to regulate its cellular concentration and to ensure an optimal supply of copper. Therefore, slightly higher or lower levels of copper can be easily levelled out by a healthy organism.^[6]

1.1.2 Metalloproteins Containing Copper

In humans, animals, bacteria and fungi, copper can be found in the active site of various metalloproteins. Being a highly redox-active element, it readily reacts with dioxygen, superoxide, nitrous oxide, thiol or thioether groups. Depending on the type of active site, copper proteins can be classified into three main categories.^[16,17] By now however, many other copper centres have been detected which do not fit into these classic categories anymore.^[5,17–20]

1.1.3 Types and Roles of Copper Proteins

Historically, copper proteins are classified into type 1-3 copper proteins depending on their spectroscopic properties and thus, reflect the geometric and electronic structure of the active site.^[17]

Type 1 includes so-called 'blue' copper proteins in which a copper ion forms the center of the protein. This copper ion is always coordinated by two nitrogen atoms of two histidine residues and two sulfur atoms of two methionine or cysteine residues. Type 1 copper proteins are mainly responsible for outer sphere electron transfer reactions: $\text{Cu}^{2+} + \text{e}^- \rightleftharpoons \text{Cu}^+$, like the

proteins plastocyanin and azurin, or they facilitate the oxidation of polyphenols and -amines or ascorbate in plants like the 'blue' oxidases laccase and ascorbate oxidase. [5,19] As Cu^+ ions prefer a tetrahedral fourfold coordination or trigonal bipyramidal coordination to the preferred tetragonal (due to the *Jahn-Teller effect*) geometry of Cu^{2+} centers, type 1 copper proteins assume a coordination sphere which lies in between those mentioned, resulting in a polyhedral geometry of the active site. [18]

Type 2 copper proteins are characterized by one copper center which is surrounded by four histidine ligands, one of which bridges the copper (II) center to a zinc (II) ion. Since the active sites of these copper proteins contain a copper (II) center, the preferred coordination geometry is a square pyramidal one, the four histidine ligands in the plane, leaving space in the axial position of the complex for another ligand to bind to the active site. [18] Copper proteins of that type are also called 'normal' (meaning 'non-blue') copper proteins and are responsible for dioxygen activation together with organic coenzymes. This includes non-blue oxidases like galactose oxidase, responsible for the oxidation of alcohol in fungi, and amine oxidases which decompose amines and are responsible for cross-linking collagen. Also, monooxygenases, e.g. dopamine- β -oxygenase, and dioxygenases, e.g. quercetinase, cytochrome-c-oxidase and copper, zinc superoxide dismutase (SOD) belong to this type. [19] The terms 'blue' and 'non-blue' copper proteins point out the fact that these two types can be easily differentiated through their spectroscopic properties. On the one hand, 'blue' copper proteins show a blue color due to the strong absorption of red light through ligand-metal-charge-transfer (LMCT) transitions between the coordinated thiolate moiety of the cysteine ligand and the metal center. On the other hand, 'non-blue' copper proteins only show a weak absorption due to weak $d \rightarrow d$ electron transitions, and therefore appear colorless to the eye. [5]

Type 3 copper proteins contain a coupled binuclear copper center in which each copper ion is coordinated by three histidine moieties. In between those copper centers oxygen can be bound reversibly. The redox conversion of those copper (I) and copper (II) centers leads to an oxygen transport. Examples of type 3 copper proteins are hemocyanin, responsible for dioxygen transport in mollusks and arthropods, tyrosinase, a monooxygenase, and catechol

oxidase, playing an important role in enzymatic browning of fruit and vegetables as well as in forming melanin in the human skin.^[5,19]

As this system of classification is merely a historic one, nowadays more copper proteins are known which do not fit into this classic system. Therefore, the system has expanded in recent years and now also includes type 4, as well as type A and type K active sites.^[19] Some important copper proteins and their biological functions are shown in Table 1.2.

Table 1.2: Selected copper proteins and their biological functions.^[18]

	Reactivity	Biological Function and Occurrence
Type 1 Copper Proteins		
Plastocyanin	Electron transfer in plants	
Azurin	Electron transfer in bacteria	
Type 2 Copper Proteins		
Monoamine oxidase (MAO)	Oxidase	Degradation of amines in bacteria, yeasts, plants and mammals
Dopamine- β -monooxygenase	Dioxygenase	Oxidation of dopamine in kidneys
Quercetin dioxygenase	Dioxygenase	Cleavage of quercetin in fungi
Galactose oxidase	Oxidase	Oxidation of alcohol in fungi
Cu, Zn superoxide dismutase (SOD)	Dismutase	Disproportionation of $O_2^{\cdot -}$ in e.g. erythrocytes (red blood cells)
Type 3 Copper Proteins		
Hemocyanin	Oxygen transport in molluscs and arthropods	

Tyrosinase	Oxygenase and Oxidase	Ortho hydroxylation of phenols and further oxidation to o-quinones in skin and pulp
Catechol Oxidase	Oxidase	Oxidation of catechols to o-quinones in plants
Non-Classical Copper Proteins		
Copper-transport-ATPase, CUP2-protein	Thionein	Regulation, storage and transport of copper
Cytochrome-c-oxidase	Electron transfer (Cu _A protein) in the respiratory chain	
N ₂ O reductase	Reductase (Cu _A protein)	Reduction of N ₂ O to N ₂ in the nitrogen cycle
laccase	Oxidase (type 2 + 3 protein)	Oxidation of polyphenols and -amines in plants
ascorbate oxidase	Oxidase (type 2 + 3 protein)	Oxidation of ascorbate to dehydroascorbate in plants

1.2 Iron

Ever since it was possible in historic times to smelter and process iron, it was extensively used instead of the relatively soft alloy bronze and thus leading the way into the iron age. As iron has a relatively high melting point (cf. Table 1.1 and Table 1.3), it was only possible to process the metal when smelting the according iron ore with an excess amount of charcoal. Before proper kilns were invented, this was done using shallow pits in which iron ore and red-hot charcoal were combined and created the high temperatures needed to smelter the metal. That way, lumps of wrought iron varying in size were obtained which could be forged afterwards and be used as spear tips, for example.^[21]

During the Middle Ages, techniques for smelting iron advanced by introducing bloomeries, furnaces which were capable of creating higher temperatures and therefore smelting the metal more effectively. Using this new technique created a problem, however. The content of carbon in the yielded metal increased leading to a lower iron content in the alloy and creating crude iron which is unforgeable and impossible to roll. Crude iron is a very brittle compound now used as cast iron and contains about 4 % of carbon and often small amounts of other impurities, such as manganese, silicon, sulfur or phosphorous. Adding lots of oxygen to the furnace and using coke instead of charcoal were the only ways of increasing the carbon content of iron at that time.^[3,21]

The introduction of blast furnaces, which were built in a way so that a constant air flow could support the smelting process, managed to fully eradicate this problem only in the second half of the 19th century. The process decreased the amount of carbon in the metal and mild steel was yielded which could be shaped through forging and rolling.

Nowadays, different types of steel (an alloy of iron and carbon with a maximum of 2.1 % carbon) are produced to meet different requirements, e.g. as building material. Sometimes other metals such as titanium, vanadium or nickel are added to the alloy to make it usable in different settings. It is also possible to yield pure iron, but as it cannot be hardened at all it is of comparably little interest to the metal industry.^[21]

Table 1.3: Some general, physical and chemical properties of elemental iron.^[3,21,22]

Appearance	Whitish silver, metallic
Atomic Number	26
Weight Per Cent in Geosphere	6.2 %
Density	7.874 g/cm ³
Melting Point	1539 °C
Boiling Point	3070 °C

Thermal Conductivity	80.4 W/(m · K)
Electrical Conductivity	$11,2 \cdot 10^6 \Omega^{-1} \text{ m}^{-1}$ at 0°C
Magnetism	Ferromagnetic
Oxidation States	+ II, + III (ranging from + I to + VI, but they are very rare)
Electron Configuration	[Ar] 4s ² 3d ⁶

Pure iron exists in three different modifications depending on the temperature; α -iron exists up to 906 °C, γ -iron up to 1401 °C and δ -iron up to 1539 °C. After aluminum, iron is the most abundant metal in our geosphere and it is the most significant metal in the world's industry. The amount of crude iron produced each year is ten times as high as that of all other metals added together.^[3]

Elemental iron is only rarely found on the Earth's surface, because it easily oxidizes. Therefore, iron is almost exclusively found as ores rich in iron oxides or sulfides like magnetite (Fe₃O₄) or pyrite (FeS₂).^[1,3]

1.2.1 Iron in Biology

In most life forms iron is very abundant and part of various compounds, either in its +II or +III oxidation state (cf. Table 1.3). Being an essential metal, iron is found in almost all living organisms including bacteria, fungi, plants and mammals. Due to its redox properties which results in an easy transition of oxidation states +II and +III, iron like copper (cf. ch. 1.1.1) is a fundamental component in a wide range of different enzymes and cofactors in living organisms, e.g. transferrin, ferritin, cytochromes, peroxidases, catalases, hemoglobin and myoglobin.^[23–25]

The best-known example in biology containing iron is probably the heme unit, a part of the metalloprotein hemoglobin, which can be found in red blood cells and is responsible for the characteristic red color of blood.^[23,26]

Being an essential metal, a continuous supply of iron is vital for most living organisms. In plants, a lack of iron leads to an interference in the synthesis of chlorophyll and to bleaching or turning yellow of green plant parts (chlorosis).^[19] The human body needs about 1 mg (men) to 2 mg (women) of iron daily. However, as iron is only resorbed relatively inefficiently from food sources the daily intake of iron needs to be a lot higher (about 5 - 9 mg for men and 14 – 18 mg for women). In plants, iron can mostly be found in its poorly soluble form, Fe^{3+} , which makes iron from plant-based food sources quite hard to absorb. Additionally, other constituents of some plants, like tannins, oxalic acid and other polyphenols inhibit the uptake of iron even more through the formation of compounds which are poorly soluble. However, taking in ascorbic acid at the same time as iron(III) compounds increases the bioavailability of iron(III).^[19] Supplementary iron in medical products therefore contain Fe(II) ions, often in combination with ascorbic acid, to facilitate resorption.

Iron taken in as hemoglobin or myoglobin from meats, on the other hand, can be more easily absorbed by the body.^[19] Therefore, vegetarians and vegan have to be very careful to take in enough iron in order to not develop any iron deficiency.

A lack of iron in the human body leads to anemia and disorder of the immune system eventually posing a dangerous health risk (cf. ch. 1.1.1).^[5] A surplus of iron on the other hand also needs to be treated, as an excess of iron stored in the functional parts of organs (parenchyma), mostly in the liver, leads to siderosis (a deposition of excess iron in the tissue). This surplus of iron can then lead to a higher susceptibility to infectious diseases such as tuberculosis, AIDS, or salmonellosis. An intake of more than 180 mg/kg of iron per day can even end lethal and an intake of 160 mg/kg per day can lead to serious health problems like liver cirrhosis or diabetes mellitus. Also, a genetic disorder known as hemochromatosis is responsible for an excess amount of iron in the body and needs to be treated medically.^[19]

Luckily, nowadays there are drugs that can balance the amount of iron accumulating in the body. Bacteria called streptomyces produce ferrioxamine b, a compound whose des-form (without iron) can be used to complex iron which is encapsuled in storage proteins. This way, excess iron can be easily disposed of via the urinary tract.^[19] In Figure 1.2, deferoxamine B is depicted.

Generally, iron is stored in metalloproteins, because the ‘free’ form of iron catalyzes the formation of highly reactive oxygen radicals which damage living organisms and can lead to a higher risk of cancer due to oxidative damage to the DNA. ^[5,19,26]

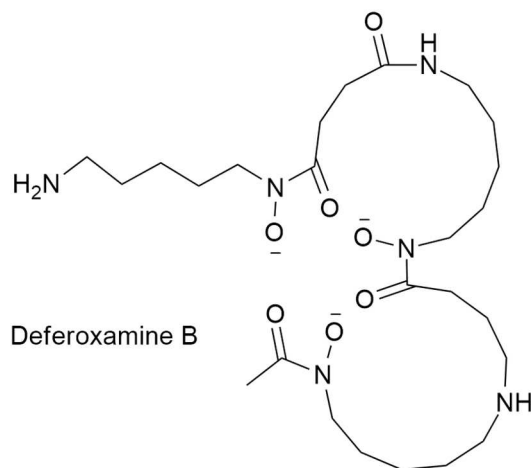


Figure 1.2: Deferoxamine B, an aliphatic molecule with three non-equivalent hydroxamate groups, which is able to coordinate iron via its six oxygen atoms (forming ferrioxamine B) and removing excess iron (e.g. after a blood transfusion) from the body that way.^[5]

1.2.2 Metalloproteins Containing Iron

Iron can be found in the active site of various metalloproteins in fungi, bacteria, animals and humans and it is the most abundant transition metal in humans. Being a highly redox-active element like copper, it readily reacts with dioxygen, nitrous oxide, cyanide and carbon monoxide which is also the reason for the toxicity of the two latter compounds.^[19] Depending on whether an iron metalloprotein contains a heme unit or not they are categorized into two main groups: heme proteins and non-heme proteins.

The heme unit itself is characterized by the existence of an iron-porphyrin sub-unit. Examples for heme iron proteins are hemoglobin and myoglobin which are both oxygen carriers in mammals.^[27] In

Figure 1.3, the heme building block, the porphyrin unit, is depicted. It is a cyclic, organic ligand which consists of four linked pyrrole components.

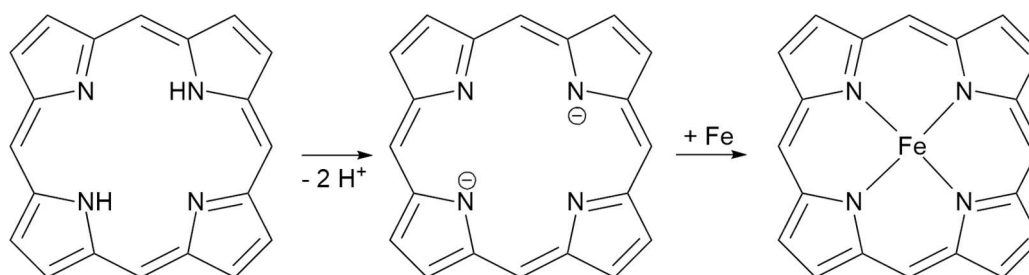


Figure 1.3: The porphyrin sub-unit (a macrocyclic, tetradentate ligand) in its protonated, deprotonated and coordinated form.^[28]

Non-heme iron proteins can be further divided into two categories: mononuclear non-heme proteins containing only one iron ion in their active site and dinuclear non-heme proteins containing two iron centers which are linked via a bridging ligand, such as a carboxylate, oxido or hydroxido species.^[28–30] In the following chapter some important examples of both types of iron proteins are presented in more detail. As opposed to copper complexes, iron complexes can have two different spin states, high spin and low spin, which affect the chemical environment of the complexes and thus the reactivity of the respective compound.

1.2.3 Types and Roles of Iron Proteins

The list of iron proteins presented in this chapter does not, by far, claim to be a complete summary of the vast field of existing iron proteins, but is supposed to give a short overview of the most distinct classes.

Compared to copper proteins, iron proteins are not as strictly classified. Merely, a distinction between heme and non-heme iron proteins is made, the latter being further sub-classified into mononuclear and dinuclear ones.

Heme proteins are all based on the porphyrin unit presented in the previous chapter and are mostly responsible for dioxygen or electron transport or catalysis. Depending on the type and pattern of the heme unit's substituents, heme proteins are further categorized into three groups: heme a, heme b and heme c. Heme a contains a long, hydrophobic chain, heme b is

characterized by two vinyl groups and heme c by two cysteine-thiol moieties linking the heme unit directly to the protein scaffolding.^[28] In Figure 1.4 those three heme units are depicted.

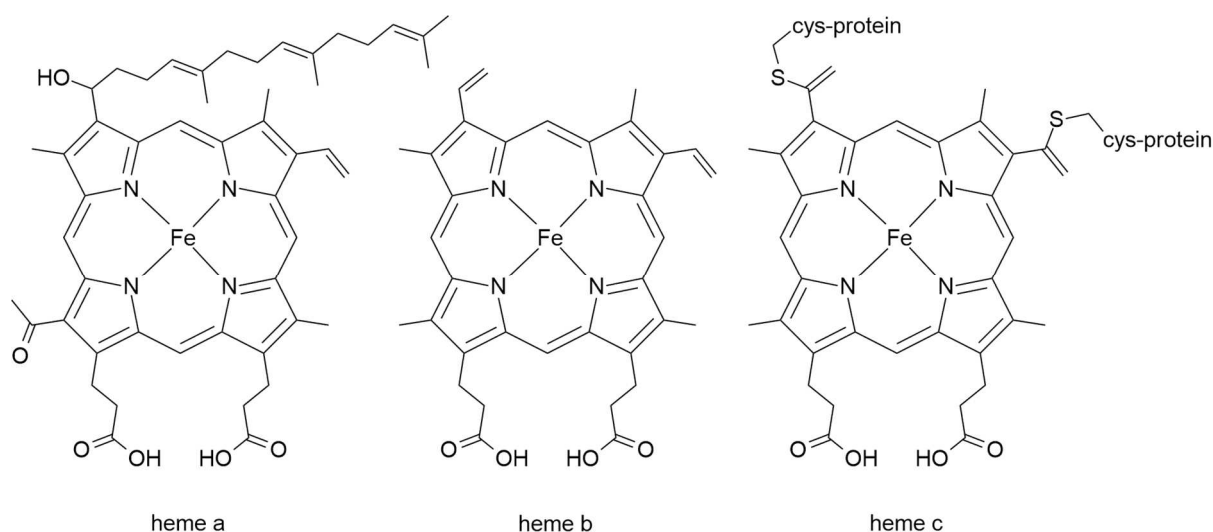


Figure 1.4: The three heme protein categories; heme a, b and c.

Coordination in heme proteins takes place at the four nitrogen atoms of the porphyrin ligand coordinating the equatorial positions around an iron center and leaving the two axial positions of the metal ion unoccupied. Those two positions can then be occupied by co-ligands in heme iron proteins. Depending on the nature of these co-ligands, the metal center either assumes a low-spin or a high-spin state, also changing the coordination sphere of the complex, as Fe^{2+} in a high-spin state does not fit into the center of the porphyrin unit anymore and therefore is forced to move ‘out of plane’ resulting in a square pyramidal coordination sphere of the heme unit. Fe^{3+} , on the other hand, fits into the pocket of the macrocyclic ligand in both spin states. The heme center in hemoglobin and myoglobin are examples for the change in steric demands of the active site in iron proteins depending on the metal center’s spin state and are depicted in Figure 1.5. In general, the iron center (in both oxidation states Fe^{2+} and Fe^{3+}) favors an octahedral coordination sphere.

Hemoglobin, a type heme b iron-porphyrin complex, is responsible for oxygen transport in most animals and humans. One of its axial positions is occupied by the imidazole ligand of a histidine moiety and contains Fe^{2+} in its high-spin state. When oxygen is bound to the sixth position of the complex, the iron center is oxidized to Fe^{3+} and assumes a low-spin state resulting in an octahedral coordination sphere of the iron center.

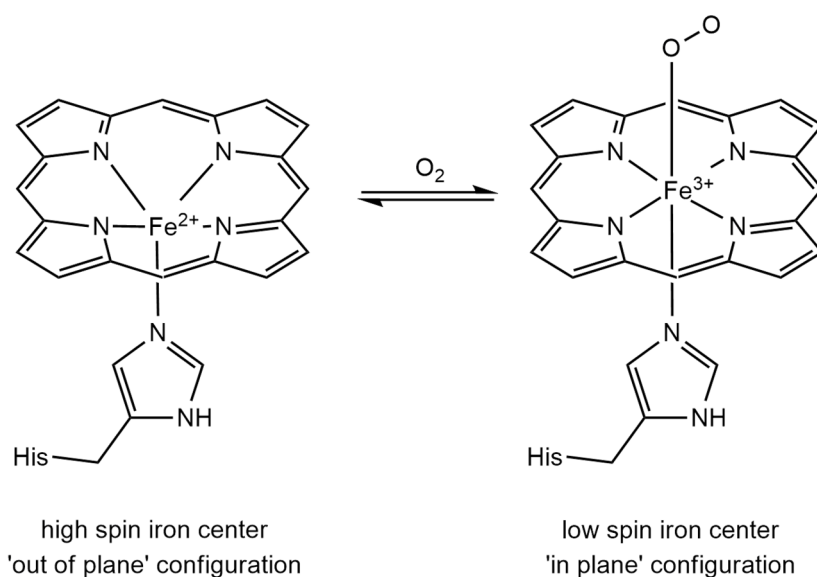


Figure 1.5: The active site of the iron proteins hemoglobin and myoglobin. Deoxygenated form on the left and oxygenated form on the right.

Mononuclear non-heme iron proteins like catechol dioxygenase or bleomycin, an anti-cancer drug made from *streptomyces verticillus*, only contain one iron metal center in their active site. This group of proteins contains many enzymes which are mono- or dioxygenases and redox synthesis enzymes play an important role in fat metabolism, amino acid synthesis and metabolizing aromats.^[5] Bleomycin is an antibiotic made from the bacteria *streptomyces verticillus* and is used as an anti-cancer agent in chemotherapy of throat and head tumors.^[19] Its effectiveness is accounted for by the formation of an iron(II) bleomycin complex in a tumor cell which is able to activate dioxygen. In this process so-called 'activated bleomycin' (cf. Figure 1.6) forms through single electron transfer. The highly reactive Fe(III) hydroperoxido intermediate reacts with the substrate (the DNA) leading to a DNA strand scission in tumor cells.^[19,29]

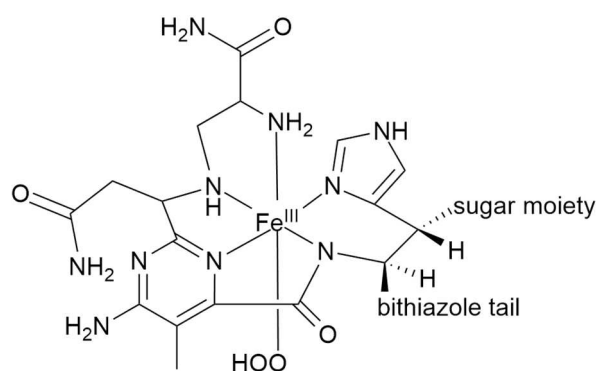


Figure 1.6: Proposed structure for 'activated bleomycin'. Adapted from^[29] and^[143].

Dinuclear non-heme iron proteins catalyze the oxidation of various organic substrates using dioxygen. They contain two iron centers in their active site which are bridged by either carboxylates and/or water-derived ligands.^[29] Examples include soluble methane monooxygenase, ribonucleotide reductase (RNR) and hemerythrin (cf. Table 1.4). As these types of proteins form the basis of interest for this thesis, some of them are discussed in more detail in the following chapter.

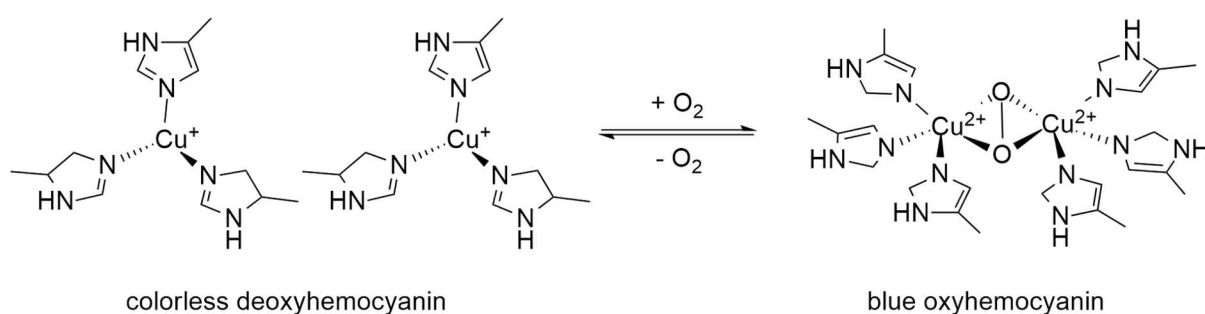
Table 1.4: A small selection of iron proteins and their biological functions.^[5,28,29,31,32]

	Reactivity	Biological Function
Heme Iron Proteins		
Myoglobin	Dioxygen storage in muscles	
Hemoglobin	Oxygen transport in lungs and blood	
Cytochrome- <i>c</i> -oxidase	Oxidase	Terminal oxidation of dioxygen to water
Heme Oxygenase	Oxygenase	Responsible for heme degradation to prevent accumulation of toxic free heme

	Reactivity	Biological Function
Heme Iron Proteins		
Heme peroxidases	Peroxidases	Catalyze peroxidase-like electron transfer reactions
Nitric Oxide Synthase 3	Synthase	Catalyzes the oxidation of the simple amino acid, L-arginine, to L-citrulline and nitric oxide
Non-Heme Iron Proteins		
Mononuclear		
Catechol dioxygenases	Dioxygenase	Catalyze ring cleavage of catechols with dioxygen
Bleomycin	Activation of dioxygen eventually leading to fragmentation of DNA in tumor cells (chemotherapeutic agent)	
Dinuclear		
Soluble methane monooxygenase hydroxylase (sMMOH)	Monooxygenase	Oxidation of methane to methanol in methanotrophs
Ribonucleotide reductase (RNR)	Reductase	Generator of tyrosyl radicals, reduces ribonucleic acids to deoxyribonucleic acids, the building blocks of DNA
Ferritins	Intracellular proteins storing iron in most living organisms	
Hemerythrin	Oxygen transport in some marine invertebrates	

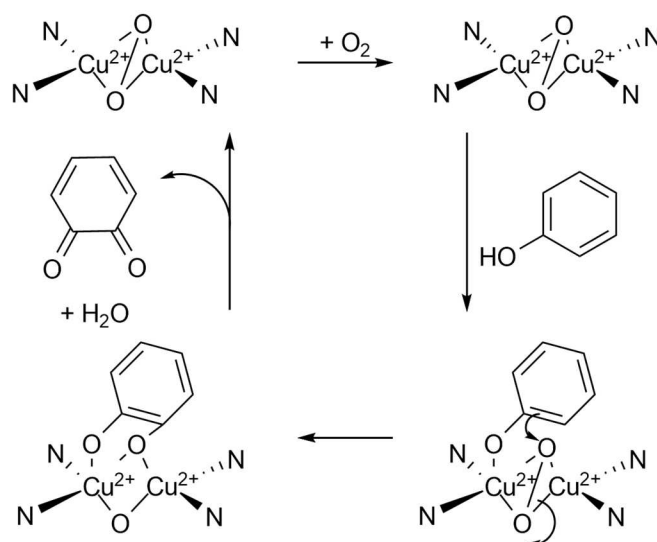
1.3 Copper and Iron Dioxygen Complexes in Nature

As already mentioned in chapters 1.1.2 and 1.1.3, there are several copper- and iron-based metalloproteins in nature which act as a carrier for dioxygen. In order to do that, those compounds need to be able to activate this small and relatively inert molecule.



Scheme 1.1: Reversible binding of dioxygen by hemocyanin.

A well-known dioxygen carrier in nature is the copper protein hemocyanin. It is responsible for transporting dioxygen in mollusks and arthropods (cf. ch. 1.1.3). In Scheme 1.1 the oxygen transfer through hemocyanin is depicted. Dioxygen binds in a $\mu\text{-}\eta^2 : \eta^2$ fashion to both copper centers resulting in an oxidation of these copper centers, reducing the added dioxygen to a peroxide.^[5,18]

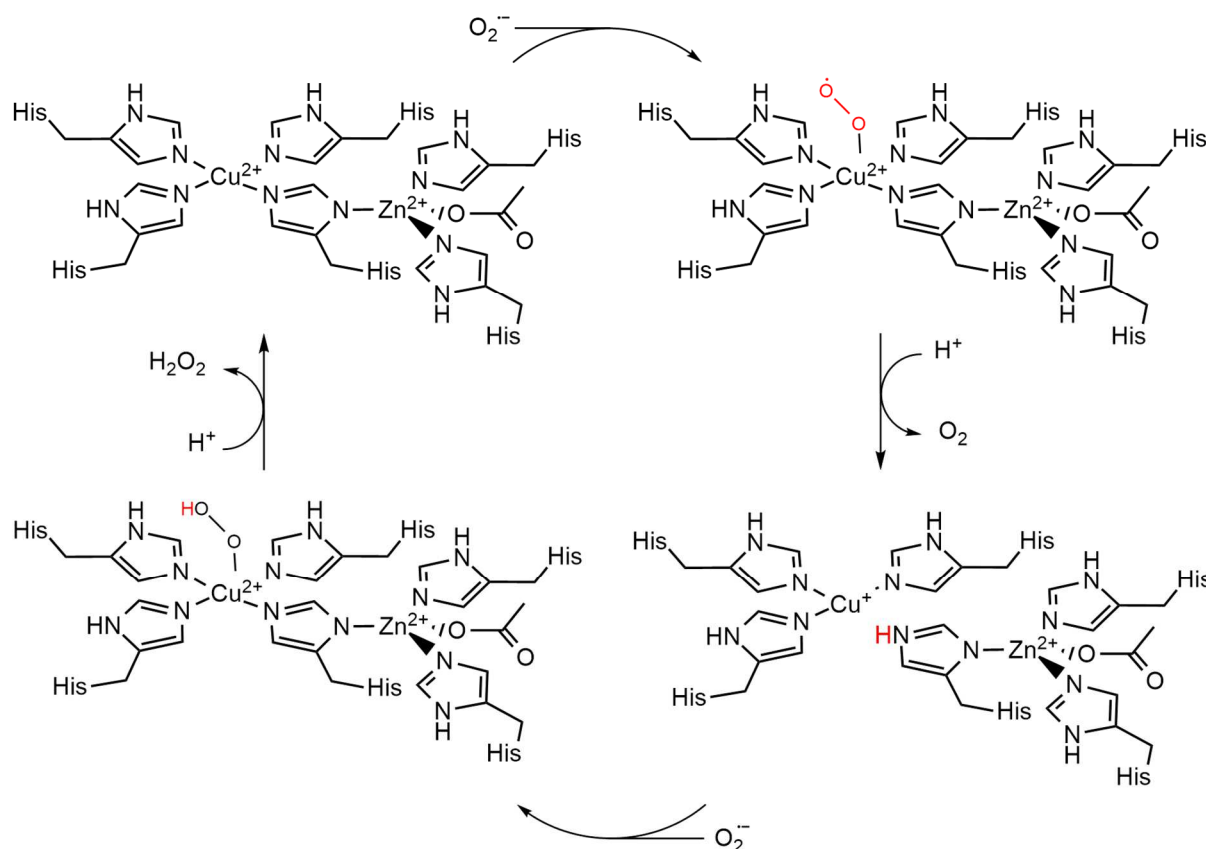


Scheme 1.2: Proposed reaction mechanism for the activation of phenol by tyrosinase. The symbol 'N' refers to the actually bound histidine imidazole group. Axial ligands are omitted for clarity.^[28]

The copper protein tyrosinase is responsible for oxidizing tyrosine to dopaquinone. Several reaction steps later, polymeric melanin pigments are formed which brown skin, hair and fruit. The reaction cycle is not entirely clear yet, but bears a strong resemblance to the reaction of the transport of dioxygen by hemocyanin. A proposed pathway for the reaction is displayed in Scheme 1.2. Comparing the active sites in hemocyanin and in tyrosinase, dioxygen is also bound by two histidine-coordinated copper(II) centers in a $\mu - \eta^2 : \eta^2$ fashion in tyrosinase. The main difference, however, is the fact that the active center of tyrosinase offers more space for the substrate and therefore allows the transfer of an oxygen atom within its coordination sphere.^[28]

Copper, zinc superoxide dismutase (SOD) is another very important protein which belongs to the category of superoxide dismutases functioning as an antioxidant in the human body. As already mentioned in Table 1.2, it is a catalyst responsible for the disproportionation of superoxide, an undesirable by-product in the respiratory chain. The mechanism for that reaction has not been entirely disclosed yet, but a proposed mechanism is shown in Scheme 1.3.^[28] SOD contains a copper and a zinc center in its active site which are connected by an imidazole group. The oxidation of the superoxide moiety takes place at the copper core forming a superoxido complex and leaving the zinc center unchanged.

In a first step, the superoxide radical attaches itself to the copper core. Then, protonation leads to the formation of dioxygen which leaves the reaction and two separate intermediates are cleft at the imidazole group in between the copper and the zinc center. This results in a copper(I) complex and a zinc(II) complex with the imidazole moiety attached to the zinc center. In the next step, another superoxide radical can bind to the copper(I) complex, reattaching the zinc center to the copper center through deprotonation of the imidazole group and binding the superoxide radical in the form of a hydroperoxido moiety, and thus re-oxidizing the copper center. Incorporating another proton, hydrogen peroxide forms and leaves the reaction, leaving behind the catalyst SOD entirely unaltered ready for a new reaction cycle.



Scheme 1.3: Proposed reaction mechanism of copper, zinc superoxide dismutase (SOD). Adapted from^[28].

Having shown multiple examples of copper proteins which display a $\mu - \eta^2 : \eta^2$ binding mode, it has to be emphasized that this mode is just one possibility of how dioxygen can be bound to the copper center in these complexes. The way dioxygen is coordinated to the metal center is based on geometric and electronic properties of the protein or the model compound used. Generally, dioxygen complexes can be divided into two categories, side-on and end-on coordinated complexes.^[33–37] In Figure 1.7 some of these possible coordination modes for copper complexes are shown, using examples that have already been characterized elsewhere.^[35,38–43] The oxidation state of the respective copper cores varies with the coordination mode of dioxygen in the complex.

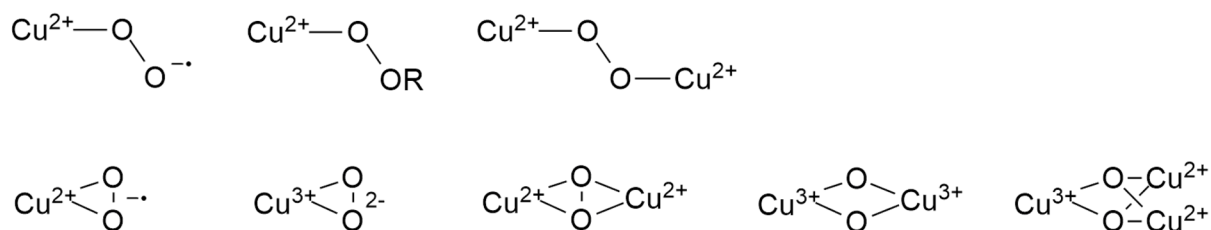
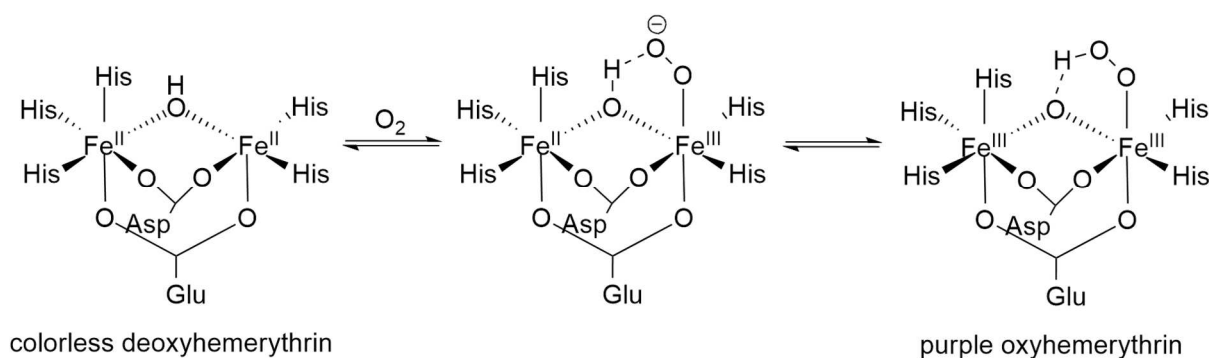


Figure 1.7: Copper-oxygen cores characterized in synthetic complexes so far.^[43] The top row shows an end-on coordination and the bottom row a side-on coordination of dioxygen to the respective copper cores.

As already mentioned in ch. 1.2.3, some marine invertebrates also use metalloproteins which contain a non-heme iron active site for reversible oxygen fixation. In Scheme 1.4 the oxygen transfer by the iron protein hemerythrin is depicted.



Scheme 1.4: Reversible binding of dioxygen by hemerythrin via a yet unobserved iron(II)/iron(III) superoxido intermediate postulated by Solomon et al.^[44]

Dioxygen binds to one iron center of deoxyhemerythrin resulting in an oxidation of both iron centers, reducing the added dioxygen to a peroxide and linking both metal centers by an oxido-bridge which then stabilizes the resulting hydroperoxido moiety on the one iron center.^[5,29,32,44,45]

Soluble methane monooxygenase hydroxylase (sMMOH) is an iron enzyme which allows methanotrophic bacteria to convert methane and dioxygen to carbon and energy. A diiron center containing two histidine and four glutamate units forms the active site of the hydroxylase component of soluble methane monooxygenase (sMMO). The enzyme transfers

one atom of the dioxygen molecule to the substrate and reduces the second atom to water.^[32,45] The active site of sMMO is shown in Figure 1.8.

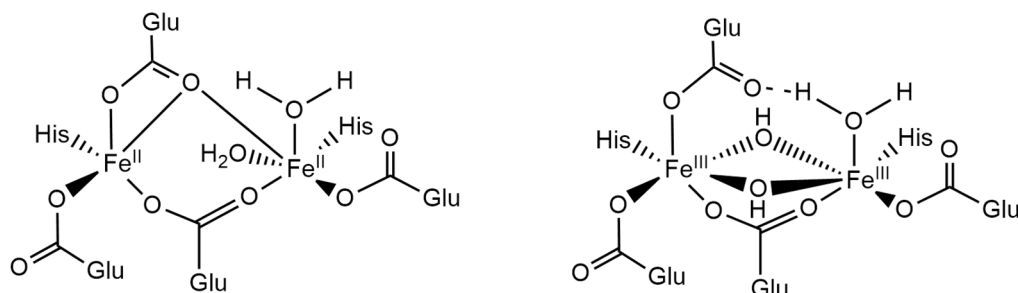
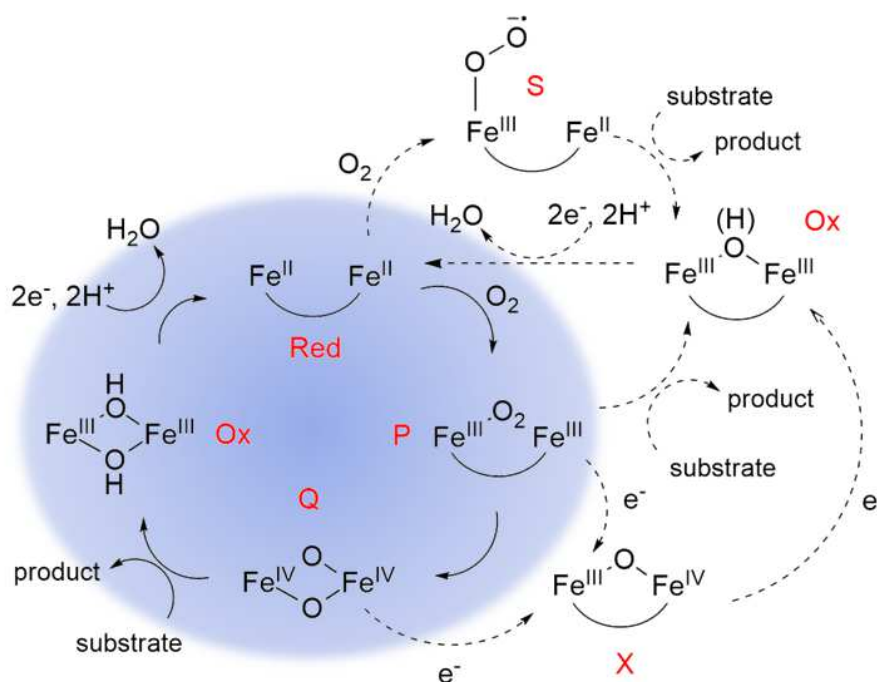


Figure 1.8: The active site of sMMO in its reduced (left) and its oxidized state (right).^[32]

The two iron centers in sMMO's active site of the hydroxylase component are coordinated by two histidine and four glutamate moieties. In its reduced state the active site contains a dinuclear iron(II) center which is oxidized through the reaction with dioxygen to a dinuclear iron(III) center containing two hydroxido-bridged ligands. Just like in copper proteins, non-heme diiron enzymes form various oxygen adduct species.



Scheme 1.5: Possible intermediates in the activation of dioxygen by non-heme diiron enzymes primarily based on the canonical mechanism for sMMOH (blue sphere). The starting point of the cycle being Red and the end being Ox. P marks a peroxidodiferric species, Q the bis(μ -oxido)diiron(IV) oxidant associated with sMMOH, X the (μ -oxido)diiron(III,IV) species that generates the catalytically essential Y122• radical in RNR R2 and S is the diiron(II,III)-superoxo species proposed for T4MOH, another non-heme diiron protein.^[45]

The canonical mechanism for sMMOH already displays an array of such species, taking into consideration that there are even more intermediates possible. Some of those intermediates that occur during the activation of dioxygen are presented in Scheme 1.5. As shown in there, end-on as well as side-on iron oxygen intermediates form during the reaction of iron enzymes with dioxygen and other substrates.

1.4 Model Compounds for Copper and Iron Proteins

Synthetic compounds which mimic the ones existing in nature are of great value when trying to optimize reaction conditions in the laboratory. Therefore, those model compounds are of high interest when researching potential new catalysts. The example of the type of reaction catalyzed by hemocyanin in comparison to tyrosinase shows that only very miniscule differences in the built of a molecule can have a huge impact on its reactivity and applicability. Building model compounds provides researchers with a better understanding of how metalloproteins function in nature and allows them to find alternative solutions for activating and transferring small molecules like dioxygen in redox reactions in the laboratory.^[25]

In recent decades, iron and copper systems have already been studied very successfully, discovering reactive intermediates and finding out more about the binding modes of dioxygen to the respective metal centers.^[20,29,32,45–48]

In 1988, the first crystal structure of a synthetic copper peroxido complex using the ligand tris(2-pyridylmethyl)amine (tmpa) was obtained by Karlin et al.^[38] As shown in Figure 1.9, tmpa is a tripodal, tetradentate ligand which forms its copper complex via three aromatic N-donor atoms and one aliphatic N-donor atom. Their research already showed that prior to the formation of the peroxido species a superoxido species forms which could be detected spectroscopically and kinetically.^[49,50] As this superoxido intermediate was of highly reactive nature, even at low temperatures, it was not possible to isolate and characterize it any further. However, the copper complex of tmpa became the first example of a model complex mimicking the protein hemocyanin and being able to bind dioxygen reversibly at low temperatures (approx. - 80°C). The difference to its natural counterpart is the binding mode

of the dioxygen molecule, because the tmpa complex favors an end-on configuration as opposed to the side-on configuration in hemocyanin.

Only in 2006, Schindler and co-workers finally managed to synthesize an end-on copper superoxido complex, which was stabilized by the sterically very demanding ligand TMG₃tren (tris(tetramethylguanidino)tren), and to isolate, crystallize and fully characterize this highly reactive oxygen intermediate at low temperatures.^[51,52] In Figure 1.9, the ligands tmpa and TMG₃tren as well as their respective oxygenated end-on copper complexes are depicted.

TMG₃tren, a derivative of tmpa, is a tripodal, aliphatic ligand which binds to the copper center via its four N-donor atoms. Steric shielding and the super-basic character of the guanidino groups leads to the stabilization of the end-on superoxido intermediate upon oxygenation at low temperatures.

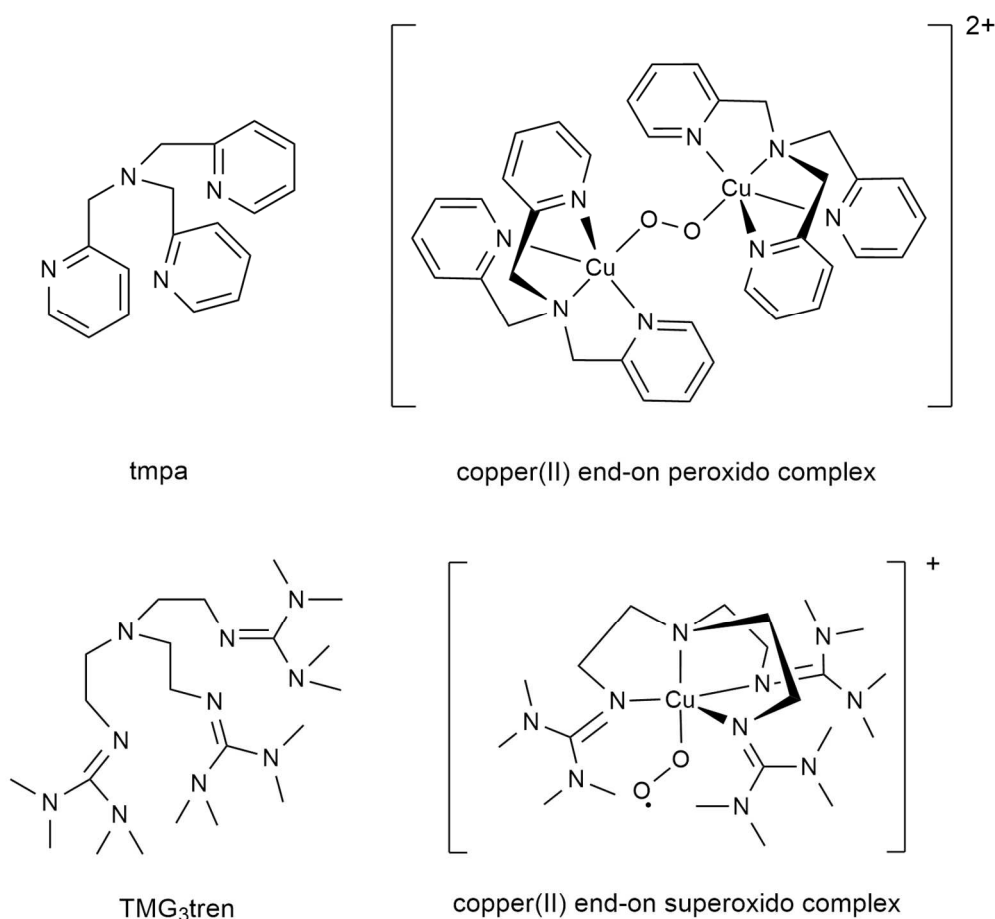


Figure 1.9: Ligands (left) used to synthesize the respective copper(II) oxygen adduct complexes (right).

In 1989, Kitajima et al. managed to synthesize the first side-on copper peroxido complex at low temperatures which could be characterized via x-ray crystallography. Using the tridentate ligand $\text{HB}(3,5\text{-iPrpz})_3$, a hydrotris(pyrazolyl)borate, and a copper(I) salt, they provided the first synthetic model complex for the copper proteins hemocyanin and tyrosinase, as the complex readily reacted with dioxygen at low temperatures.^[53]

On top of those findings, the research group also characterized the first example of a synthetic side-on copper superoxido complex using x-ray analysis in 1994. Modifying the previously used hydrotris(pyrazolyl)borate, they prepared the sterically more demanding ligand $\text{HB}(3\text{-tBu-5-iPrpz})_3$ which prevented dimerization of the oxygen adduct and therefore led to the formation of the side-on superoxido intermediate upon oxygenation.

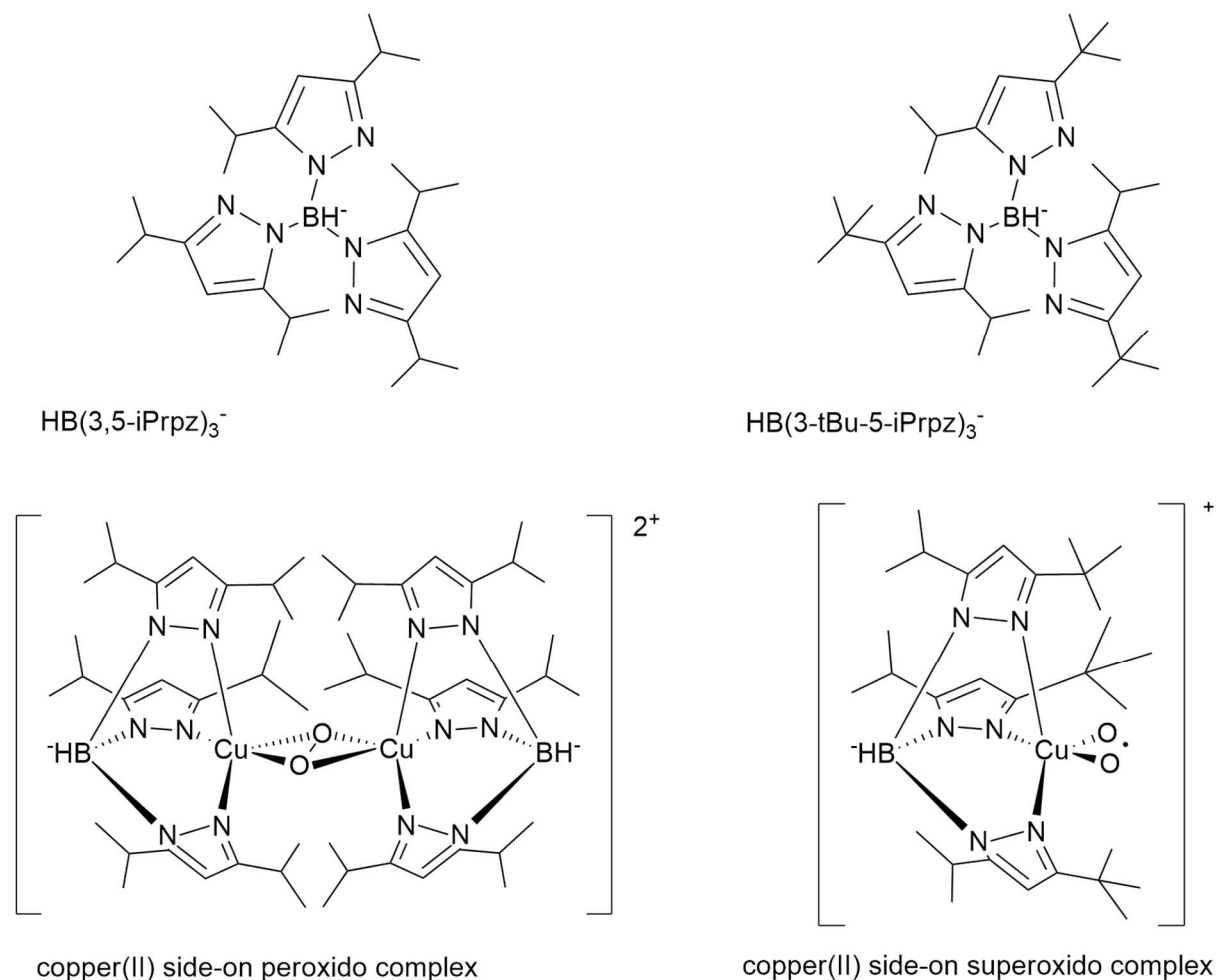


Figure 1.10: Ligands (top) used to synthesize the respective copper(II) oxygen adduct complexes (bottom).

Ligand tuning by substituting isopropyl groups of the hydrotris(pyrazolyl)borate with tert-butyl groups resulted in the stabilization of the forming superoxido intermediate.^[39] Both ligands used by Kitajima et al. as well as their corresponding copper oxygen adduct complexes are depicted in Figure 1.10.

In non-heme iron complex chemistry it was only possible to obtain five crystal structures of different model complexes which are able to mimic naturally occurring iron proteins reversibly binding dioxygen so far.^[45] There are two possible ways of creating those complexes: using a mononucleating ligand like tmpa to form an iron precursor complex which is then able to dimerize via an oxido- or a hydroxido-bridge^[54], or the direct formation of a dinuclear iron complex using a ligand which enforces dimerization instantly.^[55] These two methods are used to trap oxygen-derived diiron intermediates which are able to mimic iron proteins in nature.

The first crystal structure of a synthetic model diiron complex mimicking the core of deoxy-hemerythrin was already obtained in 1987 by Lippard et al.^[56] based on work previously done by Weiss et al.^[57] They used the tridentate cyclic ligand Me₃TACN to form the dinuclear iron(II) complex [Fe₂(μ-OH)(μ-OAc)₂(Me₃TACN)₂]⁺. In this complex, the two iron cores are bridged by two acetate and one hydroxido ligand just like in hemerythrin. However, the iron cores are neither mixed-valent like in the natural role model nor does the diiron core leave a vacant coordination site for reversible dioxygen binding. The model complex as well as the ligand Me₃TACN are depicted in Figure 1.11.

In 1996, Kim et al. reused the ligand which had been previously applied by Kitajima et al. in 1994 to generate the first example of a synthetic copper(II) side-on superoxido complex,^[39] renamed it Tp^{iPr₂} and created a (μ-1,2-peroxido)diferric complex without an additional single atom bridge to trap dioxygen.^[58] The mononuclear iron(II) carboxylate precursor complex [Fe{HB(pz')₃}(O₂CCH₂Ph)] was reacted with dioxygen at temperatures below -50°C to result in an end-on peroxido diferric adduct complex [Fe₂(μ-1,2-O₂)(μ-O₂CCH₂Ph)₂{HB(pz')₃}]₂ which could be crystallized at low temperatures. As can be seen in Figure 1.11, the two iron atoms are linked by two bridging phenylacetate ligands and a bridging peroxido ligand coordinated in a *cis*-μ-η¹:η¹ fashion. The peroxido moiety is well-shielded by the isopropyl side chains of the pyrazolylborate ligands.^[58]

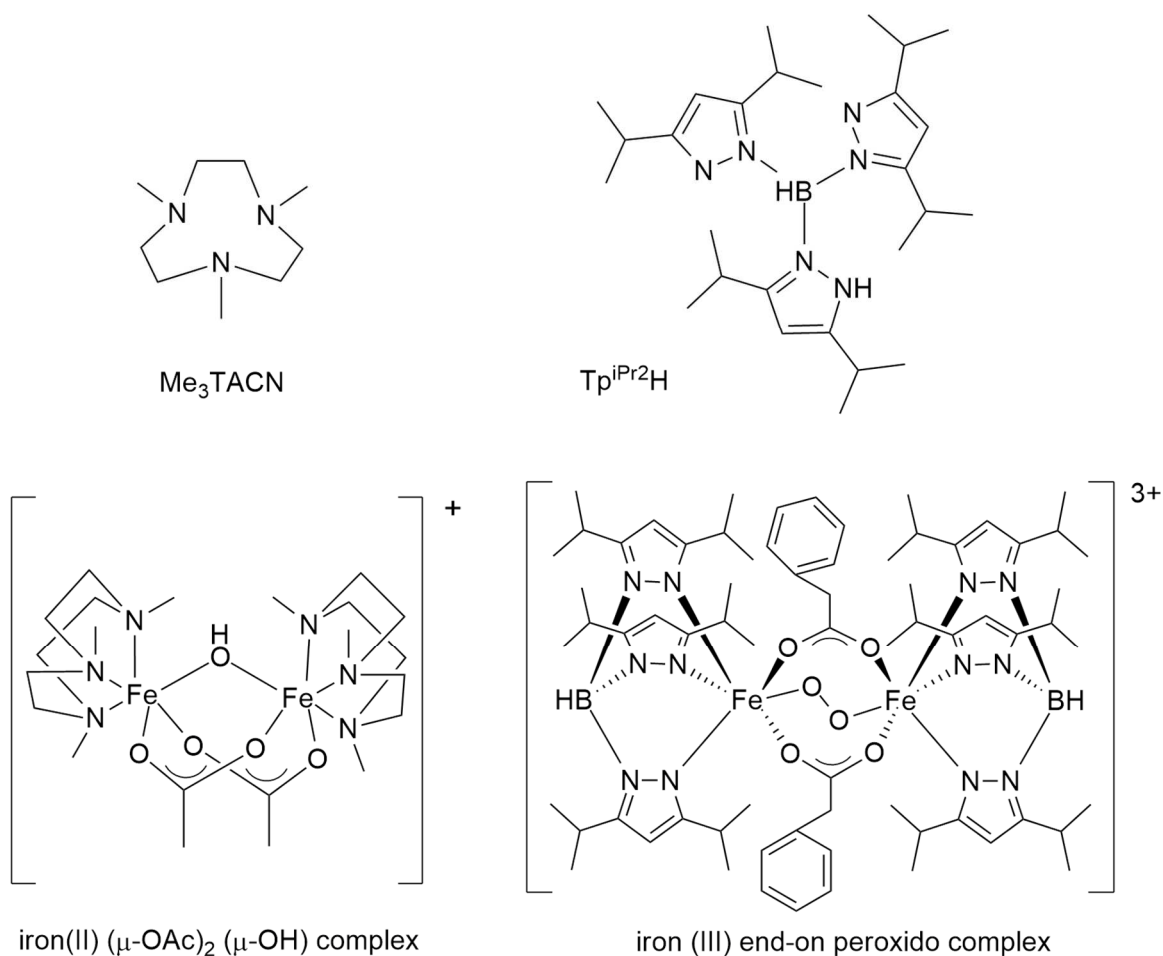


Figure 1.11: The first synthetic complex to model the active site of hemerythrin (left bottom) using the ligand Me_3TACN (left top) and one of the few non-heme iron oxygen adduct complexes determined by X-ray crystallography (right bottom) and the ligand used (right top).

As could be shown in this chapter, there have already been a lot of advances in the fields of copper dioxygen and non-heme iron dioxygen chemistry in the last three decades. However, many details still remain unexplained and have yet to be revealed. A lot more data need to be collected and interpreted to gain as much reliable information on e.g., the course of reactions or the conditions under which reactions will readily take place. These data will help to reach the goal of being able to mimic reactions of complex biological systems, for example the activation of small molecules like dioxygen under mild conditions. Additionally, smart ligand design in the laboratory is an important tool to steer reactions into a certain, desired direction.

1.5 Tripodal, Tetradentate Ligands of the Tren Family

Having elaborated on the relevance of some tripodal, tetradentate ligands mimicking copper and iron proteins in the previous chapter, the focus of this thesis lies on this type of ligand system, the formation of respective copper and iron complexes and the subsequent formation of the according oxygen adduct complexes.

TMG₃tren, being the tripodal, tetradentate ligand which was used to form and stabilize a copper end-on superoxido complex (cf. ch. 1.4), is a ligand based on the parent ligand tren (tris-(2-aminoethyl)amine). Also, tmpa which was used to stabilize and investigate the first copper end-on peroxido complex (cf. ch. 1.4) is a derivative of the tren unit.

Tren itself is an aliphatic ligand with one central N-donor atom and three attached alkyl groups, each including another N-donor atom at their ends. Being a chelating ligand, tren binds to a copper ion via its N-donor atoms and forces the resulting complex into a trigonal pyramidal geometry leaving the axial position vacant and thus allowing another atom such as dioxygen to bind to the copper center.^[59–61] Taking those facts into account, it was expected that tren would be a suitable ligand for forming complexes that produce and stabilize end-on oxygenated intermediates. However, research in the past has revealed that even if copper complexes of the ligand tren indeed tend to support the formation of a superoxido intermediate, they are not stable enough to be characterized in more detail.^[37] Therefore, the formation of a superoxido intermediate could be detected spectroscopically, but it was found that the complex is instantly protonated by the protons of the amine moieties in the ligand itself and thus leading to a very fast irreversible decay of the oxygenated intermediate.^[37,62]

In order to avoid instant decay of the oxygenated intermediate, tren was subsequently modified creating a fully methylated version of the compound, Me₆tren (tris-(2-dimethylaminoethyl)amine) and also an aromatic version, Bz₃tren (tris-(N-benzyl-N-methylaminoethyl)amine), with three benzyl moieties each one attached to the terminal nitrogen atoms of tren.^[62–64] Both ligands as well as their parent ligand tren are shown in Figure 1.12.

Me₆tren readily displayed the formation of copper end-on superoxido as well as the respective peroxido intermediate upon oxygenation which could be observed

spectroscopically.^[62] Still, crystallization of any of those two oxygenated species proved to be impossible. In 2004 however, Suzuki et al. managed to provide a crystal structure of the end-on peroxido intermediate formed by the copper(I) complex upon oxygenation using Bz₃tren. Again, a superoxido species forming prior to the respective peroxido species could be detected spectroscopically, but further characterization was not possible due to the short-lived nature of the compound.^[63]

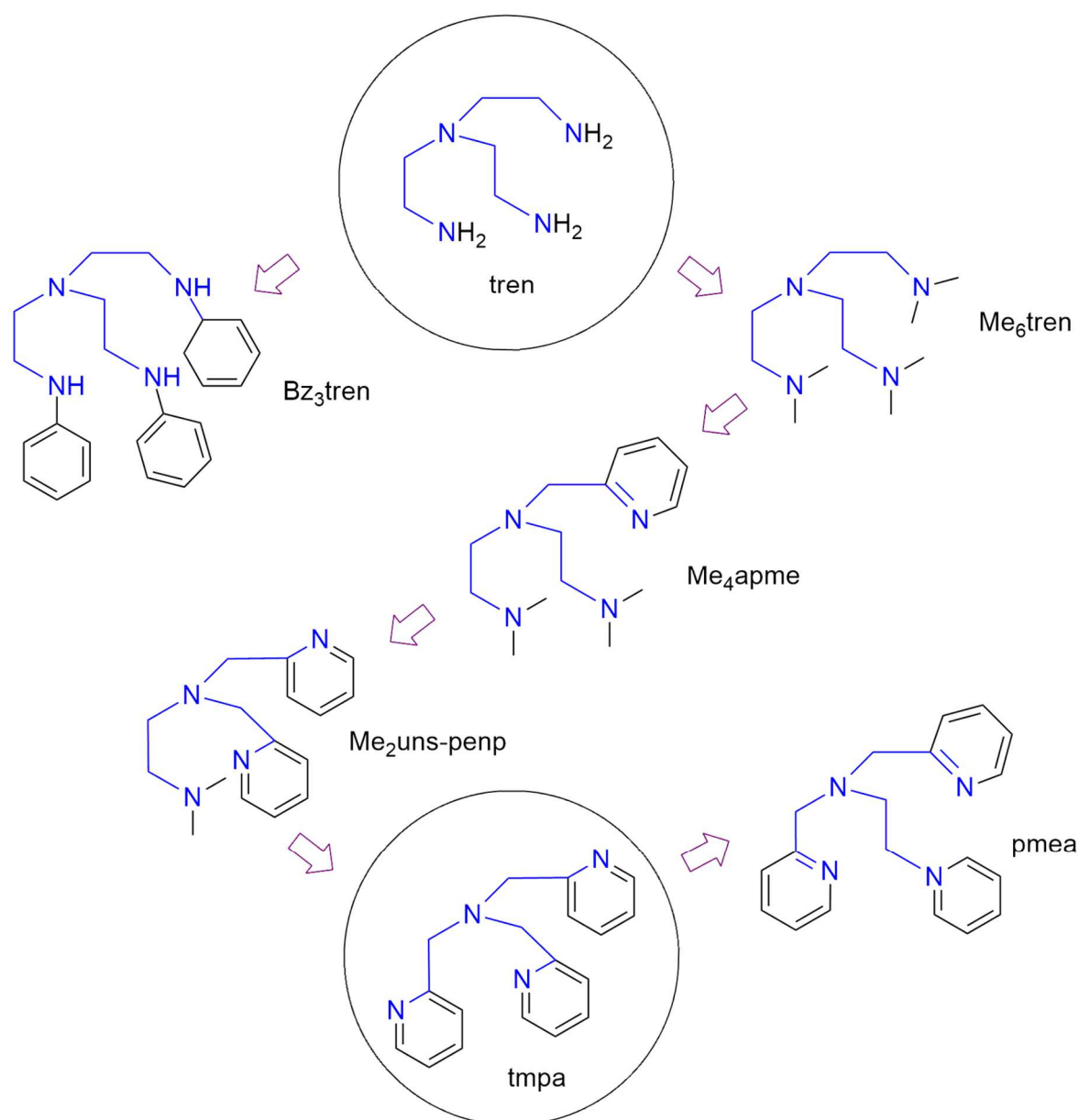


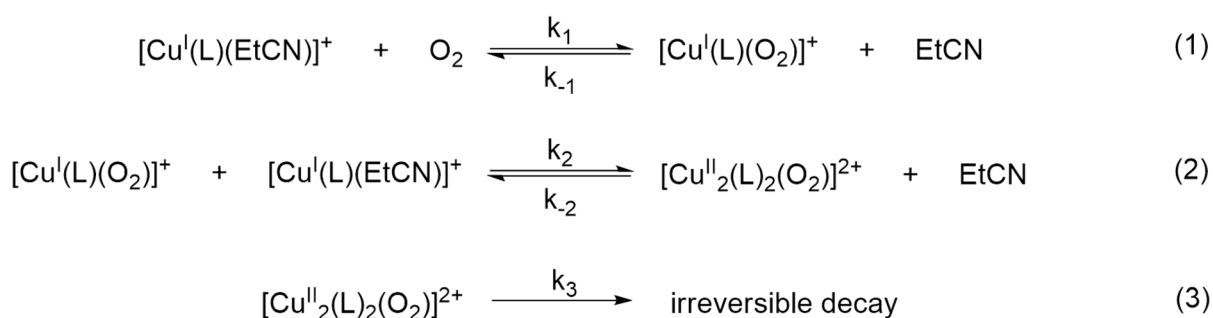
Figure 1.12: An array of tripodal, tetradentate ligands based on the tren unit used in copper and iron bioinorganic chemistry. The tren skeleton is highlighted in blue.

Based on that success, a wide range of other ligands containing the tren skeleton has been developed and investigated in copper and iron bioinorganic chemistry up to today.^[29,38,71–75,54,63,65–70] In Figure 1.12, a variety of ligands based on the tren unit is displayed. As can be seen, the tren unit can be easily modified by shortening individual arms and replacing aliphatic moieties successively by aromatic ones resulting in the ligands Me₄apme (bis-(2-dimethyl-aminoethyl)(2-methylpyridyl)amine) and Me₂uns-penp (2-dimethyl-(aminoethyl)-bis-(2-methylpyridyl)amine). Interestingly, by modifying all of the arms in that way, one arrives at the aromatic tmpa ligand which was already presented in detail in chapter 1.4.

Systematic kinetic investigations of the four ligands tmpa, Me₂unspenp, Me₄apme and Me₆tren in the past were conducted by Schindler et al. and showed that each of the copper(I) complexes with the respective ligand readily forms end-on superoxido as well as subsequent end-on peroxido complexes upon oxygenation at low temperatures.

These measurements allowed to postulate a reaction pathway of the copper(I) complexes of those ligands with dioxygen (using propionitrile as a coordinating solvent) which backs previous research in that field.^[49,64,76] The reaction pathway is shown in

Scheme 1.6.



Scheme 1.6: Reaction of $[\text{Cu}^{\text{I}}(\text{L})(\text{EtCN})]^+$ with O_2 in propionitrile (L = tmpa, Me₂uns-penp, Me₄apme, Me₆tren).^[77]

In a first step, the respective copper(I) complex in propionitrile reacts reversibly with dioxygen to form an instable 1:1 copper-dioxygen superoxido adduct (1). In a second step this 1:1 end-on copper superoxido adduct complex reacts with another copper(I) complex

resulting in a 2:1 dinuclear copper end-on peroxido complex (2). This adduct however, is not stable either and subject to irreversible decay.

As the formation and decay of oxygen intermediate complexes of copper and iron are notoriously fast (reactions are carried out at approx. - 90°C, and even then, intermediates are only detectable for a couple of seconds or minutes most of the time) low temperature UV-vis spectra using stopped flow techniques are generally recorded for characterizing the obtained species. Characteristic UV-vis data for the oxygen adduct complexes of copper mentioned in this chapter are presented in Table 1.5. Unfortunately, a similar overview for oxygen adduct complexes of iron with the same ligands is not available at this point. In non-heme iron chemistry only the iron(III) complexes with tmpa and its derivatives as well as uns-penp (aminoethyl)-bis-(2-methylpyridyl)amine) and its amide derivative acetyl-uns-penp (*N*-acetyl-*N*',*N*'-bis[(2-pyridyl)methyl]ethylenediamine) have been kinetically investigated in the past.^[29,74,75]

Table 1.5: UV-vis spectroscopic data for superoxido and peroxido complexes of tripodal tetradentate ligands discussed in this chapter.^[77,78]

Ligand (L)	[Cu(L)(O ₂)] ⁺	[Cu ₂ (L) ₂ (O ₂)] ²⁺
	λ_{max} [nm]	λ_{max} [nm]
tmpa	415	525
Me ₂ uns-penp	410	525
Me ₄ apme	414	537
Me ₆ tren	412	552
TMG ₃ tren	442	-
Bz ₃ tren	406	506

Data show that the superoxido species displays an absorbance maximum between 406 nm and 442 nm and the respective peroxido species between 506 nm and 537 nm. Therefore, when synthesizing those oxygen intermediates in bench top experiments, the color of the solution first looks sap green (indicating the end-on superoxido complex) and then purplish blue (indicating the end-on peroxido complex) to the human eye.

It was also found that the stability of the obtained end-on superoxido complexes is increased by a higher amount of hard, aliphatic N-donor atoms in the ligand used. Therefore, $[\text{Cu}(\text{Me}_6\text{tren})\text{O}_2]^+$ is the most stable superoxido complex among the four and $[\text{Cu}(\text{tmpa})\text{O}_2]^+$ the most unstable under the applied conditions. Examining the respective end-on peroxido complexes, it was found however that the stability of the complexes in propionitrile followed a rather non-systematic order: $[\text{Cu}_2(\text{Me}_2\text{uns-penp})_2\text{O}_2]^{2+}$, $[\text{Cu}_2(\text{Me}_4\text{apme})_2\text{O}_2]^{2+}$, $[\text{Cu}_2(\text{tmpa})_2\text{O}_2]^{2+}$, $[\text{Cu}_2(\text{Me}_6\text{tren})_2\text{O}_2]^{2+}$, the $\text{Me}_2\text{uns-penp}$ variety displaying the most stable and the Me_6tren variety displaying the most unstable peroxido complex of the four compounds.^[65,77]

Moreover, cyclic voltammetry of the four systems showed that soft, aromatic N-donor atoms support the copper(I) state of their respective complexes, facilitate the reduction of copper(II) complexes and also make an oxidation of copper(I) complexes more difficult. The found redox potential is more positive the more aromatic moieties exist in the ligand.^[77]

As the findings presented above have proven to be of great value for further development of dioxygen transferring model complexes, it is only logic to also develop other derivatives of the parent ligand tren and to investigate the reactivity of their copper complexes with dioxygen. Isoprop₃tren (tris[2-(isopropylamino)ethyl]amine), for example (cf. Figure 1.13), is another variety of the ligand tren which was previously used in copper chemistry to reduce a copper(II) to a copper(I) complex by nitric oxide. During this process the ligand itself undergoes trinitrosation resulting in the corresponding N-nitroso amine.^[71] Based on that research, one can assume that the copper(I) complex of Isoprop₃tren reacts similarly with dioxygen. However, details of the synthesis of the ligand neither was provided in the article cited nor could it be found anywhere else.

Taking Isoprop₃tren as a starting point for further investigations of tren-based ligands, a methylated variety of tren, Me₃tren (Tris-[2-(methylamino)ethyl]amine) as well as the methylated derivative of Isoprop₃tren, Me₃isoprop₃tren (Tris[2-(isopropylmethylamino)ethyl]amine) are expected to support the formation of end-on copper oxygen intermediate species like the ones previously found for other copper complexes of the tren family.

The copper(II) complexes of Me₃tren have already been characterized in the past and revealed a trigonal bipyramidal geometry in solid state^[79,80] which enforces the assumption that the respective copper(I) complex readily reacts with dioxygen. The copper(II) complex was investigated in the past when trying to find a more benign and effective alternative to cyanide in the process of oxidizing gold.^[80]

As TMG₃tren has already been successfully used to stabilize an end-on copper superoxido complex (cf. ch. 1.4), a smaller version of this ligand, tren's Schiff base Imine₃tren (Tris-[2-(propan-2-ylideneamino)ethyl]amine), is expected to potentially provide the required electronic (strong N-donor character) and steric properties (big bulk to prevent the superoxido species from dimerization) to stabilize such an intermediate upon oxidation and is therefore clearly worth investigating.

Even though a lot of effort has gone into researching model non-heme diiron complexes in the past, only comparatively few examples of oxygen adduct compounds could be generated so far. For example, it was possible to obtain peroxido-bridged diiron complexes as well as one example of a mononuclear iron peroxido complex, but mononuclear end-on superoxido species still remain elusive in non-heme iron chemistry.^[29,32,45,55,81,82]

1.6 Research Goals

As previously shown, copper and iron complexes are very interesting as model compounds for dioxygen activation. Characterization of these oxygen intermediates is very important for a detailed understanding of those reactions. Model compounds of copper proteins have been widely and successfully investigated for several decades. As a result, most copper oxygen adducts are well-known by now and have already been structurally characterized.^[20,37,51,64,83]

However, it is still of great interest to take a closer look at the electronic and steric influences that ligands have when forming oxygen adduct complexes. Therefore, the formation of oxygenated copper and non-heme iron adduct complexes is still of great interest to researchers (cf. ch. 1.1 to ch. 1.4). Notably, in non-heme iron chemistry only very few oxygen adduct species could be structurally characterized so far. Up to now, only bridged peroxides, iron(IV) oxido species and one mononuclear non-heme iron(III)-peroxido complex could be successfully isolated.^[29,45,55] Therefore, it is still of great interest to characterize more and different iron oxygen adduct complexes.

Having observed relatively stable oxygen intermediates with copper and iron complexes using tripodal ligands in the past, a modification of those ligands previously used promises a better insight into the formation and reactivity of metal oxygen adduct complexes: the formation of the superoxido species (a 1:1 adduct intermediate) in the first step and the consecutive peroxido or hydroperoxido species (a 2:1 adduct intermediate) in the second step before oxidation of the respective metal center.

Initially, the focus of this thesis was on copper complexes and their oxygen adduct complexes. However, as research progressed it was clear that the synthesis of one of the ligands could only be realized through a template reaction (cf. ch. 2 and ch. 3.) Hence, iron salts were introduced into the process and consequently the door to the field of iron complexes and their oxygen adduct intermediates opened up.

1.6.1 Project One: Ligand Synthesis

As already mentioned above, the ligands Me₆tren and TMG₃tren readily react with dioxygen and their oxygen adduct complex could be successfully characterized in the past, providing a valuable insight into the variety of oxygen intermediates (cf. ch. 1.3).^[29,45,51,64] They stem from the parent ligand tren, which has also already been described thoroughly elsewhere.^[59–61,84]

Keeping in mind that electronic as well as steric properties of the ligand steers the binding mode to the respective metal center, the ligands Me₃tren, Isoprop₃tren, Me₃isoprop₃tren and Imine₃tren, a Schiff-Base, were supposed to be synthesized and characterized. These ligands are direct derivatives of Me₆tren and TMG₃tren and were supposed to be investigated in

comparison to those compounds. An overview of the ligands in question can be found in Figure 1.13.

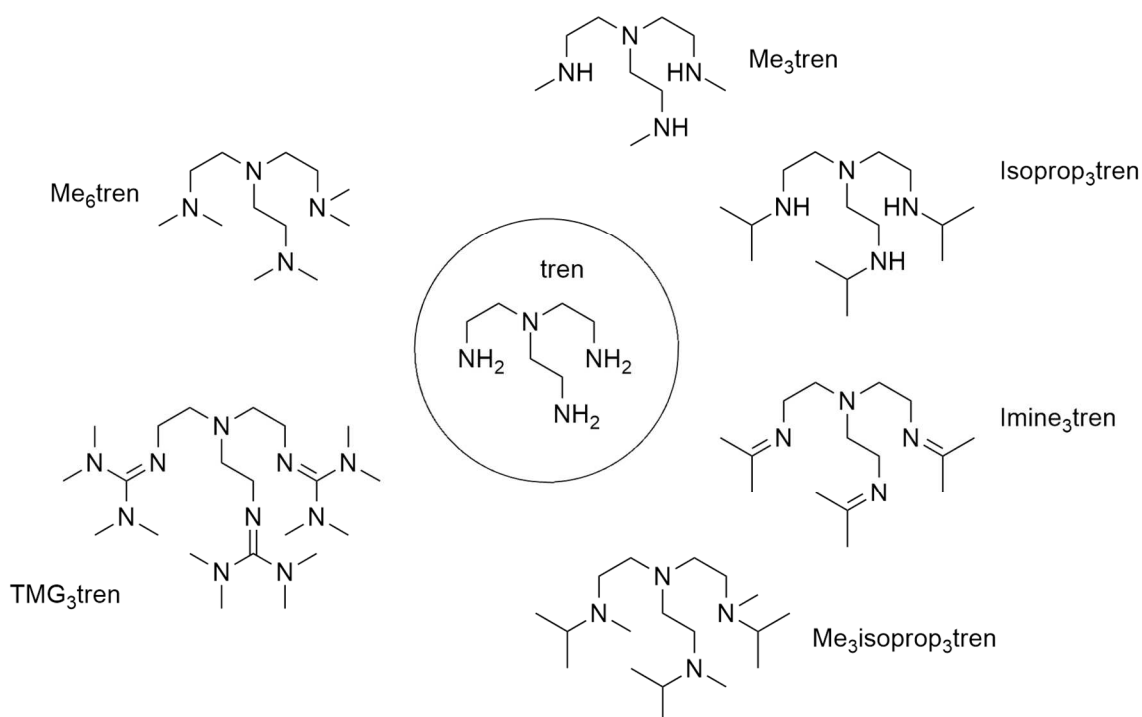


Figure 1.13: Aliphatic derivatives of the parent ligand tren. Left, already successfully investigated ligand systems elsewhere.^[51,64,85] Right, the four target ligands in this thesis, Imine₃tren being a smaller derivative of the bulky and super-basic ligand TMG₃tren and the rest being directly comparable to Me₆tren.

1.6.2 Project Two: Formation of Copper(I) and (II) Complexes and Formation of an Iron(Imine₃tren) Complex

In order to fully characterize the precursor as well as the resulting complexes after oxygenation, a wide range of research data of both, copper(I) and copper(II) complexes was supposed to be collected. As the coordination sphere of copper complexes varies greatly depending on the oxidation state and the ligands used (cf. ch. 1.1.3 and 1.3), resulting data was to be compared to other copper complexes already known to form oxygen adduct complexes. As synthesis of the ligand Imine₃tren was not possible using direct methods, a template reaction forcing the formation of the according complex by introducing an iron(II) ion was to be conducted.

1.6.3 Project Three: Formation of Copper Dioxygen Complexes and Formation of an Iron(Imine₃tren) Oxygen Adduct Complex

Consequently, oxygen adduct complexes of all copper(I) precursor complexes were to be formed, isolated and structurally characterized as detailed as possible and, attempts to crystallize oxygen adduct complexes was to be made. Also, the iron(II) complex of Imine₃tren was to be reacted with dioxygen to investigate whether a reaction would take place and potentially forming oxygen intermediates were supposed to be characterized like the according copper complexes.

2 Copper Complexes – Experiments and Results

The results described in this chapter were published in *Polyhedron* in October 2019.^[86] The Schiff-base ligand Imine₃tren, however, was impossible to obtain via a simple condensation reaction. Therefore, a template reaction had to be used in order to obtain the desired ligand. The results revolving around that ligand can be found in chapter 3 of this thesis.

2.1 Synthesis, crystal structures and reactivity towards dioxygen of copper(I) complexes with tripodal aliphatic amine ligands

Janine Will, Christian Würtele, Jonathan Becker, Olaf Walter and Siegfried Schindler

2.1.1 Abstract

Copper(I) complexes of the tripodal, tetradentate, aliphatic ligands Me₃tren (tris-(2-methylaminoethyl)amine), Isoprop₃tren (tris-(2-isopropylaminoethyl)amine) and Me₃isoprop₃tren (tris-(2-isopropylmethylaminoethyl)amine) of the Tren-family (tris(2-aminoethyl)amine) were prepared and structurally characterized. Furthermore, they were reacted in solution at low temperatures with dioxygen. All complexes formed a short-lived superoxido intermediate complex that could be observed using low temperature stopped-flow techniques prior to consecutive reactions. However, the superoxido complexes were too reactive to allow isolation and full characterization in contrast to previous work.

2.1.2 Introduction

Metalloenzymes which incorporate copper in their active site for redox-processing of molecular dioxygen, e. g. the type 3 copper protein tyrosinase (a monooxygenase responsible for hydroxylation of the amino acid tyrosine), are of great interest in bioinorganic chemistry.^[17,46,87–91] Successfully modeling these reactions would allow to use low molecular weight copper complexes as catalysts for selective oxidations of organic substrates using dioxygen/air as an oxidant.^[92,93] Especially oxidations of hydrocarbons (for example, benzene

or cyclohexane) under mild conditions are of high interest; the holy grail of these reactions being the selective oxidation of methane to methanol.^[94] Tripodal ligands have proven to be suitable for reversible uptake of dioxygen^[20,37,50,65,83,95,96] and had allowed with tris(2-pyridylmethyl)amine (tpma) to isolate and structurally characterize the first dinuclear copper peroxido complex with a $\mu\text{-}\eta^2\text{:}\eta^2$ coordination of the peroxido-ligand.^[38,76,97] Similar reactivities have been observed for tren (tris(2-aminoethyl)amine, Figure 2.1) based ligands.^[37,63,65,66,78]

Using Me₆tren (tris-(2-dimethylaminoethyl)amine, Figure 2.1) it was not only possible to structurally characterize the dinuclear peroxido copper complex, but to obtain a resonance Raman spectrum of the corresponding mononuclear end-on superoxido complex for the first time (characteristic peak at 1122 cm⁻¹ for the vibration frequency of ¹⁶O-¹⁶O).^[66,98] Due to the fast, consecutive reaction forming the dinuclear peroxido complex, it was impossible to isolate this reactive intermediate.^[64]

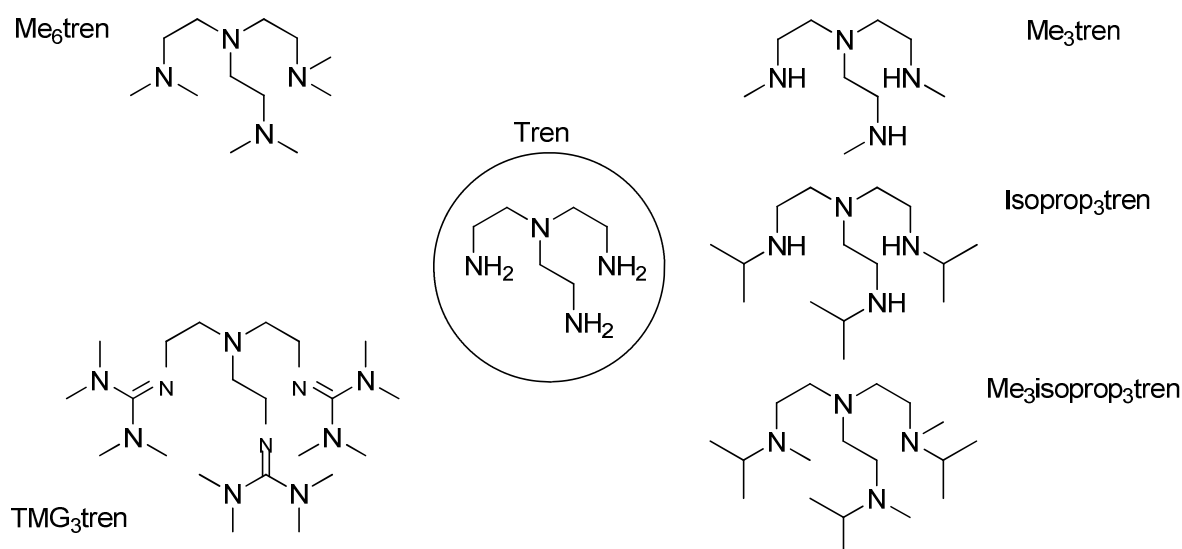


Figure 2.1: List of ligands.

However, using the guanidine derivative of tren, TMG₃tren (tris(tetramethylguanidino)tren, Figure 2.1) finally allowed (due to its electronic and steric features of this ligand) to isolate and structurally characterize the first example of such a species.^[51,99,100] The end-on superoxido binding mode had been observed previously in the active site of the copper enzyme

peptidylglycine- α -hydroxylating monooxygenase PHM.^[101] TMG₃tren belongs to the group of super bases and thus is problematic with regard to the presence of protons.^[85] Due to the importance of end-on superoxido copper complexes in general^[102–104] we used less basic aliphatic tren-based amine ligands (Me₃tren, Isoprop₃tren and Me₃isoprop₃tren (Scheme 2.1.2) with the final goal to obtain the corresponding copper superoxido complexes with a higher stability compared to the TMG₃tren-based system.

2.1.3 Experimental Section

2.1.3.1 Materials and Physical Measurements

Reagents and solvents used were of commercially available reagent quality unless stated otherwise. Solvents used for air-sensitive compounds and reactions were redistilled under argon atmosphere. All preparation, handling and storing of copper complexes was carried out under inert conditions in an argon glovebox (MBraun, Garching, Germany; water and dioxygen less than 1 ppm). Copper(I) compounds [Cu(MeCN)₄]X (X = BF₄⁻, SO₃CF₃⁻, PF₆⁻, SbF₆⁻, ClO₄⁻) were prepared according to previously published methods.^[105] The ligand tris[2-(methylamino)-ethyl]amine (Me₃tren) was obtained commercially (Acros). Acetone d₆ was purchased from Deutero GmbH (Germany), and removing oxygen from solvents was carried out by a three freeze/pump/thaw cycle. ¹H - and ¹³C - NMR spectra were recorded on a Bruker Aspect 2000/3000 400 MHz spectrometer at 298 K in 5 mm NMR tubes. The chemical shifts (δ) were obtained in deuterated solvents using TMS as an internal reference. IR measurements were performed using a JASCO FT/IR-4100 spectrometer. UV-vis spectra were measured on an Agilent 8453 spectrometer equipped with a diode array system. Cyclic voltammetry was performed using an EG&G Model 263 potentiostat at 25° C at a scan rate of 100 mV/s. The solutions under investigation contained 1 mmol/L copper complex and 0.1 mol/L [NBu₄]PF₆ in acetonitrile that had been deoxygenated by bubbling nitrogen through it. A conventional H-type cell was used, with glassy carbon, Pt, and Ag/AgCl as working, counter, and reference electrodes, respectively. Ferrocene was used as an internal standard.

2.1.3.2 X-ray Crystallography

X-ray crystallographic data were either collected on a STOE IPDS-diffractometer equipped with a low-temperature unit (Karlsruher Glastechnisches Werk), Mo-K α radiation ($\lambda = 0.71069 \text{ \AA}$) and a graphite monochromator, or a Siemens SMART 5000 CCD diffractometer. Single crystals for measurements at $-80 \text{ }^\circ\text{C}$ were mounted on the tip of a glass rod in inert oil. Cell parameters were refined using up to 5000 reflections collected with the ϕ -oscillation mode if not mentioned otherwise. The structures were solved by direct methods in SHELXS97 and refined by using full-matrix least squares in SHELXL97.^[106] All hydrogen atoms were positioned geometrically and all non-hydrogen atoms were refined anisotropically.

2.1.3.3 Stopped-Flow Instruments, Software and Handling

Rapid kinetic studies were performed using a SF-21 variable temperature stopped-flow unit (Hi-Tech Scientific (now TgK Scientific Limited, Bradford, UK), 10 or 2 mm path length cell) combined with a TIDAS/NMC301-MMS/16 VIS/500-1 diode array spectrometer (J&M, Aalen, Germany, 256 diodes 300-1100 nm, 0.8 ms minimum sampling time).^[65] Data acquisition was performed using the Kinspec program (J&M). For numerical analysis, all data were pretreated by factor analysis using the Specfit program (SPECFIT/32 is a trademark of Spectrum Software Associates, copyright 2000-2002 Spectrum Software Associates ; R. Binstead and A. D. Zuberbühler; commercially not available anymore).^[107] Maximum time-bases of the data collection was up to 2250 s for $[\text{Cu}(\text{Isoprop}_3\text{tren})]^+$, and up to 225 s for $[\text{Cu}(\text{Me}_3\text{isoprop}_3\text{tren})]^+$ and for $[\text{Cu}(\text{Me}_3\text{tren})]^+$. In a glove box, copper(I) complex solutions were transferred into a glass syringe modified for air-sensitive manipulations. Degassed and distilled solvent was transferred into a second syringe and flushed for ten minutes with dry dioxygen (grade 4.8, Messer Griesheim, Germany).

2.1.3.4 Synthesis and Characterization of Ligands

Tris[2-(isopropylamino)-ethyl]amine (Isoprop₃tren). 6 g (41.0 mmol) tris(2-aminoethyl)amine (tren), 50 mL (680.0 mmol) acetone, 90 mL water, 13 g sodium acetate and 42 mL acetic acid were mixed and cooled to $0 \text{ }^\circ\text{C}$. 25 g sodium borohydride were (660.0 mmol)

added over a time span of four hours. The mixture was then warmed to room temperature and further stirred overnight. The following day, sodium hydroxide was added until a pH of 12 was reached and two layers formed. The aqueous layer was washed five times with 100 mL of diethyl ether. The organic layers were combined and dried over magnesium sulfate. Finally, the excess amount of solvent was removed by a rotary evaporator leading to a light-yellow oil. Yield: 8.1 g (29.7 mmol, 72.4%). ^1H NMR (CDCl_3 , 400 MHz): δ 1.3 (s, 3 H, -CH), δ 2.4 (s, 12 H, -CH₂), δ 2.6 (m, 18 H, -CH₃). IR bands $\tilde{\nu}$ (cm^{-1}): 3284 s (br), 2962 s, 2822 s, 1656 m, 1580 m, 1469 s, 1380 s, 1365 s, 1338 s, 1321 m, 1245 w, 1177 s, 1123 m, 1091 m, 1053 m, 955 w, 931 w, 852 w, 738 m, 485 w.

Tris[2-(methylisopropylamino)-ethyl]amine ($\text{Me}_3\text{isoprop}_3\text{tren}$). 4 g (15.0 mmol) of $\text{Isoprop}_3\text{tren}$ were mixed with 50 mL 1,2-dichloroethane and 3.59 g (41.0 mmol) 37% formaldehyde and stirred for 15 min. Then, 8.71 g (41.0 mmol) $\text{NaBH}(\text{OAc})_3$ were added portion-wise over a time span of one hour. The mixture was then stirred overnight. 200 mL of 2 mol/L NaOH were added the next day, the organic layer separated from the aqueous layer and the latter extracted five times with 50 mL of dichloromethane. The organic fractions were combined and dried over MgSO_4 before the solvent was removed yielding a yellow colored oil. Yield: 3.43 g (10.8 mmol, 72 %). ^1H NMR (CDCl_3 , 400 MHz): δ 1.0 (d, 18 H), δ 2.2 (s, 9 H), δ 2.5 (m, 12 H), δ 2.8 (m, 3 H). ^{13}C (CDCl_3 , 100 MHz): δ 17.8, 37.7, 51, 54. IR bands $\tilde{\nu}$ (cm^{-1}): 2963 s, 2871 m, 2838 m, 2795 m, 1744 w, 1680 w, 1462 m, 1420 w, 1379 m, 1359 m, 1320 w, 1260 w, 1227 m, 1159 m, 1119 m, 1086 m, 981 m, 923 w, 876 w, 804 w, 755 w, 554 w, 494 w.

2.1.3.5 Synthesis of Copper(I) Complexes.

$[\text{Cu}(\text{Me}_3\text{tren})]\text{ClO}_4$ (**1ClO₄**). 0.1 g ($5.31 \cdot 10^{-4}$ mol) of Me_3tren were dissolved in 2 mL acetonitrile and a solution of 0.156 g ($4.78 \cdot 10^{-4}$ mol) of $[\text{Cu}(\text{MeCN})_4]\text{ClO}_4$ in 2 mL acetonitrile was added dropwise. The resulting mixture was stirred for 30 minutes at room temperature. The complex **1 ClO₄** was precipitated as a yellowish colored solid by adding the complex solution to 15 mL of Et_2O , yielding 0.146 g ($4.16 \cdot 10^{-4}$ mol, 86.9 %) based on formula of **1 ClO₄**. ^1H NMR (CDCl_3 , 400 MHz): δ 1.2(s, 12 H), δ 2.1(s, 6 H), δ 2.6(s, 6 H). Single crystals were obtained by slow vapour diffusion of Et_2O into a solution of the complex in acetonitrile.

Caution! Although we have not encountered any problems, perchlorate salts are potentially explosive and should always be handled with great care.

[Cu(Me₃tren)]BPh₄ (1 BPh₄**).** 0.1 g ($5.31 \cdot 10^{-4}$ mol) of Me₃tren was dissolved in 2 mL methanol. Into this solution, a solution of 0.15 g ($4.78 \cdot 10^{-4}$ mol) [Cu(MeCN)₄]BF₄ in 2 mL methanol was added dropwise and stirred for 30 minutes at room temperature. The resulting yellowish colored complex solution was then added to a solution of 0.163 g ($4.78 \cdot 10^{-4}$ mol) NaBPh₄ in 4 mL methanol. It was allowed to stand for 4 hours at -30 °C in order to precipitate the complex [Cu(Me₃tren)]BPh₄. The pinkish solid was filtered, washed with cold methanol and dried in vacuum for 1 hour yielding 0.248 g (90.8 %) of the product (based on formula of **1 BPh₄**). Selected IR bands $\tilde{\nu}$ (KBr, cm⁻¹): 3295 w, 3279 s, 3270 s, 3049 m, 2980 m, 2900 m, 2858 m, 2804 w, 1579 m, 1470 s, 1425 m, 1380 w, 1347 w, 1293 m, 1080 m, 1030 m, 954 m, 939 m, 806 m, 604 m, 484 m, 462 w.

[Cu(Isoprop₃tren)]SO₃CF₃ (2 SO₃CF₃**).** 0.1 g ($3.67 \cdot 10^{-4}$ mol) Isoprop₃tren were dissolved in 2 mL acetonitrile. To this solution, a solution of 0.124 g ($3.3 \cdot 10^{-4}$ mol) [Cu(MeCN)₄]SO₃CF₃ in 2 mL acetonitrile was added dropwise. The obtained complex **2 SO₃CF₃** was stirred for 30 minutes at room temperature and precipitated upon adding to 15 mL of Et₂O. Yield: 0.172 g ($3.01 \cdot 10^{-4}$ mol, 91.2 %) based on formula **2 SO₃CF₃**. ¹H NMR (CDCl₃, 400 MHz): δ 1.2(s, 27 H), δ 2.1(s, 6 H), δ 2.6(s, 6 H), Single crystals were obtained by slow vapour diffusion of Et₂O into a solution of the complex in acetonitrile.

Synthesis of [Cu(isoprop₃tren)]BPh₄ (2 BPh₄**).** 0.1 g ($3.67 \cdot 10^{-4}$ mol) of Isoprop₃tren were dissolved in 2 mL methanol to which a solution of 0.104 g ($3.3 \cdot 10^{-4}$ mol) of [Cu(MeCN)₄]BF₄ in 4 mL methanol was added slowly. The resulting yellowish complex solution was stirred for 30 minutes at room temperature and then added to a solution of 0.113 g ($3.3 \cdot 10^{-4}$ mol) NaBPh₄ in methanol. The complex precipitated as a yellowish solid after allowing the mixture to stand at -30°C for 4 hours yielding 0.192 g (88.9 %) based on formula **2 BPh₄**. Selected IR bands $\tilde{\nu}$ (KBr, cm⁻¹): 3355 w (br), 3055 w, 2970 w, 1580 w, 1481 m, 1428 m, 1366 m, 1082 s (br), 1031 s (br), 870 w, 839 w, 799 w, 750 w, 732 m, 707 m, 610 m, 551 m, 527 m, 518 m, 467 w, 411 w.

*Synthesis of [Cu(Me₃isoprop₃tren)]BPh₄ (**3 BPh₄**).* 0.1 g ($3.15 \cdot 10^{-4}$ mol) of Me₃isoprop₃tren were dissolved in 2 mL methanol to which a solution of 0.089 g ($2.83 \cdot 10^{-4}$ mol) of [Cu(MeCN)₄]BF₄ in 4 mL methanol was added slowly. The resulting yellowish complex solution was stirred for 30 minutes at room temperature and then added to a solution of 0.113 g ($2.83 \cdot 10^{-4}$ mol) NaBPh₄ in methanol. The complex precipitated as a yellowish solid after allowing the mixture to stand at – 30 °C for 4 hours. Yield: 0.17 g (85.9 %) based on formula **3 BPh₄**. Crystals suitable for X-ray measurements were obtained by ether diffusion into an acetone solution of the complex [Cu(Me₃isoprop₃tren)]BPh₄. ¹H NMR (Acetone d₆, 400 MHz): δ 1.2(d, 18 H), δ 2.3(s, 9 H), δ 2.7(t, 6 H), δ 2.8(t, 6 H), δ 3.1(m, 3 H), δ 6.7(t, 4 H), δ 6.9(t, 8 H), δ 7.3(d, 8 H). Selected IR bands $\tilde{\nu}$ (KBr, cm⁻¹): 3056 m, 2969 m, 2918 m, 2878 m, 2847 m, 1580 m, 1468 m, 1424 m, 1380 m, 1366 m, 1293 m, 1193 w, 1119 m, 1055 m, 1037 m, 971 m, 921 m, 902 m, 849 m, 746 s, 738 s, 730 s, 704 s, 611 m, 539 w, 418 w.

2.1.3.6 Synthesis of Copper(II) Complexes

*[Cu(Me₃tren)Cl]BPh₄ (**4 BPh₄**).* 0.05 g ($2.66 \cdot 10^{-4}$ mol) Me₃tren were dissolved in 2 mL methanol and added to an equimolar amount of CuCl₂ • 2 H₂O (0.045 g) in 2 mL methanol. The mixture was stirred for 30 minutes at room temperature and then added dropwise to a solution of $2.66 \cdot 10^{-4}$ mol NaBPh₄ in 2 mL methanol. 0.133 g (82.6 %) of the complex precipitated as a turquoise solid after having allowed the mixture to stand overnight at -30 °C. Selected IR bands $\tilde{\nu}$ (KBr, cm⁻¹): 3440 m (br), 3243 m, 2052 m, 1955 w, 1820 w, 1648 w (br), 1577 m, 1476 s, 1426 s, 1280 m, 1061 m, 955 m, 824 m, 749 s, 734 s, 706 s, 622 w, 610 s, 555w, 469 w.

*[Cu(Isoprop₃tren)Cl]Cl (**5 Cl₂**).* 0.05 g ($1.84 \cdot 10^{-4}$ mol) Isoprop₃tren were dissolved in 2 mL methanol. To this solution an equimolar amount (0.0314 g) of CuCl₂ • 2 H₂O in 2 mL methanol was added. Single crystals were obtained by slow vapour diffusion of Et₂O into a solution of (**5a**) in acetonitrile at -30°C.

*[Cu(Isoprop₃tren)Cl]BPh₄ (**5 BPh₄**).* 0.05 g ($1.84 \cdot 10^{-4}$ mol) Isoprop₃tren were dissolved in 2 mL methanol. To this solution, a mixture of 0.0314 g CuCl₂ • 2 H₂O in 2 mL methanol were added. The mixture was stirred for 30 minutes at room temperature. It was then added to a

solution of NaBPh₄ ($1.84 \cdot 10^{-4}$ mol) in 2 mL methanol. The resulting complex precipitated as a dark-green solid after storing it for 4 hours at -30 °C. Yield: 0.096 g (75.6 %) Selected IR bands $\tilde{\nu}$ (KBr, cm⁻¹): 3578 s, 3495 s (br), 3252 s, 3233 s, 3051 s, 2979 s, 2874 m, 1958 w, 1618 m, 1578 m, 1477 s, 1423 m, 1384 m, 1369 s, 1267 m, 912 w, 884 w, 864 w, 842 w, 788 w, 750 m, 736 s, 706 s, 611 m, 509 w, 470 w.

Synthesis of [Cu(Me₃isoprop₃tren)Cl]BPh₄ (6). 0.05 g ($1.58 \cdot 10^{-4}$ mol) Me₃isoprop₃tren were dissolved in 2 mL methanol. This solution was added to another solution containing 0.027 g ($1.58 \cdot 10^{-4}$ mol) CuCl₂ • 2 H₂O in 2 mL methanol. The complex was precipitated as a black solid upon adding the mixture to a solution of 0.054 g ($1.58 \cdot 10^{-4}$ mol) NaBPh₄ in 2 mL methanol yielding 0.079 g (68.1 %) after having cooled the mixture to - 30 °C for 4 hours. Selected IR bands $\tilde{\nu}$ (KBr, cm⁻¹): 3438 m (br), 3053 m, 2969 s, 1579 m, 1466 m, 1424 m, 1286 w, 1264 w, 1063 m, 1033 m, 734 s, 706 s, 613 m, 470 w.

2.1.4 Results and Discussion

2.1.4.1 Synthesis and General Characterizations

While we had to synthesize Me₃tren in the past^[108] it is now commercially available. Preparation of the other two ligands was performed in good yields following standard procedures. The tetradentate ligand Isoprop₃tren was synthesized through a reductive amination of tren: reacting tren with acetone and a subsequent reductive amination of the imine intermediate by adding NaBH₄ was carried out at 0 °C under acidic conditions using an acetate buffer (Scheme 2.1). More recently, this amine became commercially available as well (Sigma Aldrich). Me₃isoprop₃tren was synthesized through an Eschweiler-Clarke reaction^[109,110] of the ligand Isoprop₃tren with formaldehyde and formic acid.

The monomeric copper(I) complexes $[\text{Cu}(\text{Me}_3\text{tren})]^+$ (**1**), $[\text{Cu}(\text{Isoprop}_3\text{tren})]^+$ (**2**) and $[\text{Cu}(\text{Me}_3\text{isoprop}_3\text{tren})]^+$ (**3**) were prepared by adding 1 equiv. of $[\text{Cu}(\text{MeCN})_4]\text{X}$ ($\text{X} = \text{BF}_4^-, \text{ClO}_4^-, \text{SO}_3\text{CF}_3^-$ or SbF_6^-) to the corresponding ligand in MeCN, EtCN or acetone under argon in a glove box. Solid copper(I) complexes were obtained by adding diethyl ether as a fine powder of light-yellow color. In contrast to related copper(I) complexes with pyridyl based ligands it is difficult or even impossible to obtain copper(I) complexes with aliphatic amines as solids or to prepare solutions in higher concentrations.^[64,98] Due to disproportionation and decomposition it was unfortunately impossible to fully characterize the bulk material. However, single crystals for crystallographic characterization were obtained by recrystallization and/or slow diffusion of ether into solutions of the complexes. Crystals were obtained for $[\text{Cu}(\text{Me}_3\text{tren})]\text{ClO}_4$ (**1 ClO₄**), $[\text{Cu}(\text{Isoprop}_3\text{tren})]\text{SO}_3\text{CF}_3$ (**2 SO₃CF₃**), $[\text{Cu}(\text{Me}_3\text{isoprop}_3\text{tren})]\text{BPh}_4$ (**3 BPh₄**) and molecular structures of the cations of these complexes are presented in Figure 2.2. Crystallographic data are reported in chapter 2.2.1.

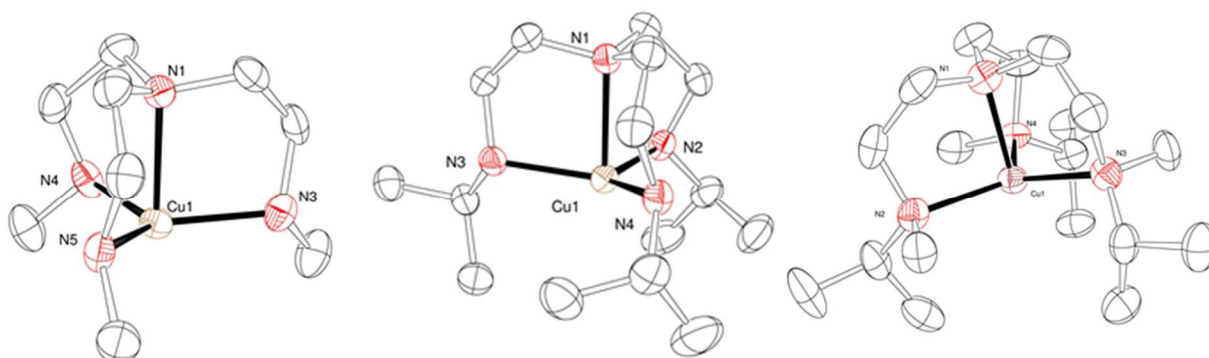


Figure 2.2: Molecular structures of the cations of (from left to right): $[\text{Cu}(\text{Me}_3\text{tren})]\text{ClO}_4$ (**1 ClO₄**), $[\text{Cu}(\text{Isoprop}_3\text{tren})]\text{SO}_3\text{CF}_3$ (**2 SO₃CF₃**) and $[\text{Cu}(\text{Me}_3\text{isoprop}_3\text{tren})]\text{BPh}_4$ (**3 BPh₄**).

All three complexes reveal their trigonal pyramidal geometry in solid state, quite similar to the molecular structure of $[\text{Cu}(\text{Me}_6\text{tren})]^+$ reported previously.^[62] In each case, the bridgehead amine nitrogen occupies an axial position and the three pendant amines (either secondary in the case of Me_3tren and $\text{Isoprop}_3\text{tren}$ or tertiary in the case of $\text{Me}_3\text{isoprop}_3\text{tren}$) form the equatorial plane. Interestingly, even when MeCN was used as a solvent, in none of the complexes the remaining axial position was occupied by a solvent molecule in contrast to the copper(I) complexes of tmpa .^[111]

However, this has been observed previously for the copper(I) Me₆tren complex and with other derivatives of tmpa.^[50,66] The mean distance Cu1-N1 in **1** amounts to 2.205 Å which is very similar to the distance Cu1-N1 found in the complex [Cu(Me₆tren)]⁺ measuring 2.200 Å.^[62] However, the bond lengths of the surrounding nitrogen atoms to the copper center are slightly shorter in complex **1** with an average of 2.051 Å than the one measured for [Cu(Me₆tren)]⁺ with an average of 2.122 Å. As expected, bond angles of complex **1** are also very much comparable to those found in [Cu(Me₆tren)]⁺ previously. Comparing molecular structures of complexes **2** and **3** with each other reveals that the bond lengths between the copper(I) atom and the respective bridgehead nitrogen atom are slightly shorter in complex **3** (2.138 Å) than in **2** (2.208 Å). Therefore, the shape of complex **3** is slightly more compressed than the shape of complex **2** which is reflected in comparatively longer bond distances of the equatorial nitrogen atoms to the copper(I) center in complex **3**. The bond length for the complex [Cu(TMG₃tren)]⁺ of 2.190(3) Å of the bridgehead nitrogen atom to the copper(I) center^[85] thus is in between those found for complexes **2** and **3**. The bond lengths of the equatorial nitrogen atoms in [Cu(TMG₃tren)]⁺, however, are notably shorter (2.052(2) Å) than the correspondent bond distances in complexes **2** and **3**.

Copper(II) complexes herein were only prepared for completion, but not further investigated. However, molecular structures of copper(II) complexes with chloride as an additional ligand can provide some useful information in terms of a possible binding mode of dioxygen.^[62] Copper(II) complexes of the ligand Me₃tren have already been described elsewhere.^[80,108] Fischmann et al. reported the crystal structure of [Cu(Me₃tren)MeCN](ClO₄)₂ in which the fifth, axial position within the complex is occupied by an acetonitrile (solvent) molecule. Furthermore, Thaler et al. previously reported the molecular structure of a dimeric cyanide bridged species of the copper(II) Me₃tren complex. Monoclinic crystals of [Cu(Isoprop₃tren)Cl]Cl (**5 Cl₂**) were obtained in a bluish-green color and its molecular structure is presented in Figure 2. Crystallographic data are reported in chapter 2.2.1.

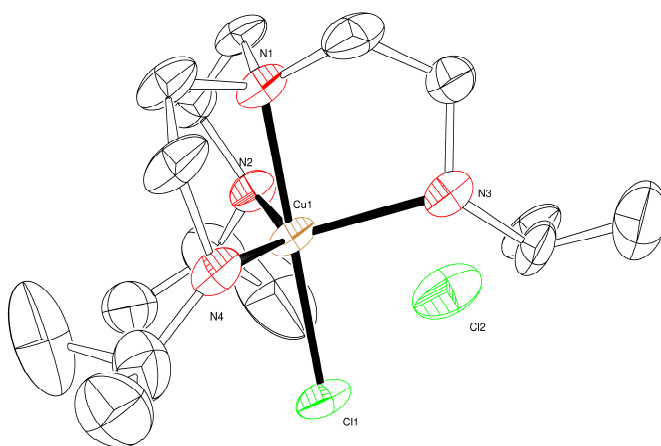


Figure 2.3: Molecular structure of $[\text{Cu}(\text{Isoprop}_3\text{tren})\text{Cl}]\text{Cl}$.

The τ parameter has become a useful tool describing the geometry of five-coordinate metal centers ($\tau = 1.00$ being perfectly trigonal bipyramidal and $\tau = 0.00$ being perfectly square pyramidal).^[112] The τ parameter for $[\text{Cu}(\text{Me}_3\text{tren})\text{MeCN}](\text{ClO}_4)_2$ is close to **1** and therefore represents a nearly ideal trigonal bipyramidal system.^[80]

In contrast, the τ parameter of **5** could be determined at $\tau = 0.63$ revealing a distorted geometry that can be described as being in between a square pyramidal and a trigonal bipyramidal shape of the complex compared to the τ parameter of $[\text{Cu}(\text{TMG}_3\text{tren})\text{Cl}]\text{Cl}$ ^[85] which was determined at $\tau = 0.96$ and therefore, being of almost perfect trigonal bipyramidal shape. The bond length of the copper(II) center to the axial nitrogen atom in the complex $[\text{Cu}(\text{TMG}_3\text{tren})\text{Cl}]\text{Cl}$ was found at $2.111(3)$ Å whereas it was determined slightly shorter in complex **5** at $2.039(3)$ Å. The equatorial nitrogen atoms in complex **5** surround the copper(II) center at a length between $2.120(4)$ Å to $2.197(4)$ Å, while the copper(II) center in the complex $[\text{Cu}(\text{TMG}_3\text{tren})\text{Cl}]\text{Cl}$ is surrounded by equatorial nitrogen atoms at a distance between $2.091(3)$ to $2.109(3)$ Å, again, binding more closely to the copper(II) center than the nitrogen atoms in complex **5**.

Furthermore, we could obtain crystals and solve the molecular structure for the corresponding perchlorate complex $[\text{Cu}(\text{Isoprop}_3\text{tren})\text{CH}_3\text{CN}](\text{ClO}_4)_2$ (also with a value of $\tau = 0.6$), but due to the fact that an identical crystal structure of this complex together with

the molecular structure of a perchlorate salt of the ligand has already been described previously it is not reported herein.^[71]

So far, it has been impossible to obtain single crystals suitable for X-ray crystallography of the of the complex $[\text{Cu}(\text{Me}_3\text{Isoprop}_3\text{tren})]^{2+}$ (**6**). However, it is expected that the molecular structure should be quite similar to other copper(II) complexes with related ligands.

For UV-vis measurements additional copper(II) complexes of the type $[\text{Cu}(\text{X})\text{Cl}]\text{Cl}$ ($\text{X} = \text{Me}_3\text{tren}$, $\text{Isoprop}_3\text{tren}$, $\text{Me}_3\text{isoprop}_3\text{tren}$) were prepared *in situ* by adding equimolar amounts of ligand X and $\text{CuCl}_2 \cdot 2 \text{H}_2\text{O}$ in MeCN to get an idea of final product solutions after the oxidation/decomposition of the respective copper(I) complexes (cf. ch. 2.3.6). UV-vis spectra showed for $[\text{Cu}(\text{Me}_3\text{tren})\text{Cl}]\text{Cl}$ (MeCN) λ_{max} , nm; (ϵ , $\text{M}^{-1} \text{cm}^{-1}$): 288 (7111), 710 (167); for $[\text{Cu}(\text{Isoprop}_3\text{tren})\text{Cl}]\text{Cl}$ (MeCN) λ_{max} , nm; (ϵ , $\text{M}^{-1} \text{cm}^{-1}$): 292 (6154), 466 (110); and for $[\text{Cu}(\text{Me}_3\text{isoprop}_3\text{tren})\text{Cl}]\text{Cl}$ (MeCN) λ_{max} , nm; (ϵ , $\text{M}^{-1} \text{cm}^{-1}$): 302 (6484), 322 (6264), 655 (275).

The UV-vis spectra provided information that the coordination geometry of the complexes in solid state is retained in solution. While $[\text{Cu}(\text{Me}_3\text{tren})\text{Cl}]\text{Cl}$ displays a more trigonal bipyramidal geometry, the other two complexes are much more distorted towards a square pyramidal geometry. In the past, this has been also supported by EPR measurements for related complexes.^[113,114]

Cyclic voltammetry demonstrated irreversible reduction of copper(II) complexes with the ligands $\text{Isoprop}_3\text{tren}$ and $\text{Me}_3\text{isoprop}_3\text{tren}$. Surprisingly, the copper(II) complex with the ligand Me_3tren could be reduced reversibly electrochemically with a potential of -0.2 V (-0.7 V vs. ferrocene) In general, redox potentials of these type of complexes can have a quite wide range.^[63]

2.1.4.2 Bench Top Experiments of the Reaction of Copper(I) Complexes with Dioxygen

Taking into consideration the results of our previous investigations on the copper(I) complexes of Me_6tren and TMG_3tren , it was expected that the three ligands described herein could be suitable for the stabilization of a copper superoxido complex. Investigations and

results by other research groups supported this assumption as well. For example, based on earlier work by us,^[78] Komiyama et al. reported stabilization of an *end-on* copper superoxido complex using the methylated ligand Bz₃Me₃tren.^[63] Quite surprisingly, they were able to structurally characterize the dinuclear peroxide complex with the ligand Bz₃tren (due to amine protons) in excellent work. Furthermore, Itoh and co-workers demonstrated reversible formation of dioxygen binding to a copper complex using the highly sterically demanding ligand HIPT₃tren (a well-known ligand that has also been used successfully for binding and activation of N₂ by the corresponding molybdenum complex^[115]).^[116] Based on these findings it is obvious that small changes in the ligand system can lead to dramatic stabilization effects.

Due to charge transfer transitions "dioxygen adduct" complexes can be easily detected by their very intense color in solution in so called bench top experiments. Copper(I) complexes with the three ligands were exposed to pure dioxygen at -80°C in a Schlenck tube. They revealed different colors upon oxygenation as well as of the final products. Bench top experiments were performed using acetone as a non-coordinating solvent.

When a colorless solution of **1** (Figure 2.4, left) was exposed to dioxygen an extremely fast change to a sap green color was observed that then turned to the darker green colored solution shown in Figure 2.4 (middle). In a few minutes the color of the solution changed to a deep brown color (Figure 2.4, right). In contrast, solutions of complexes **2** and **3** kept a sap green color after reaction with dioxygen for a short time before turning into a light bluish-green color (decomposition to copper(II) complexes). With regard to previous studies, the sap green solutions indicated the formation of *end-on* superoxido copper complexes as the first intermediate in these reactions. In order to verify those assumptions, low-temperature stopped-flow measurements were conducted.

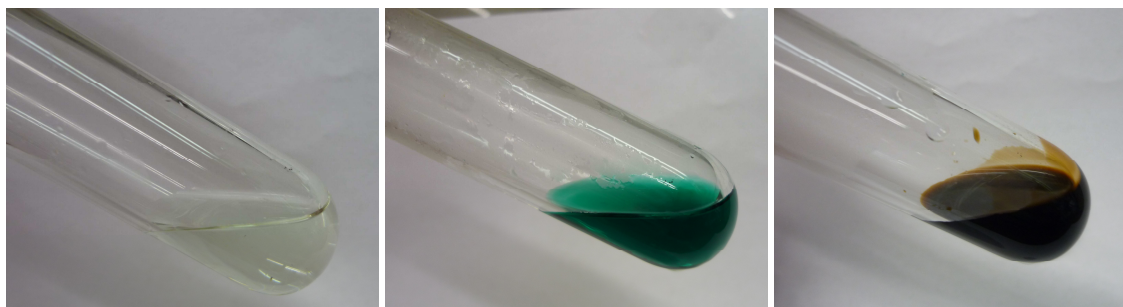


Figure 2.4: Reacting **1** with dioxygen in acetone in a bench top experiment at -80 °C.

2.1.4.3 Low Temperature Stopped-Flow Measurements

Low temperature stopped-flow measurements are useful to obtain information about the occurrence and stability of reactive intermediate complexes.^[65,76,97] Confirming observations of the bench top experiments described above, reactions of all three complexes with dioxygen in acetone confirmed the formation of an intermediate *end-on* copper superoxido complex with a characteristic UV absorbance maximum at around 410 nm. Unfortunately however, none of the superoxido complexes turned out to be persistent – even at low temperatures – and thus our original goal, to improve the stability of such a species comparable to our previously characterized superoxido complex with the TMG₃tren ligand, was not accomplished. Therefore, no detailed further kinetic analyses were performed.

Previous experiments applying the ligand Me₃tren had indicated that there might be a possibility to stabilize a superoxido complex using this ligand.^[37] Further support came from theoretic modelling on this system.^[117] However, first experiments had failed due to low availability of the ligand itself (synthesis had turned out to be a bit tedious).^[108] Commercially available Me₃tren now allowed to perform a much more detailed investigation. Unfortunately, we could still only confirm previous findings, which is the very fast formation of an end-on copper superoxido complex (according to our UV-vis data at the beginning of our stopped-flow measurements with its characteristic absorbance maximum at 410 nm) prior to its decomposition to products that we could not identify so far. An example of time resolved UV-vis spectra for this reaction at -76 °C is presented in Figure 2.5.

The decrease of the absorbance at 410 nm is caused by the decomposition of the superoxido species due to consecutive reactions leading to the final brown solution. Parallel to the formation of the superoxido complex, an additional but smaller amount of the corresponding dinuclear peroxide complex can be observed with characteristic absorbance maxima at around 500 and 570 nm.^[62,96]

However, calculation of the value of approximately 4000 cm⁻¹mol⁻¹L (at 410 nm) for the absorption coefficient accounts for the formation of a much larger amount of the superoxido complex (in accordance with published data).^[63]

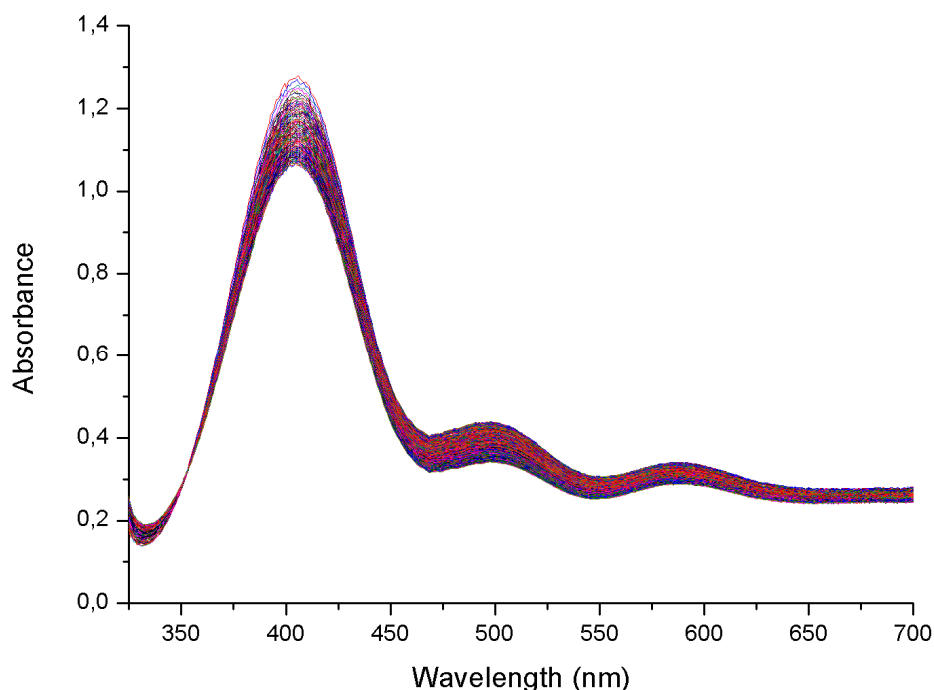


Figure 2.5: Reaction of $[\text{Cu}(\text{Me}_3\text{tren})]^+$ (**1**) ($[\text{complex}] = 0.30 \text{ mmol/L}$) with a saturated solution of dioxygen in acetone at -76°C over 22.5 s.

In contrast to **1**, the reaction of **2** with dioxygen looks much cleaner. The only difference between the two complexes is that Isoprop₃tren is a sterically more demanding ligand than Me₃tren. With **2** however, it was still possible to observe the formation of the superoxido complex (Figure 2.6) within 0.05 s (complete formation according to the absorption maximum at 410 nm) at -90°C .

Often, these reactions are so fast that they cannot be observed by stopped-flow techniques, because they already occur during the mixing time of the instrument. Sometimes, it can be interesting to compare the reaction of dioxygen to the analogous reaction with nitrogen oxide. Most of the time NO reacts even faster than O₂ (monoradical vs. diradical). So far, to the best of our knowledge, previous studies with NO were only performed with the copper(II) Isoprop₃tren complex **4**, by Sarma et al. leading to the reduction and a trinitrosation of the ligand.^[71]

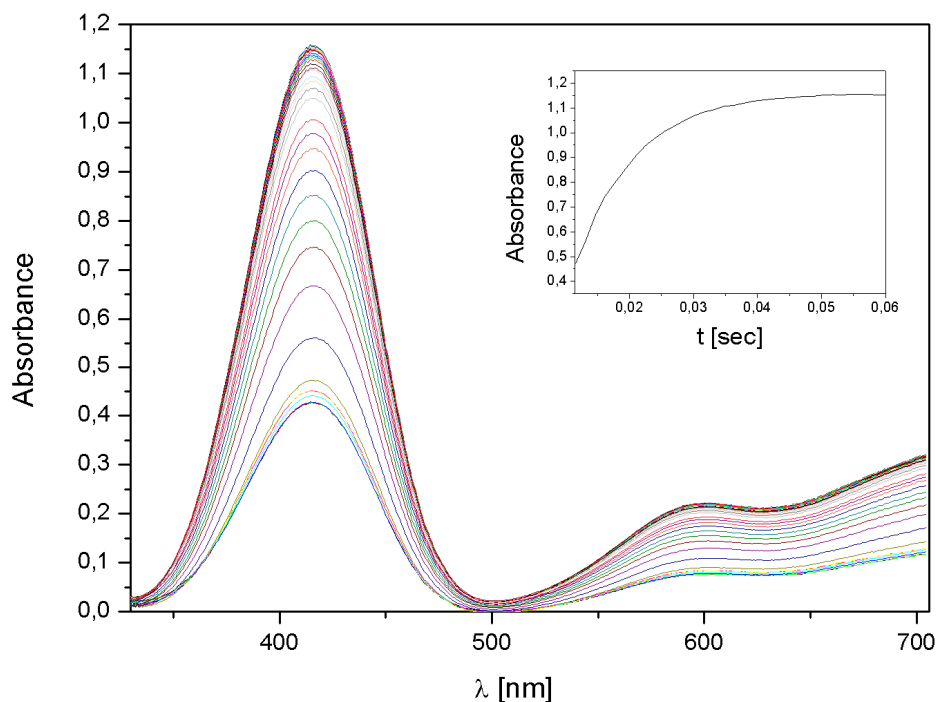


Figure 2.6: Reaction of $[\text{Cu}(\text{Isoprop}_3\text{tren})]^+$ (**2**⁺) ([complex] = 0.12 mmol/L) with a saturated solution of dioxygen in acetone at -90.4°C . Measured over 0.075 s. Insert shows the absorbance vs. time trace at 414 nm.

In contrast to the decomposition reaction described above for **1**, the superoxido complex formed from **2** did react further to a new species (Figure 2.7) that we assign to a hydroperoxido complex due to the similarity of its UV-vis spectrum of related complexes.^[114,118–121] The proton and electron needed herein can be easily provided through a similar mechanism described previously for the copper Bz_3tren system.^[78] Still, additional investigations are necessary to support this assumption.

Kinetic analysis turned out to be difficult, most likely due to further reactions such as, e. g. the formation of a dinuclear side-on peroxido complex caused by bond cleavage of one of the amine arms of the ligand. Concomitant formation of a copper superoxido complex with such a dinuclear peroxide complex has been observed previously for the copper HIPT_3tren complex.^[116] Moreover, intramolecular ligand hydroxylation could occur at one point.

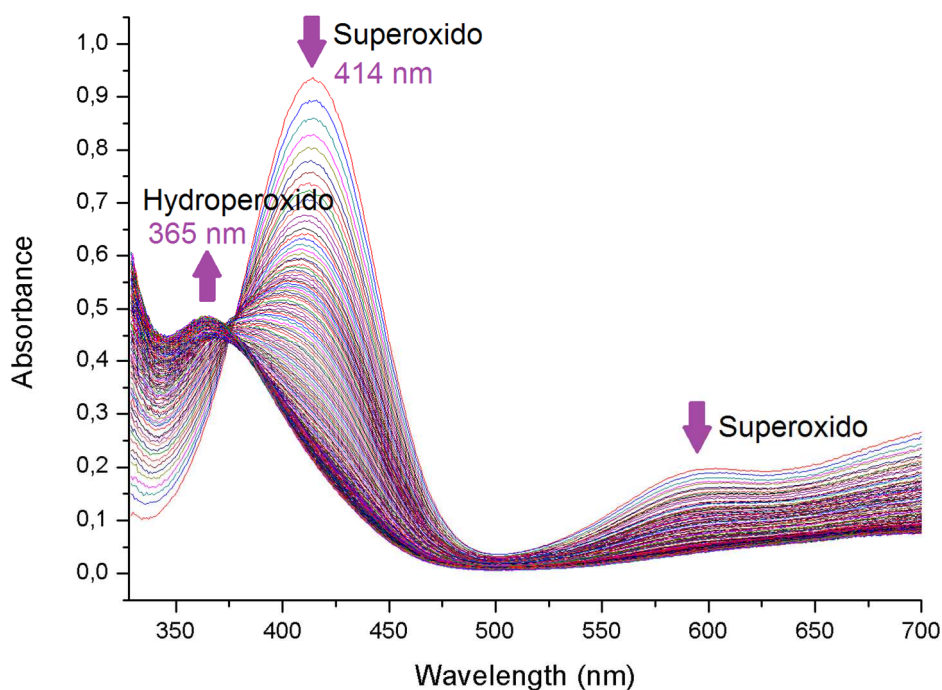


Figure 2.7: Reaction of $[\text{Cu}(\text{Isoprop}_3\text{tren})]^+$ (**2**) ($[\text{complex}] = 0.12 \text{ mmol/L}$) with a saturated solution of dioxygen in acetone at -95°C . Measured over 2250 s.

Due to previous results for the formation of a quite stable mononuclear copper superoxido complex from the reaction of dioxygen with the $\text{Bz}_3\text{Me}_3\text{tren}$ copper(I) complex,^[63] expectations were highest for the reactivity of **3** (better sterical shielding, no amine protons). In accordance with these expectations, the sole formation of the mononuclear superoxido complex was observed in our stopped-flow measurement (Figure 2.8). However, the complex is not stable and reacts further in a fast, consecutive reaction. Therefore, only the decrease of the absorbance at 410 nm can be observed. Most likely, intermediate oxido-bridged copper complexes form during this reaction. After workup only the copper(II) $\text{Me}_3\text{isoprop}_3\text{tren}$ complex was obtained and obviously, no stabilization (despite the lack of amine protons) was achieved.

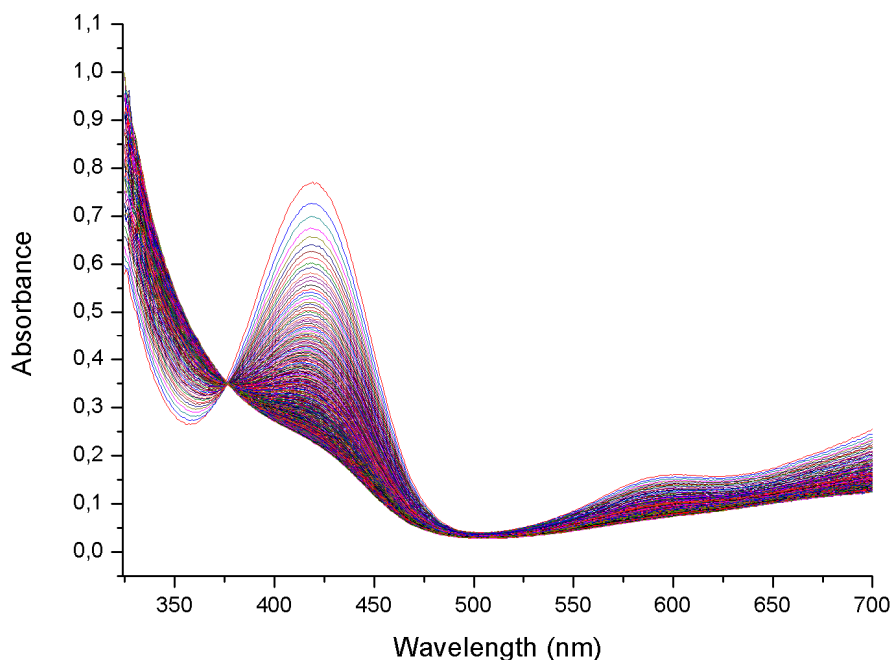


Figure 2.8: Reaction of $[\text{Cu}(\text{Me}_3\text{isoprop}_3\text{tren})]^+$ (**3**) ([complex] = 0.42 mmol/L) with a saturated solution of dioxygen in acetone at -86°C . Measured over 90 s.

2.1.5 Conclusions and Outlook

As the ligand systems Me_6tren and TMG_3tren have already proven to be of great success in stabilizing intermediate oxygenated copper adduct complexes, the study of copper complexes which incorporate the ligands mentioned in this paper were a logic consequence of these previous studies. While our expectations to further stabilize a mononuclear copper *end-on* superoxido complex using a tripodal ligand were not achieved, the results are important with regard to a better understanding and ligand design for further investigations in that research field. Small changes in the ligand design can lead to quite dramatic stabilization of these usually highly reactive species. The possibility of this kind of ligand modification has been demonstrated previously with the TMG_3tren system^[51] and by a recent report on a dinuclear *side-on* copper peroxido complex that turned out to be extremely stable using a macrocyclic ligand with sterically demanding residues.^[122] In terms of further investigations of complexes **1** and **2**, work is in progress to study these complexes at much lower temperatures (as low as down to -140°C) that are likely to allow observation and stabilization of the individual species.

This approach has already been successfully applied by Stack and co-workers for their complexes with propylene diamine ligands (also containing amine protons).^[123]

2.2 Supporting Information

2.2.1 Selected Crystallographic Data

Table 2.1: Crystal data and structure refinement for [Cu(Me₃tren)]ClO₄

CCDC No 1909701

Color	Light yellow	
Crystal size	0.400 x 0.280 x 0.200 mm ³	
Empirical formula	C ₉ H ₂₄ ClCuN ₄ O ₄	
Formula weight	351.31	
Temperature	193(2) K	
Wavelength	0.71073 Å	
Crystal system	Orthorhombic	
Space group	<i>Pna</i> 2 ₁	
Unit cell dimensions	<i>a</i> = 12.3260(14) Å	$\alpha = 90^\circ$
	<i>b</i> = 8.8897(9) Å	$\beta = 90^\circ$
	<i>c</i> = 14.033(2) Å	$\gamma = 90^\circ$
Volume	1537.6(3) Å ³	
<i>Z</i>	4	
Density (calculated)	1.518 Mg/m ³	
Absorption coefficient	1.609 mm ⁻¹	
<i>F</i> (000)	736	
Theta range for data collection	2.712 to 27.096°	
Index ranges	-15 ≤ <i>h</i> ≤ 15, -10 ≤ <i>k</i> ≤ 11, -17 ≤ <i>l</i> ≤ 17	
Reflections collected	12125	
Independent reflections	3379 [<i>R</i> (int) = 0.0592]	
Completeness to theta = 25.242°	99.3 %	
Absorption correction	None	
Refinement method	Full-matrix least-squares on <i>F</i> ²	
Data / restraints / parameters	3379 / 140 / 200	
Goodness-of-fit on <i>F</i> ²	0.932	
Final <i>R</i> indices [<i>I</i> > 2σ(<i>I</i>)]	<i>R</i> 1 = 0.0321, <i>wR</i> 2 = 0.0698	
<i>R</i> indices (all data)	<i>R</i> 1 = 0.0449, <i>wR</i> 2 = 0.0736	
Absolute structure parameter	-0.003(9)	
Largest diff. peak and hole	0.706 and -0.315 e.Å ⁻³	

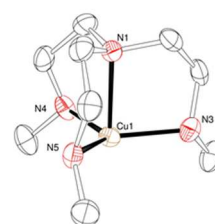


Table 2.2: Selected bond lengths [Å] and angles [°] for [Cu(Me₃tren)]ClO₄

Cu1-N1	2.206(2)	Cu1-N2	2.048(3)	Cu1-N3	2.056(2)
Cu1-N4	2.047(3)				
N1-Cu1-N2	85.49(10)	N1-Cu1-N3	84.64(10)	N1-Cu1-N4	85.15(10)
N2-Cu1-N3	118.17(11)	N2-Cu1-N4	120.46(10)	N3-Cu1-N4	119.20(11)

Table 2.3: Crystal data and structure refinement for [Cu(Isoprop₃tren)]SO₃CF₃

CCDC No 1909700

Color	Light orange	
Crystal size	0.500 x 0.300 x 0.200 mm ³	
Empirical formula	C ₁₆ H ₃₆ CuF ₃ N ₄ O ₃ S	
Formula weight	485.09	
Temperature	193(2) K	
Wavelength	0.71073 Å	
Crystal system	Monoclinic	
Space group	<i>P</i> 2 ₁ / <i>n</i>	
Unit cell dimensions	<i>a</i> = 9.3379(19) Å	$\alpha = 90^\circ$
	<i>b</i> = 16.565(3) Å	$\beta = 91.85(3)^\circ$
	<i>c</i> = 15.292(3) Å	$\gamma = 90^\circ$
Volume	2364.2(8) Å ³	
Z	4	
Density (calculated)	1.363 Mg/m ³	
Absorption coefficient	1.057 mm ⁻¹	
F(000)	1024	
Theta range for data collection	1.813 to 27.103°	
Index ranges	-11 ≤ <i>h</i> ≤ 11, -21 ≤ <i>k</i> ≤ 21, -19 ≤ <i>l</i> ≤ 19	
Reflections collected	29874	
Independent reflections	5212 [<i>R</i> (int) = 0.0376]	
Completeness to theta = 25.242°	99.9 %	
Absorption correction	Semi-empirical from equivalents	
Refinement method	Full-matrix least-squares on <i>F</i> ²	
Data / restraints / parameters	5212 / 3 / 268	
Goodness-of-fit on <i>F</i> ²	0.967	
Final <i>R</i> indices [<i>I</i> > 2σ(<i>I</i>)]	<i>R</i> 1 = 0.0290, <i>wR</i> 2 = 0.0712	
<i>R</i> indices (all data)	<i>R</i> 1 = 0.0486, <i>wR</i> 2 = 0.0758	
Largest diff. peak and hole	0.283 and -0.266 e.Å ⁻³	

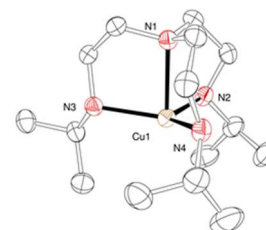


Table 2.4: Selected bond lengths [Å] and angles [°] for [Cu(Isoprop₃tren)]SO₃CF₃

Cu1-N1	2.2082(16)	Cu1-N2	2.0861(16)	Cu1-N3	2.0894(16)
Cu1-N4	2.0579(16)				
N1-Cu1-N2	83.96(6)	N1-Cu1-N3	84.36(5)	N1-Cu1-N4	85.50(6)
N2-Cu1-N3	111.27(7)	N2-Cu1-N4	120.94(7)	N3-Cu1-N4	125.17(7)

Table 2.5: Crystal data and structure refinement for [Cu(Me₃isoprop₃tren)]BPh₄

CCDC No 1909702

Color	Light yellow	
Crystal size	0.280 x 0.200 x 0.160 mm ³	
Empirical formula	C ₄₂ H ₆₂ BCuN ₄	
Formula weight	697.30	
Temperature	193(2) K	
Wavelength	0.71073 Å	
Crystal system	Monoclinic	
Space group	<i>P</i> 2 ₁	
Unit cell dimensions	<i>a</i> = 10.571(2) Å	$\alpha = 90^\circ$
	<i>b</i> = 17.564(4) Å	$\beta = 113.90(3)^\circ$
	<i>c</i> = 11.465(2) Å	$\gamma = 90^\circ$
Volume	1946.3(8) Å ³	
<i>Z</i>	2	
Density (calculated)	1.190 Mg/m ³	
Absorption coefficient	0.595 mm ⁻¹	
<i>F</i> (000)	752	
Theta range for data collection	2.499 to 28.184°	
Index ranges	-14 ≤ <i>h</i> ≤ 13, -23 ≤ <i>k</i> ≤ 23, -15 ≤ <i>l</i> ≤ 15	
Reflections collected	17272	
Independent reflections	9188 [<i>R</i> (int) = 0.0743]	
Completeness to theta = 25.242°	99.8 %	
Absorption correction	None	
Refinement method	Full-matrix least-squares on <i>F</i> ²	
Data / restraints / parameters	9188 / 1 / 442	
Goodness-of-fit on <i>F</i> ²	0.803	
Final <i>R</i> indices [<i>I</i> > 2σ(<i>I</i>)]	<i>R</i> 1 = 0.0493, <i>wR</i> 2 = 0.0931	
<i>R</i> indices (all data)	<i>R</i> 1 = 0.1141, <i>wR</i> 2 = 0.1093	
Absolute structure parameter	-0.020(11)	
Largest diff. peak and hole	0.535 and -0.286 e.Å ⁻³	

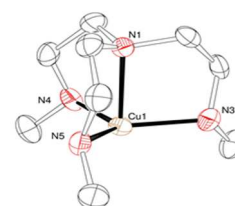


Table 2.6: Selected bond lengths [Å] and angles [°] for [Cu(Me₃isoprop₃tren)]BPh₄

Cu1-N1	2.138(4)	Cu1-N2	2.147(4)	Cu1-N3	2.153(4)
Cu1-N4	2.113(4)				
N1-Cu1-N2	85.73(16)	N1-Cu1-N3	86.02(15)	N1-Cu1-N4	87.32(15)
N2-Cu1-N3	118.79(14)	N2-Cu1-N4	120.11(14)	N3-Cu1-N4	119.90(14)

Table 2.7: Crystal data and structure refinement for [Cu(Isoprop₃tren)Cl]Cl

CCDC No 1909699

Color	Dark turquoise	
Crystal size	0.35 x 0.10 x 0.03 mm ³	
Empirical formula	C ₁₅ H ₃₆ Cl ₂ CuN ₄	
Formula weight	406.92	
Temperature	200(2) K	
Wavelength	0.71073 Å	
Crystal system	Monoclinic	
Space group	<i>P</i> 2 ₁ / <i>c</i>	
Unit cell dimensions	<i>a</i> = 10.851(3) Å	$\alpha = 90^\circ$
	<i>b</i> = 15.199(4) Å	$\beta = 106.369(4)^\circ$
	<i>c</i> = 13.809(3) Å	$\gamma = 90^\circ$
Volume	2185.2(9) Å ³	
<i>Z</i>	4	
Density (calculated)	1.237 Mg/m ³	
Absorption coefficient	1.246 mm ⁻¹	
<i>F</i> (000)	868	
Theta range for data collection	1.96 to 28.44°	
Index ranges	-14 ≤ <i>h</i> ≤ 14, -19 ≤ <i>k</i> ≤ 19, -18 ≤ <i>l</i> ≤ 18	
Reflections collected	25966	
Independent reflections	5353 [<i>R</i> (int) = 0.1201]	
Completeness to theta = 28.44°	93.6 %	
Absorption correction	Semi-empirical from equivalents	
Refinement method	Full-matrix least-squares on <i>F</i> ²	
Data / restraints / parameters	5353 / 0 / 220	
Goodness-of-fit on <i>F</i> ²	0.909	
Final <i>R</i> indices [<i>I</i> > 2σ(<i>I</i>)]	<i>R</i> 1 = 0.0538, <i>wR</i> 2 = 0.1242	
<i>R</i> indices (all data)	<i>R</i> 1 = 0.1590, <i>wR</i> 2 = 0.1579	
Largest diff. peak and hole	0.874 and -1.265 e.Å ⁻³	

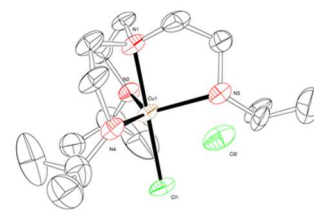
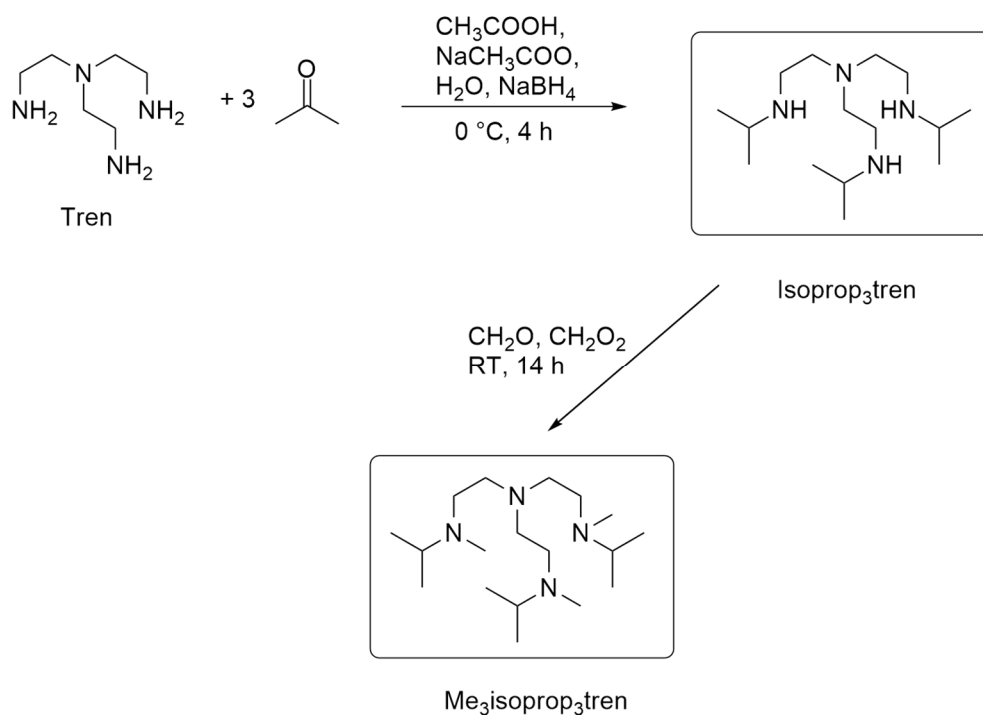


Table 2.8: Selected bond lengths [Å] and angles [°] for [Cu(Isoprop₃tren)Cl]Cl

Cu1-N1	2.039(3)	Cu1-N2	2.120(4)	Cu1-N3	2.197(4)
Cu1-N4	2.130(4)	Cu1-Cl1	2.2409(12)		
N1-Cu1-N2	83.75(14)	N1-Cu1-N3	82.57(15)	N1-Cu1-N4	83.46(14)
N2-Cu1-N3	115.43(16)	N2-Cu1-N4	138.35(17)	N3-Cu1-N4	101.92(16)
N1-Cu1-Cl1	176.41(10)				

2.3 Additional Material and Unpublished Results

2.3.1 Synthesis of Ligands



Scheme 2.1: Visual reaction pathway of the syntheses of the ligands prepared.

2.3.2 Synthesis of [Cu(L)]BF₄

Synthesis of [Cu(Me₃tren)]BF₄

0.15 g ($4.78 \cdot 10^{-4}$ mol) of $[\text{Cu}(\text{MeCN})_4]\text{BF}_4$ were dissolved in 2 mL methanol and added dropwise to 0.1 g ($5.31 \cdot 10^{-4}$ mol) of Me₃tren diluted in 2 mL of methanol. The resulting yellowish solution was stirred for 30 minutes at room temperature. The complex was then

precipitated as a light yellow solid upon adding 15 mL of Et₂O. The remaining liquid was decanted and the resulting crystalline solid filtered and washed with Et₂O. The product was dried in vacuum to yield 0.124 g (3.66×10^{-4} mol, 76.6 %) of [Cu(Me₃tren)]BF₄.

Synthesis of [Cu(Isoprop₃tren)]BF₄

0.104 g ($3.3 \cdot 10^{-4}$ mol) of [Cu(MeCN)₄]BF₄ were dissolved in 2 mL methanol and added dropwise to 0.1 g ($3.67 \cdot 10^{-4}$ mol) of Isoprop₃tren diluted in 2 mL of methanol. The resulting yellowish solution was stirred for 30 minutes at room temperature. Upon adding 15 mL of Et₂O, the complex was precipitated as a light yellow solid. The remaining liquid was decanted and the resulting crystalline solid filtered and washed with Et₂O. The product was dried in vacuum to yield 0.127 g ($3 \cdot 10^{-4}$ mol, 91 %) of [Cu(Isoprop₃tren)]BF₄.

Synthesis of [Cu(Me₃isoprop₃tren)]BF₄




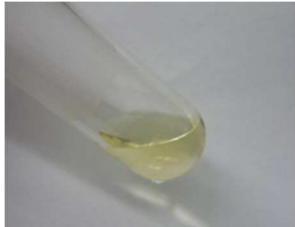

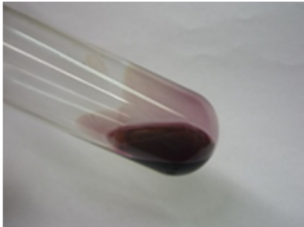
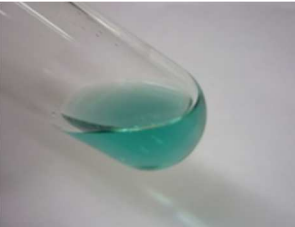



0.089 g ($2.83 \cdot 10^{-4}$ mol) of [Cu(MeCN)₄]BF₄ were dissolved in 2 mL methanol and added dropwise to 0.1 g ($3.15 \cdot 10^{-4}$ mol) of Me₃isoprop₃tren diluted in 2 mL methanol. The resulting yellowish solution was stirred for 30 minutes at room temperature. The complex was precipitated as a light yellow solid upon adding 15 mL of Et₂O. The remaining liquid was decanted and the resulting crystalline solid filtered and washed with Et₂O. The product was dried in vacuum to yield 0.118 g ($2.52 \cdot 10^{-4}$ mol, 89.2 %) of [Cu(Me₃isoprop₃tren)]BF₄.

2.3.3 Bench Top Experiments

Bench top experiments oxygenating copper(I) complexes as [Cu(L)]BF₄ (L= Me₃tren or Me₃isoprop₃tren) in acetone and in EtCN were carried out at -86°C in an ethanol/liquid nitrogen bath and color changes were photographed where possible. The sap green superoxido intermediates were (even at those low temperatures) extremely unstable and reacted very fast to further species visible through color changes. Therefore, none of the forming superoxido intermediates could be photographed. Formation of a characteristic sap green end-on superoxido intermediate could only be seen in the case of the reaction of [Cu(Me₃isoprop₃tren)]BF₄ in acetone. All other expected end-on superoxido species were so short-lived that they could not be spotted by the eye. Subsequent oxygen intermediates could

be photographed as well as their respective decomposed products at low temperatures and at room temperature. All photographs taken are shown in Table 2.9.

Table 2.9: Photographs of copper(I) complexes reacting with pure dioxygen at low temperatures in acetone and in EtCN.

$[\text{Cu}(\text{Me}_3\text{tren})]\text{BF}_4$	$[\text{Cu}(\text{Me}_3\text{tren})]\text{BF}_4$	$[\text{Cu}(\text{Me}_3\text{isoprop}_3\text{tren})]\text{BF}_4$	$[\text{Cu}(\text{Me}_3\text{isoprop}_3\text{tren})]\text{BF}_4$
in acetone	in EtCN	in acetone	in EtCN
			
Oxygenation at - 86°C			
		N.a. since the intermediate reacted to subsequent species too fast for photographic documentation	
			



in acetone



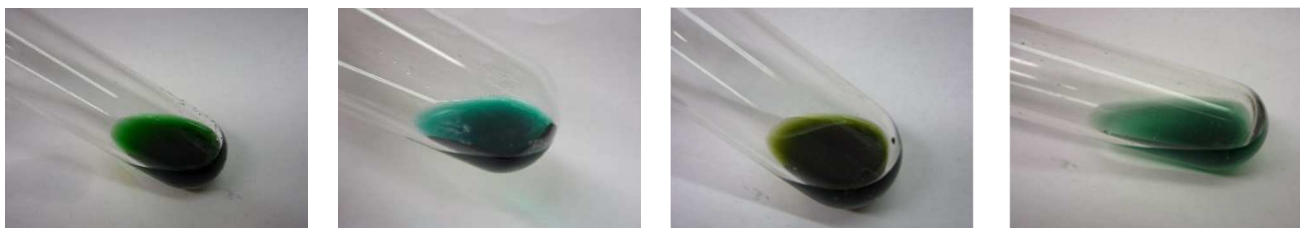
in EtCN



in acetone



in EtCN

Decomposed products at room temperature

Low temperature bench top experiments can only give a first indication of whether a certain copper(I) complex will react with dioxygen and if so, whether the intermediate species vary in color and therefore in configuration in different solvents. EtCN is a coordinating solvent and was used because a slower reaction of each copper(I) complex with dioxygen was expected. As there were visible differences in colors upon oxygenation, low temperature stopped flow measurements were subsequently not only carried out in acetone, but for the complexes $[\text{Cu}(\text{Me}_3\text{tren})]^+$ and $[\text{Cu}(\text{Isoprop}_3\text{tren})]^+$ also in EtCN.

2.3.4 Low Temperature Stopped Flow Measurements of $[\text{Cu}(\text{Me}_3\text{tren})]\text{ClO}_4$ in EtCN

Under the inert conditions of an argon-filled glove box, a solution of $[\text{Cu}(\text{Me}_3\text{tren})]\text{ClO}_4$ (0.6 mmol) in EtCN was mixed with a solution of oxygen-saturated EtCN at -92°C . The reaction was observed using low temperature stopped flow techniques (1 UV-vis spectrum per 1 ms). The formation of the superoxido species $[\text{Cu}(\text{Me}_3\text{tren})\text{O}_2]^{2+}$ could be detected, but even at these low temperatures it is extremely fast so that a more detailed kinetic characterization of this reaction was not possible. Noticeable in Figure 2.9, however, is the presence of an isosbestic point at 352 nm indicating the formation of another oxygenated intermediate species. Unfortunately, neither temperature variation nor variation in time recording the spectra provided more information about the nature of that intermediate.

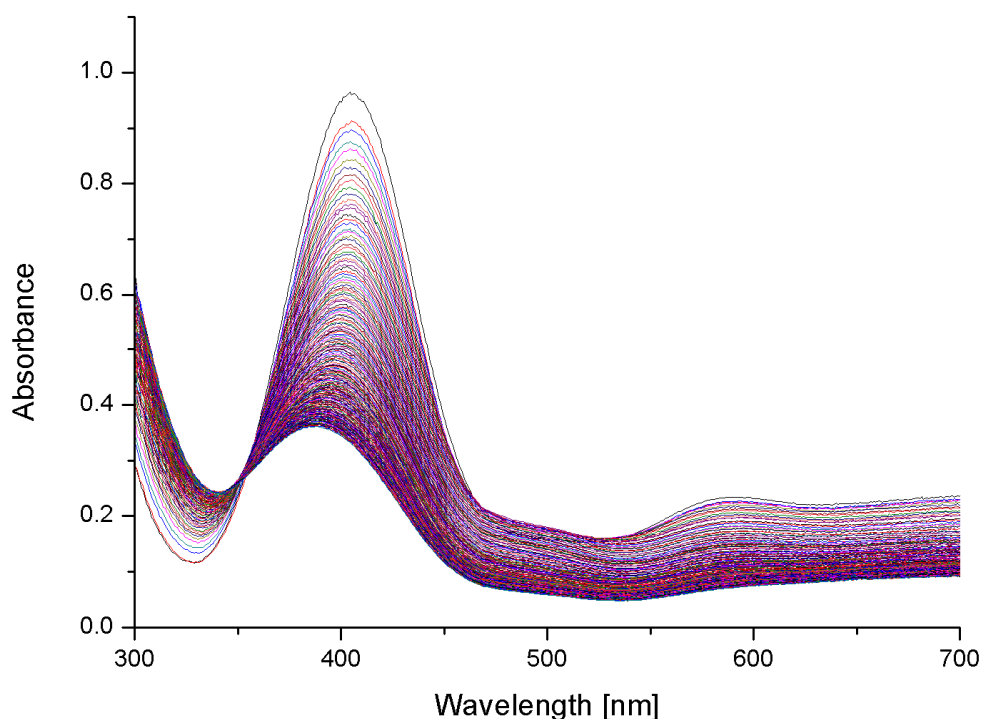


Figure 2.9: Time-resolved spectra of the reaction of $[\text{Cu}(\text{Me}_3\text{tren})\text{ClO}_4]$ with dioxygen using low temperature stopped flow techniques. The spectra show the formation and the decay of absorption maxima at 405 nm and 588 nm indicating an end-on superoxido species and displaying an isosbestic point at 352 nm.

2.3.5 Low Temperature Stopped Flow Measurements of $[\text{Cu}(\text{Isoprop}_3\text{tren})]\text{SbF}_6$ in EtCN

Under the inert conditions of an argon-filled glove box, a solution of $[\text{Cu}(\text{Isoprop}_3\text{tren})\text{SbF}_6]$ (0,345 mmol) in EtCN was mixed with a solution of oxygen-saturated EtCN at -89°C . The reaction was observed using low temperature stopped flow techniques (1 UV-vis spectrum per 1 ms). The formation of the superoxido species $[\text{Cu}(\text{Isoprop}_3\text{tren})\text{O}_2]^+$ could be detected at 408 nm and 601 nm, but like in the case of the respective Me_3tren complex the reaction is extremely fast, so that a more detailed kinetic characterization was not possible either. The recorded spectra are shown in Figure 2.10.

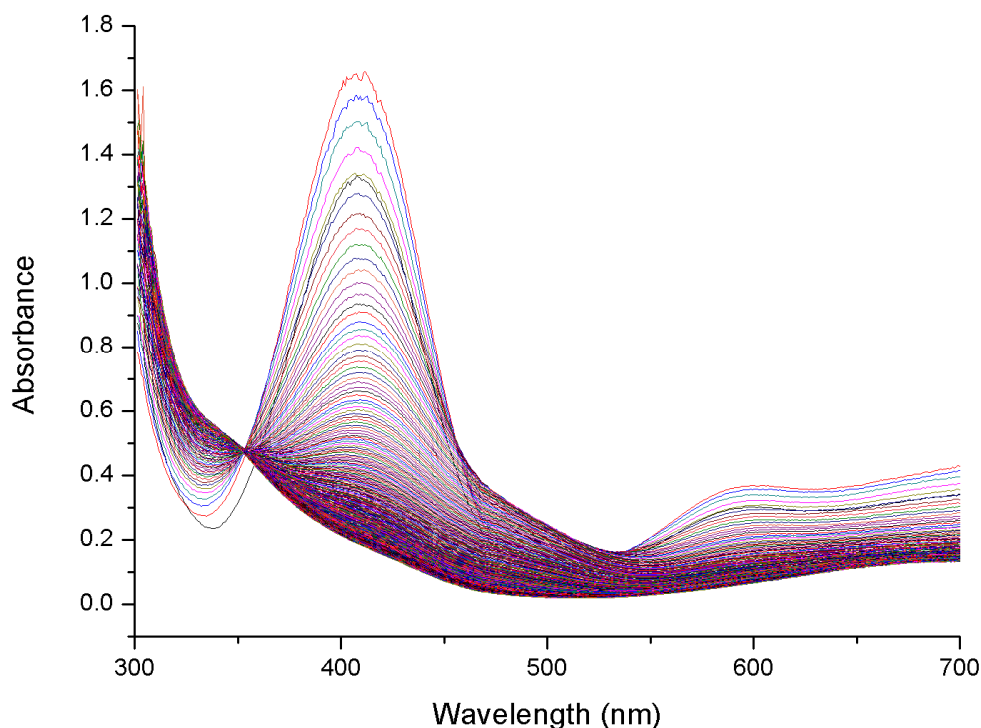


Figure 2.10: Time-resolved spectra of the reaction of $[\text{Cu}(\text{Isoprop}_3\text{tren})]\text{SbF}_6$ with dioxygen using low temperature stopped flow techniques. The spectra show the formation and the decay of the end-on superoxido species in absorption bands with maxima at 408 nm and 601 nm as well as an isosbestic point at 353 nm.

The presence of an isosbestic point at 351 nm and the formation of another shoulder at 340 nm indicates the formation of another oxygenated intermediate species. The formation of this species was faster than the one observed in the same reaction in acetone. Due to the coordinating properties of EtCN as a solvent, the reaction of the copper(I) complex with dioxygen was expected to be slower than the same reaction in acetone, but this was not the case. However, neither temperature variation nor variation in times used for recording those spectra revealed more information about the nature of that intermediate.

2.3.6 UV-vis Measurements of Copper(II) Complexes

In order to gain an understanding of how dioxygen could coordinate to the copper(I) complexes of the ligands in solution, according copper(II) complexes using chloride as an anion were prepared and characterized using UV-vis technique (cf.ch. 2.1.4.1). The spectra of those measurements are displayed in Figure 2.11.

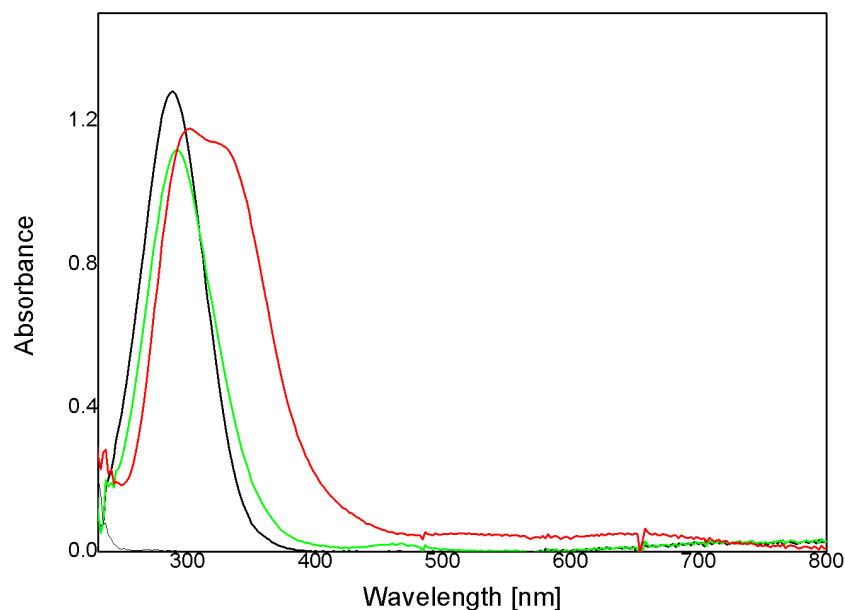


Figure 2.11: UV-vis data of the copper(II) complexes $[\text{Cu}(\text{Me}_3\text{tren})\text{Cl}]\text{Cl}$ (black line), $[\text{Cu}(\text{Isoprop}_3\text{tren})\text{Cl}]\text{Cl}$ (green line) and $[\text{Cu}(\text{Me}_3\text{isoprop}_3\text{tren})\text{Cl}]\text{Cl}$ (red line). All spectra taken in a MeCN solution.

3 Iron Complexes – Experiments and Results

The results presented in this chapter were published in the *Israel Journal of Chemistry* in January 2020.^[124]

3.1 Synthesis and Reactivity of Iron(II) Complexes with a New Tripodal Imine Ligand

*Janine Will, Lars Schneider, Jonathan Becker, Sabine Becker, Andreas Miska,
Christopher Gawlig and Siegfried Schindler*

3.1.1 Abstract

A new tripodal imine ligand tris(2-(propan-2-ylideneamino)ethyl)amine (Imine₃tren) was prepared in order to stabilize high valent iron-oxido complexes. Iron complexes were synthesized in template reactions from iron(II) salts, tris(2-aminoethyl)amine (tren) and acetone. Due to the reversibility of the imine formation, complexes with different ligands were obtained depending on the reaction conditions. Three complexes, [Fe(Imine₃tren)(OAc)₂] (**1**), [Fe(Imine₃tren)(OAc)]OTf (**2**) and [Fe₂(Imine₃tren)F₂](SbF₆)₂(**4**), could be synthesized and structurally characterized. However, reactions with hydrogen peroxide, iodosobenzene or ozone did not lead to any kind of an "oxygen adduct" complex that could be observed spectroscopically.

3.1.2 Introduction

Interaction of dioxygen with iron compounds leading to different iron "oxygen complexes" plays an important role in the active sites of a large number of iron proteins/enzymes.^[30,45,125] Especially non-heme iron enzymes have been investigated in great detail to learn how to model their functionality in order to accomplish the selective oxidation of organic substrates with dioxygen (air) as the sole oxidant.^[29,126] In that respect, iron complexes with tripodal ligands such as tris[(2-pyridyl)-methyl]amine (abbreviated either as tmpa or tpa, Figure 3.1.a) and derivatives have been quite useful in the past to gain better understanding on the reactivity of iron enzymes towards dioxygen.^[29,45,127] Furthermore, tris(2-amino-ethyl)amine (tren, Figure 3.1b), the aliphatic relative of tmpa is an excellent building block for a series of ligands. For example with the tripodal ligand tris[(*N'*-*tert*-butylureaylato)-*N*-ethyl]aminato

([H₃1]³⁻, Figure 3.1c) it was possible to stabilize monomeric M–O and M–OH iron(III) complexes by H-bonding.^[128,129]

Using the guanidine derivative of tren (TMG₃tren, Figure 3.1d) allowed to obtain one of the few examples of an iron(IV) oxido complex in the high spin state ($S = 2$).^[130] In contrast to the trigonal bipyramidal geometry adopted by the [Fe(TM_G₃tren)O](OTf)₂ complex, the $S = 1$ iron(IV) oxido complexes reported previously mainly have an octahedral geometry.^[131,132] High valent iron(IV) oxido complexes play an important role as catalysts for oxidations of relatively inert substrates.^[131,133]

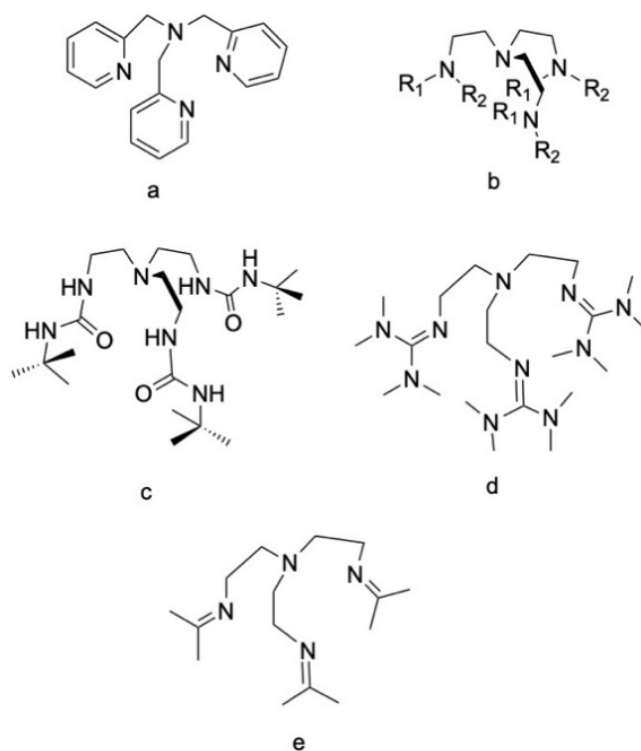


Figure 3.1: Tripodal ligands a) tmpa, b) tren ($R_1 = R_2 = H$), c) protonated [H₃1]³⁻, d) TMG₃tren and e) Imine₃tren.

Surprisingly, so far Imine₃tren (Figure 3.1.e) has not been used as a ligand, most likely because of the difficulties to obtain this compound in pure form. Due to the fact that its position is somewhat based in between the amine, guanidine and amide-based ligands, it was considered that it could have properties that can support the stabilization of high valent iron complexes. Therefore, it seemed to be a valid approach to prepare iron(II) complexes with this

ligand and to study their reactivity towards oxidants such as dioxygen, hydrogen peroxide, iodosobenzene and ozone.

3.1.3 Results and Discussion

3.1.3.1 Synthesis and crystallographic characterization of iron complexes

Up to now, all our attempts to synthesize the ligand Imine₃tren in pure form have not been successful. Efforts to prepare the corresponding nickel or iron complexes in a template reaction under different conditions only led to the isolation of nickel or iron tren complexes.^[134] Still, a dinuclear oxido-bridged iron(III) tren complex (**5**) could be structurally characterized. However, there are many examples of related complexes reported in the literature and therefore we did not investigate this compound any further. Crystallographic details of **5** are described in chapter 3.2.6.1. In previous work, we showed that iron(II) ions can be very useful to support related template reactions when $[\text{Fe}(\text{py})_4(\text{SCN})_2]$ is reacted with acetone together with the ligands uns-penp or apme.^[68,135] However, it was not possible to obtain the iron(II) Imine₃tren complex that way.

Recently, we observed the formation of a new tridentate macrocyclic ligand (Figure 3.2a) with a pendant donor arm when iron(II) chloride is reacted together with tren in acetone.^[134] These reactions (using an iron(II) salt, tren and acetone) are quite problematic in general, due to the reversibility of the imine formation reactions which lead to different reaction products. These reactions also strongly depend on several specific reaction conditions, e.g. solvent, metal cation and anion.

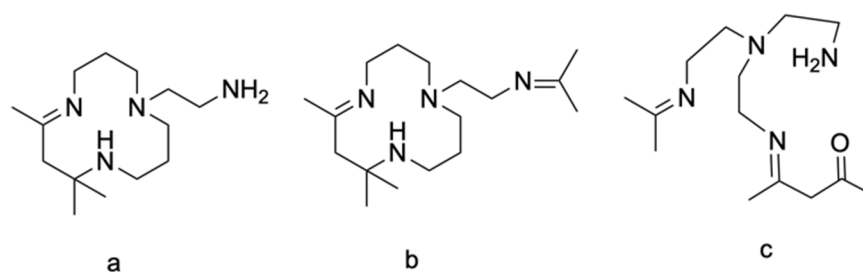


Figure 3.2: Different ligands obtained from the template reaction of iron(II) salts with tren and acetone.

Using iron(II) acetate finally allowed us to synthesize and crystallize the iron(II) Imine₃tren acetate complex [Fe(Imine₃tren)(OAc)₂] (**1**). The molecular structure of this complex is presented in Figure 3.3 (Crystallographic data are reported in Table 3.1 and Table 3.2. CV measurements showed irreversible redox reactions (see ch. 3.2.2).

Table 3.1: Crystal data and structure refinement for [Fe(Imine₃tren)(OAc)₂] (1**), [Fe(Imine₃tren)(OAc)OTf] (**2**) and [(Fe(Imine₃tren))₂F₂](SbF₆)₂ (**4**)**

	[Fe(Imine ₃ tren)(OAc) ₂] 1	[Fe(Imine ₃ tren)(OAc)OTf] 2	[(Fe(Imine ₃ tren)) ₂ F ₂](SbF ₆) ₂ 4
Empirical formula	C ₁₉ H ₃₆ FeN ₄ O ₄	C ₁₈ H ₃₃ F ₃ FeN ₄ O ₅ S	C ₁₅ H ₃₀ F ₇ FeN ₄ Sb
M _t	440.37	530.39	577.03
Crystal size [mm]	0.300 x 0.257 x 0.130	0.597 x 0.234 x 0.196	0.250 x 0.250 x 0.150
Crystal system	Triclinic	Monoclinic	Monoclinic
Space group	<i>P</i> $\bar{1}$	C2/c	<i>P</i> 2 ₁ / <i>n</i>
a [Å]	8.9920(5)	26.5956(7)	11.814(2)
b [Å]	11.1010(6)	12.0482(3)	14.283(3)
c [Å]	11.7729(6)	16.8118(4)	13.510(3)
α [°]	93.559(2)	90	90
β [°]	102.539(2)	114.5970(10)	111.47(3)
γ [°]	106.448(2)	90	90
V [Å ³]	1090.58(10)	4898.2(2)	2121.5(8)
Z	2	8	4
F(000)	472	2224	1152

$\rho_{\text{calcd.}} [\text{Mg m}^{-3}]$	1.341	1.438	1.807
$\mu [\text{mm}^{-1}]$	0.722	0.759	2.025
Total reflections	47156	57100	39698
Unique reflections	3856	6596	4895
R(int)	0.0849	0.0593	0.0409
Scan range θ_{max} [°]	2.436 to 25.058	2.490 to 29.130	2.338 to 27.602
Completeness to θ_{max} [%]	97.8	99.9	99.8
Index ranges	-10<=h<=10,	-36<=h<=36	-14<=h<=15,
	-13<=k<=13,	-16<=h<=16	-18<=k<=18,
	-14<=l<=14	-23<=h<=23	-17<=l<=17
Data/restraints/ parameters	3856 / 0 / 261	6590 / 90 / 363	4895 / 874 / 324
R1, ^{[a],[b]} wR2 [I>2 σ (I)] ^[c]	0.0390, 0.0730	0.0388, 0.0899	0.0248, 0.0586
R1, ^{[a],[b]} wR2 [all data] ^{[c] [d]}	0.0517, 0.0766	0.0539; 0.0961	0.0318, 0.0618
Goodness/of-fit on F ²	1.098	1.040	1.042
Mx./min. el. dens. [e*Å ⁻³]	0.304, -0.313	0.507, -0.391	0.395, -0.851

As can be seen in Figure 3.3, one arm of the Imine₃tren ligand is not coordinated to the metal center. Instead, coordination to an acetate anion is observed. One of the acetate ions

could either be replaced by triflate (**2**) or by tetraphenylborate (**3**) as anions leading to a full coordination of the ligand. The molecular structure of the cation of $[\text{Fe}(\text{Imine}_3\text{tren})(\text{OAc})]\text{OTf}$ (**2**) is presented in Figure 3.4. Crystallographic data of complex (**3**) are reported in chapter 3.2.6.1.

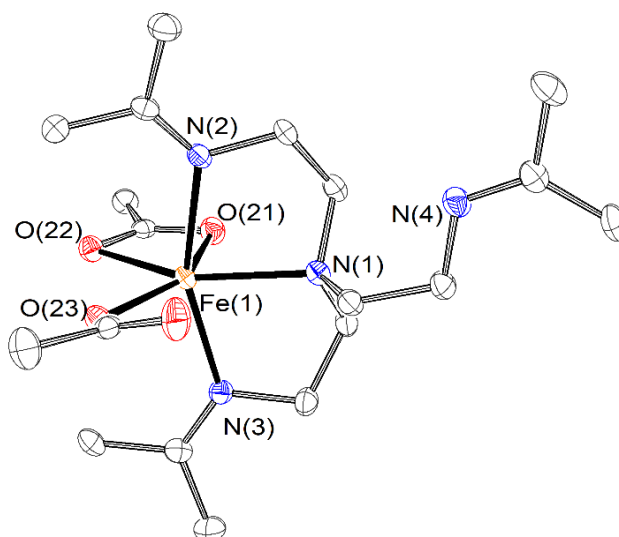


Figure 3.3: Molecular structure of $[\text{Fe}(\text{Imine}_3\text{tren})(\text{OAc})_2]$ (**1**).

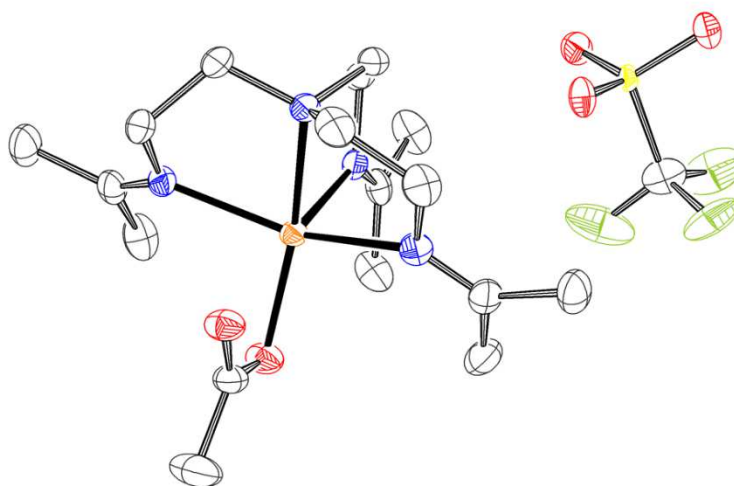


Figure 3.4: Molecular structure of $[(\text{Fe}(\text{Imine}_3\text{tren})(\text{OAc}))\text{OTf}]$ (**2**).

Fe-N bond lengths are only slightly different in $[(\text{Fe}(\text{Imine}_3\text{tren})(\text{OAc})_2)]$ (**1**) and $[(\text{Fe}(\text{Imine}_3\text{tren})(\text{OAc}))\text{OTf}]$ (**2**) caused by the coordination of either one or two acetate ions.

Bond lengths are also quite similar to those observed for the related complex $[\text{Fe}(\text{TMG}_3\text{tren})(\text{OTf})]\text{OTf}$.^[130]

The problems with reversible imine bond formation became obvious when the template reaction was performed using different amounts of the base NEt_3 (the presence of NEt_3 seemed to improve template reactions). Either **1** formed, or again, a macrocyclic iron complex (**6**) formed (see ch. 3.2). However, this time the free "amine arm" of the macrocycle had also reacted with another acetone molecule (Figure 3.2 b).

Table 3.2: Selected interatomic distances [Å] and angles [°] for $[\text{Fe}(\text{Imine}_3\text{tren})(\text{OAc})_2]$ (1**)**

Fe(1)-N(1)	2.242	Fe(1)-N(1)-N(2)	78.48
Fe(1)-N(2)	2.198	Fe(1)-N(1)-N(3)	79.22
Fe(1)-N(3)	2.192	Fe(1)-N(1)-O(21)	85.18
Fe(1)-O(21)	2.226	Fe(1)-N(1)-O(22)	143.18
Fe(1)-O(22)	2.297	Fe(1)-N(1)-O(23)	126.95
Fe(1)-O(23)	2.009	Fe(1)-N(2)-N(3)	157.67
		Fe(1)-N(2)-O(21)	89.83
		Fe(1)-N(2)-O(22)	98.00
		Fe(1)-N(2)-O(23)	97.66
		Fe(1)-N(3)-O(21)	87.19
		Fe(1)-N(3)-O(22)	99.14
		Fe(1)-N(3)-O(23)	96.60
		Fe(1)-O(21)-O(22)	58.05
		Fe(1)-O(21)-O(23)	147.82
		Fe(1)-O(22)-O(23)	89.86

Changing reaction conditions (e.g., different amounts of NEt_3 added) often led to mixtures of products. Crystallization of an iron(II) complex with a partially reacted tren ligand (Figure 3.2 c) clearly demonstrated some of the reactions occurring during the course of the imine formation, either leading to the $\text{Imine}_3\text{tren}$ or to the macrocyclic ligand. The molecular structures of two iron complexes with this ligand and different anions (**7**, **8**) are reported in chapter 3.2.6.1. Efforts to obtain the ligand or corresponding complexes using hexafluoroacetone instead of acetone were not successful. Only iron tren complexes were obtained, co-crystallized with an iron hexafluoroacetone complex in which the hexafluoroacetone had reacted with water (**9**, see ch. 3.2.6.1).

Table 3.3: Selected interatomic distances [Å] and angles [°] for [(Fe(Imine₃tren)(OAc))OTf (2)

Fe(1)-N(1)	2.19	N(1)-Fe-N(2)	78.33
Fe(1)-N(2)	2.20	N(1)-Fe-N(3)	80.64
Fe(1)-N(3)	2.17	N(2)-Fe-N(3)	95.98
Fe(1)-N(4)	2.20	N(1)-Fe-O(22)	165.58
Fe(1)-O(22)	2.11	N(2)-Fe-O(22)	97.38
Fe(1)-O(21)	2.29	N(3)-Fe-O(22)	113.63

Finally, it was possible to obtain an iron(II) complex with fully coordinated Imine₃tren using the iron(II) salt [Fe(CH₃CN)₆](SbF₆)₂ whose molecular structure is shown in Figure 3.5. Crystallographic data are reported in Table 3.4. Unfortunately, only a few crystals were obtained after several months that merely allowed structural characterization. Due to the lack of material, no further characterizations or investigations were possible.

As can be seen in Figure 3.5, a fluoride abstraction from the anion must have occurred which is then coordinated in between the two iron centers of the dinuclear complex [(Fe(Imine₃tren))₂F₂](SbF₆)₂ (**2**). Furthermore, crystallographic characterization with a different anion was accomplished (**10**, see ch. 3.2.6.1). However, fluoride abstraction is not unusual and has been observed previously.^[136]

Unfortunately, all of our efforts to obtain other iron(II) complexes without a coordinating anion have been unsuccessful so far.

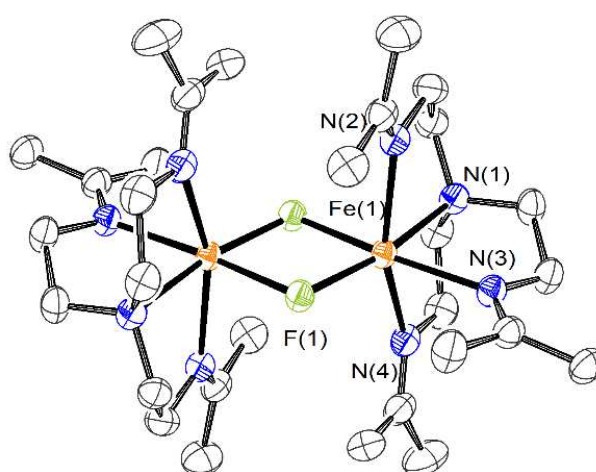
**Figure 3.5: Molecular structure of the cation of the cation of [(Fe(Imine₃tren))₂(F)₂](SbF₆)₂ (**4**).**

Table 3.4: Selected interatomic distances [Å] and angles [°] for [(Fe(Imine₃tren))₂(F)₂](SbF₆)₂ (4**).**

Fe(1)-N(1)	2.146	Fe(1)-N(1)-N(2)	77.78
Fe(1)-N(2)	2.222	Fe(1)-N(1)-N(3)	81.08
Fe(1)-N(3)	2.171	Fe(1)-N(1)-N(4)	77.61
Fe(1)-N(4)	2.232	Fe(1)-N(1)-F(1)	166.54
Fe(1)-F(1)	1.923	Fe(1)-N(1)-F(1)_i	88.32
Fe(1)-(F1)_i	2.153	Fe(1)-N(2)-N(3)	92.42
		Fe(1)-N(2)-N(4)	155.37
		Fe(1)-N(2)-F(1)	101.96
		Fe(1)-N(2)-F(1)_i	89.98
		Fe(1)-N(3)-N(4)	82.82
		Fe(1)-N(3)-F(1)	112.33
		Fe(1)-N(3)-F(1)_i	168.37
		Fe(1)-N(4)-F(1)	102.19
		Fe(1)-N(4)-F(1)_i	90.28
		Fe(1)-F(1)-F(1)_i	78.21

3.1.3.2 Reactivity of the iron(II) complexes **1** and **3** towards dioxygen, peroxides and ozone

Our hopes, to stabilize high valent iron complexes with the Imine₃tren ligand, were not fulfilled. Only a sluggish reaction of **1** or **3** with dioxygen was observed. Also, in contrast to related work, no peroxido, hydroperoxido or oxido complexes were spectroscopically detected when **1** was reacted with either hydrogen peroxide, iodosobenzene or ozone. Most likely, the ligand decomposed under these conditions.

3.1.4 Summary

So far, it has not been possible to obtain the new tripodal imine ligand Imine₃tren (fig. 3.2.2) in pure form. However, it was possible to obtain the corresponding iron(II) complexes [Fe(Imine₃tren)(OAc)₂] (**1**), [Fe(Imine₃tren)(OAc)]OTf (**2**) and [(Fe(Imine₃tren))₂(F)₂](SbF₆)₂ (**4**) in template reactions with iron(I) salts and to structurally characterize them. Fluoride abstraction of the anion caused the formation of the dinuclear fluoro-bridged complex. Complexes **1** and **2** did not show any formation of a spectroscopically detectable "oxygen adduct" iron complex when oxidized with different oxidants.

3.1.5 Experimental

3.1.5.1 General

All chemicals used were of p.a. quality and were purchased from either Acros Organics or Sigma Aldrich. Dry solvents purchased for air sensitive synthesis were redistilled under argon. The preparation and handling of air sensitive compounds were performed in a glovebox or under standard Schlenk-techniques. Electrospray-ionization MS (ESI-MS) measurements were performed on a Bruker microTOF mass spectrometer. Elemental analysis was performed by a Thermo Scientific FlashEA 1112.

3.1.5.2 Crystallographic Characterization

Details for X-ray crystal structure determination are described in chapter 3.2.6.

3.1.5.3 Synthesis of [Fe(Imine₃tren)(OAc)₂] (1)

Fe(OAc)₂ (174 mg, 1.00 mmol) was added to acetone (1 mL). Afterwards, a solution of tren (147 mg, 1.01 mmol) in acetone (1 mL) was added dropwise. The yellow suspension was stirred for 3 h at room temperature. After filtration, a greenish solution was obtained. The solution was stored at -40 °C and after 1 – 2 months crystals could be separated from the solution. They were washed with diethyl ether three times and dried. Yield: 94 mg (21%). Anal. Calc. for FeC₁₉H₃₆N₄O₄: C, 51.8; H 8.2; N 12.7. Found: C, 50.5; H, 8.2; N, 12.8. ESI-MS (*m/z*): calculated for the ligand (C₁₅H₃₀N₄ + H⁺) 267,255; found, 227.256 (Imin₃tren + H⁺) calculated for the complex (C₁₇H₃₃FeN₄O₂⁺) 381.195; found, 381.198 (Fe(Imin₃tren)OAc⁺). IR data are reported in the SI. Obtained crystals were suitable for structural characterization.

3.1.5.4 Synthesis of [Fe(Imine₃tren)(OAc)]OTf (2)

A solution of tren (73 mg, 0.50 mmol) in 1 mL of acetone was added dropwise to a solution of NEt₃ (30 mg, 0.30 mmol) and Fe(OAc)₂ (87 mg, 0.50 mmol) in 1 mL of acetone. After stirring for 3 h, AgOTf (128 mg, 0.50 mmol) was added. It was stirred for 5 min. and stored at -40°C for 30min. The resulting, gray suspension was filtered, then added to diethyl ether and kept at -40°C. Light yellow crystals which turned out to be suitable for X-ray analysis were obtained.

3.1.5.5 Synthesis of $[(\text{Fe}(\text{Imine}_3\text{tren}))_2(\text{F})_2](\text{SbF}_6)_2$ (4)

To a suspension of $[\text{Fe}(\text{MeCN})_6](\text{SbF}_6)_2$ (154 mg, 0.02 mmol) in acetone (1 mL) a solution of tren (28 mg, 0.02 mmol) in acetone (1 mL) was added dropwise. The light orange coloured solution was stirred for 3 h at room temperature. It was then filtered and diethyl ether was added. Slow evaporation at $-40\text{ }^\circ\text{C}$ was allowed. After storage for eight months, a few orange-coloured crystals formed that turned out to be suitable for crystallographic characterization.

3.2 Supporting Information & Additional Material

3.2.1 Synthesis of Iron Complexes

3.2.1.1 Synthesis of $[\text{Fe}(\text{Imine}_3\text{tren})(\text{OAc})]\text{BPh}_4$ (3)

To a solution of $[\text{Fe}(\text{Imine}_3\text{tren})](\text{OAc})_2$ (147 mg, 1.01 mmol) in acetone NaBPh_4 was added. After stirring for 3 h, the solution was filtered, added to diethyl ether and stored at $-40\text{ }^\circ\text{C}$. The product could be obtained as light-yellow crystals which turned out to be suitable for X-ray analysis.

3.2.1.2 Synthesis of $[\text{Fe}_2(\text{tren})_2(\text{Oxido})_2](\text{OTf})_2$ (5)

A solution of tren (146 mg, 1.00 mmol) in 1 mL of acetone was added dropwise to a solution of $[\text{Fe}(\text{MeCN})_2(\text{OTf})_2]$ (440 mg, 1.01 mmol) in 1 mL of acetone. After stirring the solution for 48 hours, it was filtered and diethyl ether was added. Slow evaporation at $-40\text{ }^\circ\text{C}$ was allowed. After four months, the product could be obtained as purple crystals which turned out to be suitable for X-ray analysis.

3.2.1.3 Synthesis of $[\text{Fe}(\text{ClEt})_2(\text{H}_2\text{O})(\text{OAc})](\text{OAc})$ (6)

A solution of tren (147 mg, 1.01 mmol) in acetone was added dropwise to a solution of triethylamine (50 mg, 0.50 mmol) and $\text{Fe}(\text{OAc})_2$ (174 mg, 1.00 mmol) in acetone. After stirring for 3 h, the solution was filtered and stored at $-40\text{ }^\circ\text{C}$. The product could be obtained as yellow crystals which turned out to be suitable for X-ray analysis.

3.2.1.4 Synthesis of $[\text{Fe}(\text{Imine}_1\text{amine}_1\text{aldol}_1\text{tren})(\text{OH}_2)](\text{NTf}_2)_2$ (7)

$[\text{Fe}(\text{H}_2\text{O})_6](\text{NTf}_2)_2$ (145 mg, 0.20 mmol) was added to an acetone/triethylamine (1:1) mixture and a solution of tren (29 mg, 0.20 mmol) in acetone/triethylamine (1:1) was added dropwise. The final solution was stirred for 3 h at room temperature. After filtration, an orange solution was obtained. The solution was stored at -40 °C and after a few days, crystals could be obtained which turned out to be suitable for X-ray analysis.

3.2.1.5 Synthesis of $[\text{Fe}(\text{Imine}_1\text{amine}_1\text{aldol}_1\text{tren})(\text{OH}_2)](\text{PF}_6)_2$ (8)

$[\text{Fe}(\text{MeCN})_6](\text{PF}_6)_2$ (178 mg, 0.30 mmol) was added to an acetone/triethylamine (1:1) mixture and a solution of tren (44 mg, 0.30 mmol) in acetone/triethylamine (1:1) was added dropwise. The yellow suspension was stirred for 3 h at room temperature. After filtration, a yellow solution was obtained. The solution was stored at -40 °C and after a few days, green crystals could be obtained which turned out to be suitable for X-ray analysis.

3.2.1.6 Synthesis of $2 [\text{Fe}(\text{tren})](\text{MeCN})_2^{2+} + [\text{Fe}((\text{CF}_3)_2\text{C}(\text{OH})(\text{O}))_4]^{2-} + [\text{Fe}((\text{CF}_3)_2\text{C}(\text{OH})(\text{O}))_4(\text{MeCN})]^{2-}$ (9)

A solution of tren (146 mg, 1.00 mmol) in acetonitrile was added to a solution of MgSO_4 (124 mg, 1.03 mmol), FeCl_2 (127 mg, 1.00 mmol) and acetonitrile. After stirring for a few minutes, $\text{HFA} \cdot 1.5 \text{ H}_2\text{O}$ (Hexafluoroacetone sesquihydrate, 583 mg, 3.51 mmol) was added. The blue suspension was stirred for 3 h, filtered and stored at -40 °C. The product could be obtained in form of purple crystals after one week which turned out to be suitable for X-ray analysis.

3.2.1.7 Synthesis of $[(\text{Fe}(\text{Imine}_3\text{tren}))_2(\text{F})_2](\text{BPh}_4)_2$ (10)

A solution of tren (29 mg, 0.20 mmol) in acetone was added dropwise to a suspension of $[\text{Fe}(\text{H}_2\text{O})_6](\text{PF}_6)_2$ (91 mg, 0.20 mmol) in acetone over molecular sieves (3 Å). After stirring for 5 h, the suspension was filtered and NaBPh_4 (137 mg, 0.40 mmol) was added. It was stirred overnight, filtered and added to diethyl ether. The solution was stored at -40 °C. After two weeks orange crystals were obtained which turned out to be suitable for X-ray analysis.

3.2.2 Electrochemical Measurements

Electrochemical data were recorded with a Princeton PAS 263 potentiostat using an H-type cell, equipped with a glassy carbon electrode as the working electrode, a platinum wire (counter electrode), and a Ag/AgCl reference electrode. The solvent was acetonitrile together with NMe_4BF_4 (0.1 mol/L). Complex concentrations were 1×10^{-3} mol/L. Ferrocene was used as an internal standard ($E^0 = 0.1$ V under these conditions) and the scan rate was at 50 mV/s.

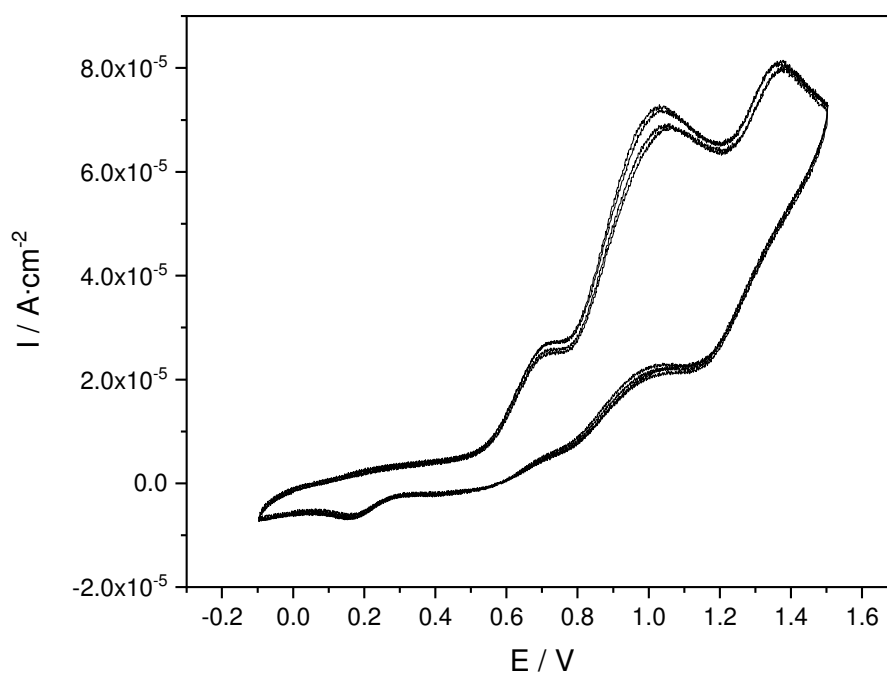


Figure 3.6: Cyclic voltammogram of $[\text{Fe}(\text{Imine}_3\text{tren})(\text{OAc})_2]$ (**1**).

3.2.3 IR Measurements

IR spectroscopy measurements were performed with a Jasco FTIR 4100 spectrometer. The samples were measured as KBr pellets.

Table 3.5: Theoretic and measured IR data of $[\text{Fe}(\text{Imine}_3\text{tren})(\text{OAc})_2]$ (1).

Modes of vibration	Intensity	Theoretic	Measured
$\nu(\text{C-H})$ (CH_3) $\nu(\text{C-H})$ (CH_2)	m	2850-2960	2986-2915
$\nu(\text{C=N})$ (CNR) $\nu(\text{C=O})$ (OCO)	s	1640-1690 1550-1610	1651-1570
$\delta(\text{C-H})$ (CH_3) $\delta(\text{C-H})$ (CH_2) $\delta(\text{C-H})$ (CH_3CO)	s	1370-1390 1430-1470 1365-1385	1460-1375
$\nu(\text{C-O})$ (OCO)	s	1300-1420	1329
$\nu(\text{C-N})$ (NR_3)	m	1250-1020	1043
$\delta(\text{C-H})$ (CH_2)	m	700-750	735
$\delta(\text{C-O})$ (OCO)	m	700-400	664

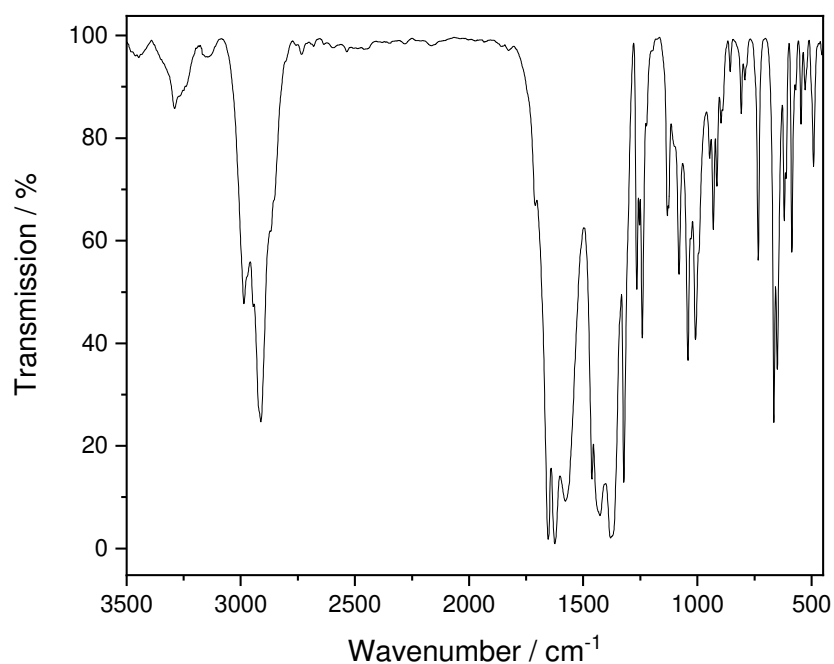


Figure 3.7: IR spectrum of $[\text{Fe}(\text{Imine}_3\text{tren})(\text{OAc})_2]$ (1).

3.2.4 UV-vis Measurements

UV-vis spectra were recorded with an Agilent 8453 spectrometer using a 10 mm quartz cuvette.

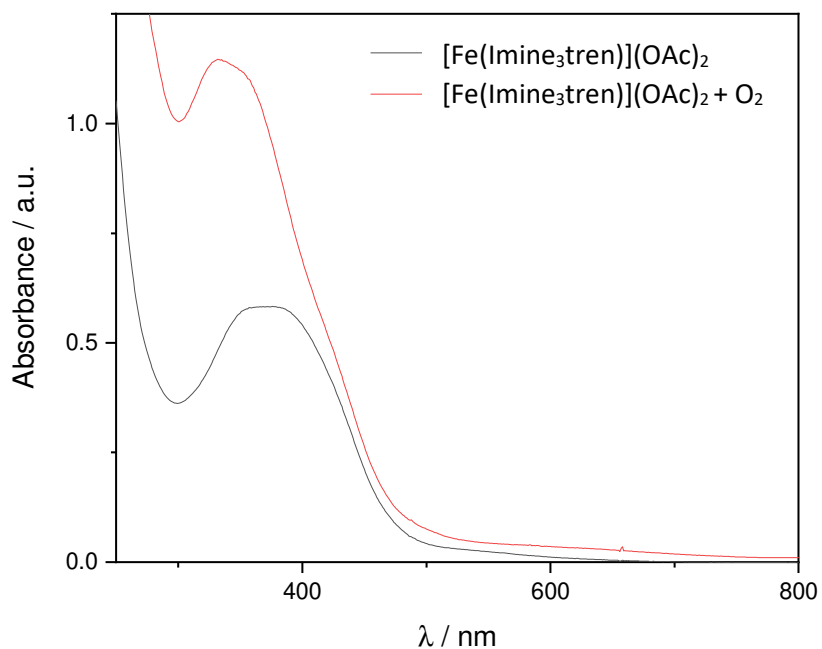


Figure 3.8: UV-vis spectra of $[\text{Fe}(\text{Imine}_3\text{tren})](\text{OAc})_2$ (1) (10^{-3} mol/L) before and after the reaction with O_2 in EtCN (O_2 was introduced at -80°C and then warmed to room temperature).

3.2.5 Low Temperature Stopped Flow Measurements

Low-temperature stopped-flow measurements were performed using a commercial HI-TECH SF-61SX2 instrument (TgK Scientific, Bratford-on-Avon, UK). Solvents used for stopped-flow measurements and experiments under inert conditions were obtained as already pure chemicals and distilled under argon atmosphere prior to transferring them into a glovebox (MBraun, Garching, Germany).

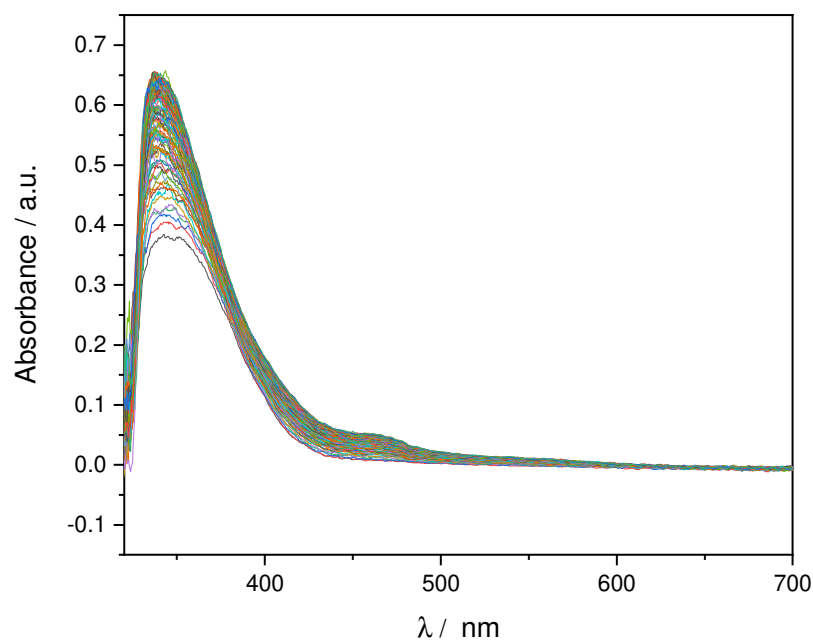


Figure 3.9: Stopped-flow measurements of the reaction of $[\text{Fe}(\text{Imine}_3\text{tren})(\text{OAc})_2]$ (**1**) (10^{-3} mol/L) with O_2 in acetone at 25 °C (total time = 32 s).

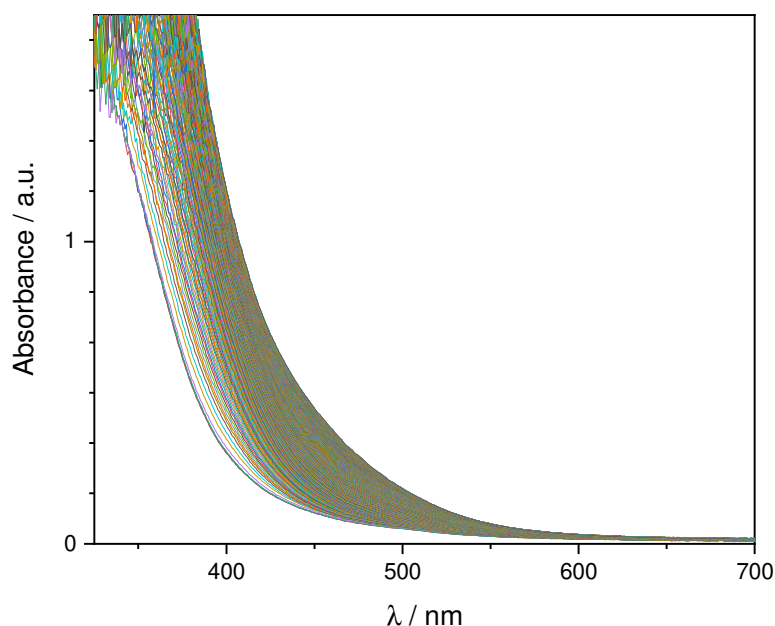


Figure 3.10: Stopped-flow measurements of the reaction of $[\text{Fe}(\text{Imine}_3\text{tren})(\text{OAc})_2]$ (**1**) (2×10^{-3} mol/L) with H_2O_2 (4×10^{-2} mol/L) in methanol at -40°C (total time = 0.75 s).

3.2.6 Details of X-ray Crystal Structure Determination

Diffraction data for all samples except for $[(\text{Fe}(\text{Imine}_3\text{tren}))_2\text{F}_2](\text{SbF}_6)$ were collected at low temperatures (100K) using ϕ - and ω -scans on a BRUKER D8 Venture System equipped with dual $\text{I}\mu\text{S}$ microfocus sources, a PHOTON100 detector and an OXFORD CRYOSYSTEMS 700 low temperature system. Mo- $\text{K}\alpha$ radiation with a wavelength of 0.71073 \AA and a collimating Quazar multilayer mirror were used.

X-ray crystallographic data for $[(\text{Fe}(\text{Imine}_3\text{tren}))_2\text{F}_2](\text{SbF}_6)$ were collected using a BRUKER/NONIUS KappaCCD detector with a BRUKER/NONIUS FR591 rotating anode radiation source and an OXFORD CRYOSYSTEMS 600 low temperature system at 193 K using ϕ - and ω -scans. Mo- $\text{K}\alpha$ radiation with a wavelength of 0.71073 \AA and a graphite monochromator were used.

Semi-empirical absorption corrections from equivalents were applied using SADABS.^[137] The structures were solved by direct methods using SHELXT^[138] and refined against F^2 on all data by full-matrix least squares using SHELXL^[138]. All non-hydrogen atoms were refined anisotropically and C-H hydrogen atoms were positioned at geometrically calculated positions and refined using a riding model. The N-H and O-H hydrogen atoms were located in the Fourier

difference map and set to ideal distances. The isotropic displacement parameters of all hydrogen atoms were fixed to 1.2x or 1.5x (CH_3 and OH hydrogens) the U_{eq} value of the atoms they are linked to. All crystallographic data were deposited with the Cambridge Crystallographic Database as 1951611-1951620 and can be obtained free of charge.^[139]

3.2.6.1 Selected Crystallographic Data

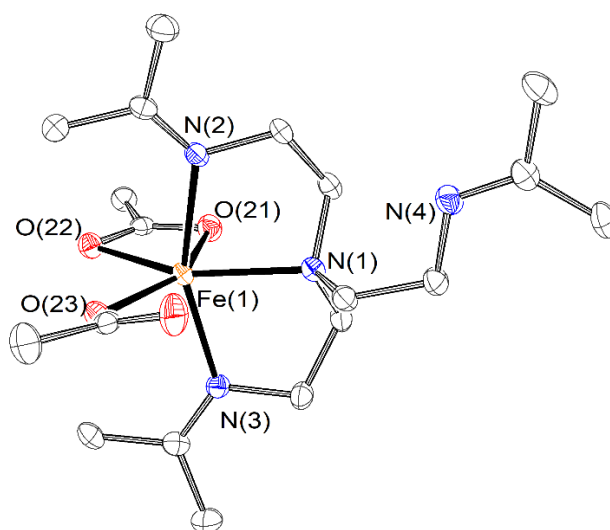


Figure 3.11: Molecular structure of $[\text{Fe}(\text{Imine}_3\text{tren})(\text{OAc})_2]$ (1).

The structure was solved in the triclinic space group $P\bar{1}$ and contains one molecule in the asymmetric unit.

Table 3.6: Crystal data and structure refinement for $[\text{Fe}(\text{Imine}_3\text{tren})(\text{OAc})_2]$ (1).

CCDC No 195161

Crystal size	0.400 x 0.280 x 0.200 mm ³
Empirical formula	$\text{C}_{19} \text{H}_{36} \text{Fe} \text{N}_4 \text{O}_4$
Formula weight	440.37
Temperature	100(2) K
Wavelength	0.71073 Å
Crystal system	Triclinic
Space group	$P\bar{1}$

Unit cell dimensions	$a = 8.9937(5) \text{ \AA}$ $b = 11.1032(6) \text{ \AA}$ $c = 11.7756(6) \text{ \AA}$	$\alpha = 93.565(2)^\circ$ $\beta = 102.532(2)^\circ$ $\gamma = 106.449(2)^\circ$
Volume	$1091.26(10) \text{ \AA}^3$	
Z	2	
Density (calculated)	1.340 mg/m^3	
Absorption coefficient	0.722 mm^{-1}	
F(000)	472	
Crystal size	$0.300 \times 0.257 \times 0.130 \text{ mm}^3$	
Theta range for data collection	2.436 to 26.731° .	
Index ranges	$-11 \leq h \leq 11$, $-14 \leq k \leq 13$, $-14 \leq l \leq 14$	
Reflections collected	52779	
Independent reflections	4628 [R(int) = 0.0922]	
Completeness to theta = 25.242°	99.9 %	
Absorption correction	Semi-empirical from equivalents	
Refinement method	Full-matrix least-squares on F^2	
Data / restraints / parameters	4628 / 0 / 261	
Goodness-of-fit on F^2	1.050	
Final R indices [$I > 2\sigma(I)$]	R1 = 0.0398, wR2 = 0.0828	
R indices (all data)	R1 = 0.0630, wR2 = 0.0918	
Largest diff. peak and hole	0.415 and $-0.358 \text{ e.\AA}^{-3}$	

Table 3.7: Selected bond lengths [\AA] and angles [$^\circ$] for $[\text{Fe}(\text{Imine}_3\text{tren})(\text{OAc})_2] \text{ (1)}$.

Fe1-N1	2.2420(17)	Fe1-N2	2.1976(18)	Fe1-N3	2.1918(18)
Fe1-O23	2.0085(15)	Fe1-O21	2.2269(16)	Fe1-O22	2.2974(15)
O23-Fe1-N2	97.66(6)	N3-Fe1-O21	87.19(6)	O23-Fe1-O21	147.82(6)
O23-Fe1-N3	96.60(7)	N2-Fe1-O21	89.83(6)	N3-Fe1-N2	157.67(7)
O23-Fe1-N1	126.95(6)	N3-Fe1-N1	79.22(6)	N2-Fe1-N1	78.48(6)
O21-Fe1-N1	85.18(6)	O23-Fe1-O22	89.86(6)	N3-Fe1-O22	99.14(6)
N2-Fe1-O22	98.00(6)	O21-Fe1-O22	58.05(5)	N1-Fe1-O22	143.18(6)

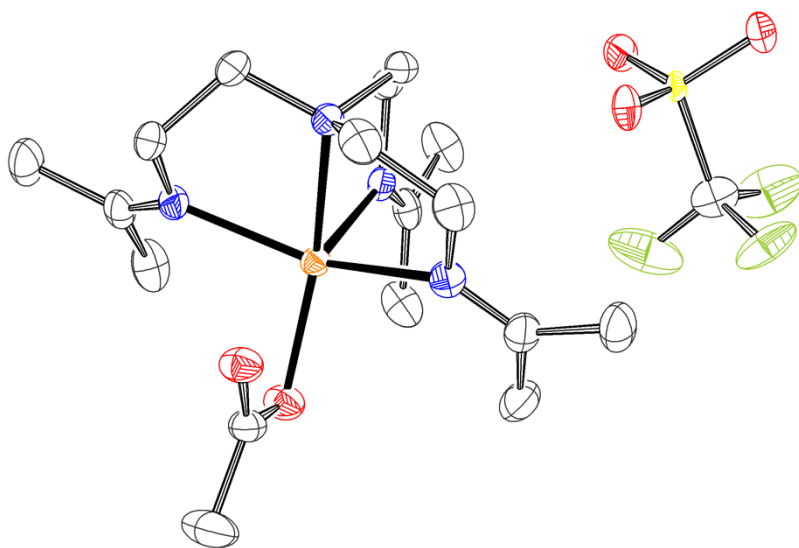


Figure 3.12: Molecular structure of the cation of [Fe(Imine₃tren)OAc]OTf (2).

CCDC No 1951615

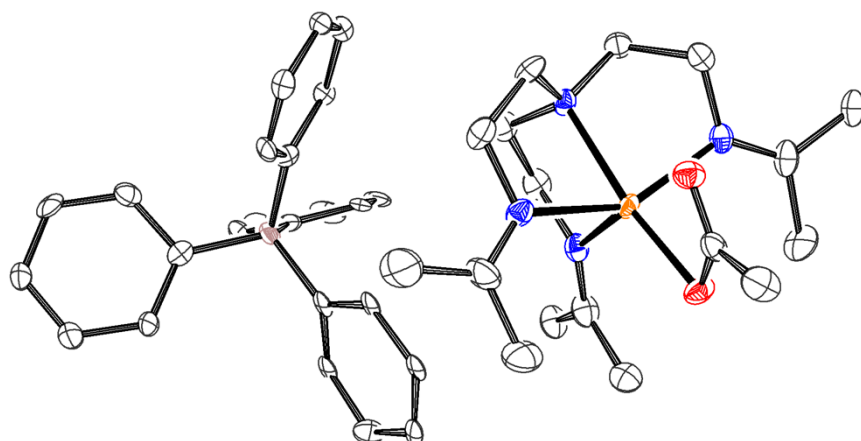
Table 3.8: Crystal data and structure refinement for [Fe(Imine₃tren)OAc]OTf (2).

Empirical formula	C ₁₈ H ₃₃ F ₃ Fe N ₄ O ₅ S	
Formula weight	530.39	
Temperature	100(2) K	
Wavelength	0.71073 Å	
Crystal system	Monoclinic	
Space group	C2/c	
Unit cell dimensions	a = 26.5956(7) Å	α = 90°.
	b = 12.0482(3) Å	β = 114.5970(10)°.
	c = 16.8118(4) Å	γ = 90°.
Volume	4898.2(2) Å ³	
Z	8	
Density (calculated)	1.438 mg/m ³	
Absorption coefficient	0.759 mm ⁻¹	
F(000)	2224	
Crystal size	0.597 x 0.234 x 0.196 mm ³	
Theta range for data collection	2.490 to 29.130°.	
Index ranges	-36 ≤ h ≤ 36, -16 ≤ k ≤ 16, -23 ≤ l ≤ 23	
Reflections collected	57199	
Independent reflections	6596 [R(int) = 0.0593]	
Completeness to theta = 25.242°	99.9 %	

Absorption correction	Semi-empirical from equivalents
Refinement method	Full-matrix least-squares on F^2
Data / restraints / parameters	6596 / 90 / 363
Goodness-of-fit on F^2	1.040
Final R indices [$I > 2\sigma(I)$]	R1 = 0.0388, wR2 = 0.0899
R indices (all data)	R1 = 0.0539, wR2 = 0.0961
Largest diff. peak and hole	0.507 and -0.391 e.Å ⁻³

Table 3.9: Selected bond lengths [Å] and angles [°] for [Fe(Imine₃tren)OAc]OTf (2).

Fe1-O22	2.1125(13)	Fe1-N1	2.1935(15)	Fe1-N4	2.2063(16)
Fe1-N3	2.1699(15)	Fe1-N2	2.1955(15)	Fe1-O21	2.2877(14)
O22-Fe1-N3	113.63(6)	N1-Fe1-N2	78.33(6)	O22-Fe1-O21	59.76(5)
O22-Fe1-N1	165.58(6)	O22-Fe1-N4	102.38(6)	N3-Fe1-O21	173.39(5)
N3-Fe1-N1	80.64(6)	N3-Fe1-N4	96.18(6)	N1-Fe1-O21	105.97(5)
O22-Fe1-N2	97.38(6)	N1-Fe1-N4	77.03(6)	N2-Fe1-O21	85.47(5)
N3-Fe1-N2	95.98(6)	N2-Fe1-N4	150.26(6)	N4-Fe1-O21	85.55(5)

Figure 3.13: Molecular structure of the cation of $[\text{Fe}(\text{Imine}_3\text{tren})\text{OAc}]\text{BPh}_4$ (3).

CCDC No 1951614

Table 3.10: Crystal data and structure refinement for $[\text{Fe}(\text{Imine}_3\text{tren})\text{OAc}]\text{BPh}_4$ (3).

Empirical formula	$\text{C}_{41} \text{H}_{53} \text{B Fe N}_4 \text{O}_2$	
Formula weight	700.53	
Temperature	100(2) K	
Wavelength	0.71073 Å	
Crystal system	Monoclinic	
Space group	$P2_1/c$	
Unit cell dimensions	$a = 18.649(13)$ Å	$\alpha = 90^\circ$.
	$b = 15.391(11)$ Å	$\beta = 114.43(2)^\circ$.
	$c = 15.972(12)$ Å	$\gamma = 90^\circ$.
Volume	$4174(5)$ Å ³	
Z	4	
Density (calculated)	1.115 mg/m^3	
Absorption coefficient	0.397 mm^{-1}	
F(000)	1496	
Crystal size	$0.221 \times 0.154 \times 0.018 \text{ mm}^3$	
Theta range for data collection	2.399 to 27.099° .	
Index ranges	$-23 \leq h \leq 23$, $-19 \leq k \leq 19$, $-20 \leq l \leq 20$	
Reflections collected	98068	
Independent reflections	9206 [$R(\text{int}) = 0.0971$]	
Completeness to $\theta = 25.242^\circ$	99.9 %	
Absorption correction	Semi-empirical from equivalents	

Refinement method	Full-matrix least-squares on F^2
Data / restraints / parameters	9206 / 2398 / 680
Goodness-of-fit on F^2	1.008
Final R indices [$I > 2\sigma(I)$]	R1 = 0.0411, wR2 = 0.0852
R indices (all data)	R1 = 0.0698, wR2 = 0.0941
Largest diff. peak and hole	0.355 and -0.332 e.Å ⁻³

Table 3.11: Selected bond lengths [Å] and angles [°] for [Fe(Imine₃tren)(OAc)]BPh₄ (3).

Fe(1)-O(1)	2.0804(18)	Fe(1)-N(4)	2.151(14)	Fe(1)-N(3)	2.181(14)
Fe(1)-N(2)	2.147(14)	Fe(1)-N(1)	2.165(13)	Fe1-O2	2.3137(16)
O1-Fe1-N2	163.7(3)	N4-Fe1-N1	98.2(7)	O1-Fe1-O2	59.88(5)
O1-Fe1-N4	113.8(3)	O1-Fe1-N3	102.2(5)	N2-Fe1-O2	103.9(3)
N2-Fe1-N4	82.4(5)	N2-Fe1-N3	110.5(3)	N4-Fe1-O2	173.1(4)
O1-Fe1-N1	98.1(5)	N4-Fe1-N3	98.3(7)	N1-Fe1-O2	85.8(7)
N2-Fe1-N1	80.4(5)	N1-Fe1-N3	149.5(5)	N3-Fe1-O2	84.9(7)

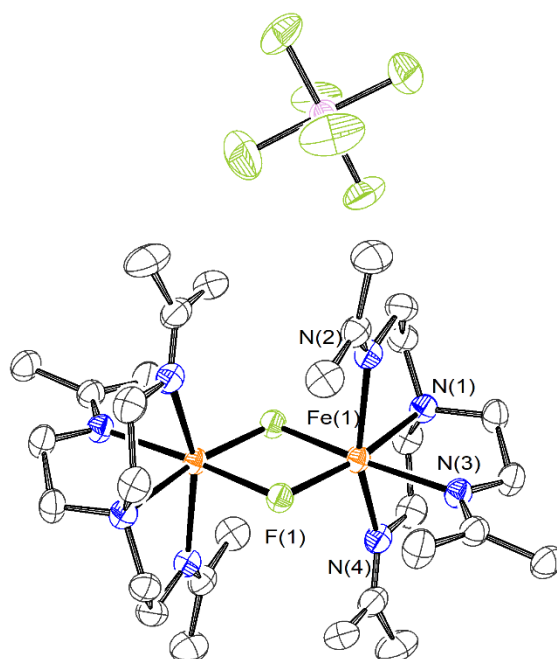


Figure 3.14: Molecular structure of $[(\text{Fe}(\text{Imine}_3\text{tren}))_2\text{F}_2](\text{SbF}_6)_2$ (4). Only one of the SbF_6^- anions is shown.

The structure was solved in the monoclinic space group $P2_1/n$. The asymmetric unit contains half of the complex and an SbF_6^- anion. The anion was found to be disordered, the disorder was modeled with the help of same distance restraints on 1,2 and 1,3 distances, similarity restraints on the anisotropic displacement parameters,^[140] advanced rigid bond restraints^[141] and the disorder ratio was allowed to refine freely and converged to 0.53(2).

CCDC No 1951616

Table 3.12: Crystal data and structure refinement for $[(\text{Fe}(\text{Imine}_3\text{tren}))_2\text{F}_2](\text{SbF}_6)$ (4).

Empirical formula	$\text{C}_{15} \text{H}_{30} \text{F}_7 \text{Fe} \text{N}_4 \text{Sb}$
Formula weight	577.03
Temperature	193(2) K
Wavelength	0.71073 Å
Crystal system	Monoclinic
Space group	$P2_1/n$

Unit cell dimensions	a = 11.814(2) Å b = 14.283(3) Å c = 13.510(3) Å	$\alpha = 90^\circ$. $\beta = 111.47(3)^\circ$. $\gamma = 90^\circ$.
Volume	2121.5(8) Å ³	
Z	4	
Density (calculated)	1.807 mg/m ³	
Absorption coefficient	2.025 mm ⁻¹	
F(000)	1152	
Crystal size	0.250 x 0.250 x 0.150 mm ³	
Theta range for data collection	2.338 to 27.602°.	
Index ranges	-14<=h<=15, -18<=k<=18, -17<=l<=17	
Reflections collected	39698	
Independent reflections	4895 [R(int) = 0.0409]	
Completeness to theta = 25.242°	99.8 %	
Absorption correction	Semi-empirical from equivalents	
Refinement method	Full-matrix least-squares on F ²	
Data / restraints / parameters	4895 / 874 / 324	
Goodness-of-fit on F ²	1.042	
Final R indices [I>2sigma(I)]	R1 = 0.0248, wR2 = 0.0586	
R indices (all data)	R1 = 0.0318, wR2 = 0.0618	
Largest diff. peak and hole	0.395 and -0.851 e.Å ⁻³	

Table 3.13: Selected bond lengths [Å] and angles [°] for [(Fe(Imine₃tren))₂F₂](SbF₆) (4).

Fe1-F1	1.9230(12)	Fe1-F1#1	2.1526(12)	Fe1-N3	2.1707(16)
Fe1-N1	2.1464(17)	Fe1-N2	2.2224(18)	Fe1-N4	2.2324(18)
F1-Fe1-N1	166.54(6)	F1#1-Fe1-N3	168.38(6)	F1-Fe1-N4	102.20(6)
F1-Fe1-F1#	78.21(5)	F1-Fe1-N2	101.95(6)	N1-Fe1-N4	77.61(7)
N1-Fe1- F(1)#1	88.32(6)	N1-Fe1-N2	77.78(7)	F1#1-Fe1-N4	90.28(6)
F1-Fe1-N3	112.33(6)	F1#1-Fe1-N2	89.98(6)	N3-Fe1-N4	82.82(6)
N1-Fe1-N3	81.08(7)	N3-Fe1-N2	92.42(7)	N2-Fe1-N4	155.37(7)
				Fe1-F1-Fe1#1	101.78(5)

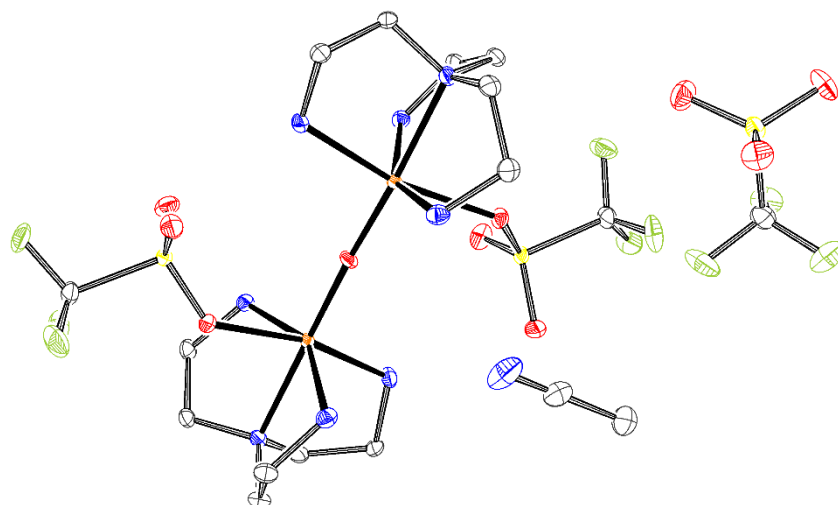


Figure 3.15: Molecular structure of $[(\text{Fe}(\text{tren}))_2\text{O}](\text{OTf})_2$ (5).

The structure was solved in the orthorhombic space group $P2_12_12$. The absolute structure was determined successfully with a Parsons parameter of 0.011(4). The asymmetric unit contains one half of the molecule with a triflate anion and an acetonitrile solvent molecule connected via hydrogen bonds and another triflate anion.

CCDC No 1951612

Table 3.14: Crystal data and structure refinement for $[(\text{Fe}(\text{tren}))_2\text{O}](\text{OTf})_2$ (5).

Empirical formula	$\text{C}_{20} \text{H}_{42} \text{F}_{12} \text{Fe}_2 \text{N}_{10} \text{O}_{13} \text{S}_4$	
Formula weight	1098.57	
Temperature	100(2) K	
Wavelength	0.71073 Å	
Crystal system	Orthorhombic	
Space group	$P2_12_12$	
Unit cell dimensions	$a = 14.3833(6)$ Å	$\alpha = 90^\circ$.
	$b = 16.7147(7)$ Å	$\beta = 90^\circ$.
	$c = 8.3845(4)$ Å	$\gamma = 90^\circ$.
Volume	$2015.74(15)$ Å ³	
Z	2	
Density (calculated)	1.810 mg/m ³	
Absorption coefficient	1.052 mm ⁻¹	

F(000)	1120
Crystal size	0.503 x 0.154 x 0.074 mm ³
Theta range for data collection	2.429 to 30.032°.
Index ranges	-20<=h<=20, -23<=k<=23, -11<=l<=11
Reflections collected	129832
Independent reflections	5915 [R(int) = 0.0592]
Completeness to theta = 25.242°	99.9 %
Absorption correction	Semi-empirical from equivalents
Refinement method	Full-matrix least-squares on F^2
Data / restraints / parameters	5915 / 6 / 295
Goodness-of-fit on F^2	1.071
Final R indices [$I > 2\sigma(I)$]	R1 = 0.0259, wR2 = 0.0615
R indices (all data)	R1 = 0.0294, wR2 = 0.0627
Absolute structure parameter	0.011(4)
Largest diff. peak and hole	0.513 and -0.355 e.Å ⁻³

Table 3.15: Selected bond lengths [Å] and angles [°] for [(Fe(tren))₂O](OTf)₂ (5).

Fe1-O1	1.7867(3)	Fe1-N4	2.140(2)	Fe1-O11	2.1869(15)
Fe1-N3	2.121(2)	Fe1-N1	2.1509(19)	Fe1-N2	2.2502(17)
O1-Fe1-N3	104.75(10)	N4-Fe1-N1	94.74(8)	O1-Fe1-N2	176.40(9)
O1-Fe1-N4	100.96(9)	O1-Fe1-O11	94.07(4)	N3-Fe1-N2	78.24(8)
N3-Fe1-N4	150.48(8)	N3-Fe1-O11	81.39(7)	N4-Fe1-N2	76.67(7)
O1-Fe1-N1	98.64(5)	N4-Fe1-O11	82.59(7)	N1-Fe1-N2	78.96(7)
N3-Fe1-N1	95.47(8)	N1-Fe1-O11	167.29(7)	O11-Fe1-N2	88.34(6)
				Fe1-O1-Fe1#1	173.65(15)

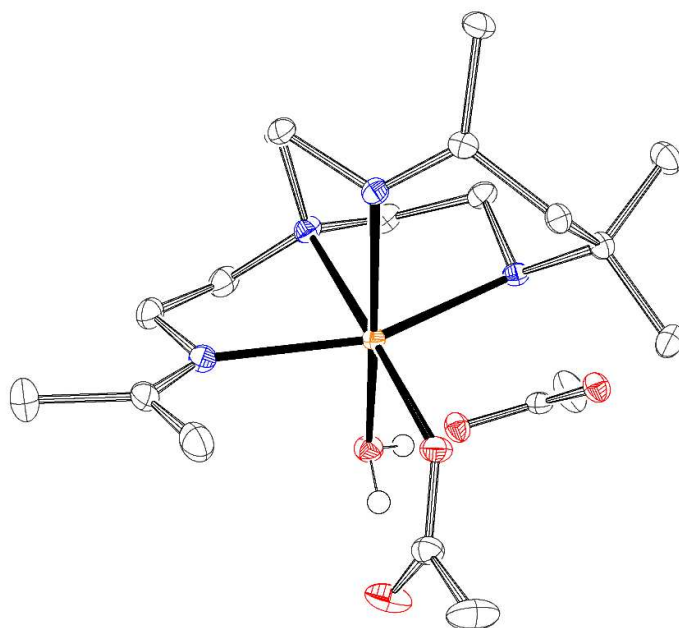


Figure 3.16: Molecular structure of $[\text{Fe}(\text{CIEI})(\text{H}_2\text{O})(\text{OAc})]\text{OAc}$ (6).

The structure was solved in the monoclinic space group $C2/c$. The asymmetric unit contains one complex molecule with an acetate anion and 1.5 water molecules bonded by hydrogen bonds and half of an acetone molecule. The $-\text{CH}_3$ moiety of one of the acetates was found to be disordered and the disordered hydrogen atoms were positioned using the AFIX 123 instruction. The disorder ratio was allowed to refine freely and converged to 0.58(2).

CCDC No 1951613

Table 3.16: Crystal data and structure refinement for $[\text{Fe}(\text{CIEI})(\text{H}_2\text{O})(\text{OAc})]\text{OAc}$ (6).

Empirical formula	$\text{C}_{20.5} \text{H}_{44} \text{Fe} \text{N}_4 \text{O}_7$	
Formula weight	514.44	
Temperature	100(2) K	
Wavelength	0.71073 Å	
Crystal system	Monoclinic	
Space group	$C2/c$	
Unit cell dimensions	$a = 18.9898(13)$ Å	$\alpha = 90^\circ$.
	$b = 15.7162(12)$ Å	$\beta = 96.824(4)^\circ$.
	$c = 17.8928(12)$ Å	$\gamma = 90^\circ$.
Volume	$5302.2(7)$ Å ³	
Z	8	

Density (calculated)	1.289 mg/m ³
Absorption coefficient	0.612 mm ⁻¹
F(000)	2216
Crystal size	0.590 x 0.510 x 0.146 mm ³
Theta range for data collection	2.592 to 30.027°.
Index ranges	-26<= <i>h</i> <=26, -22<= <i>k</i> <=22, -25<= <i>l</i> <=25
Reflections collected	167362
Independent reflections	7754 [R(int) = 0.0886]
Completeness to theta = 25.242°	99.9 %
Absorption correction	Semi-empirical from equivalents
Refinement method	Full-matrix least-squares on <i>F</i> ²
Data / restraints / parameters	7754 / 9 / 321
Goodness-of-fit on <i>F</i> ²	1.040
Final R indices [<i>I</i> >2σ(<i>I</i>)]	R1 = 0.0306, wR2 = 0.0698
R indices (all data)	R1 = 0.0415, wR2 = 0.0737
Largest diff. peak and hole	0.445 and -0.316 e.Å ⁻³

Table 3.17: Selected bond lengths [Å] and angles [°] for [Fe(CIEI)(H₂O)(OAc)]OAc (6).

Fe1-O21	2.0414(8)	Fe1-N4	2.1853(10)	Fe1-N1	2.2572(10)
Fe1-O1	2.1648(9)	Fe1-N2	2.2277(10)	Fe1-N3	2.2596(9)
O21-Fe1-O1	89.16(3)	N4-Fe1-N2	75.73(4)	O21-Fe1-N3	99.58(3)
O21-Fe1-N4	104.90(4)	O21-Fe1-N1	102.71(4)	O1-Fe1-N3	91.69(3)
O1-Fe1-N4	165.26(4)	O1-Fe1-N1	89.17(3)	N4-Fe1-N3	81.74(3)
O21-Fe1-N2	178.64(4)	N4-Fe1-N1	91.98(4)	N2-Fe1-N3	81.68(4)
O1-Fe1-N2	90.32(4)	N2-Fe1-N1	76.03(4)	N1-Fe1-N3	157.70(4)

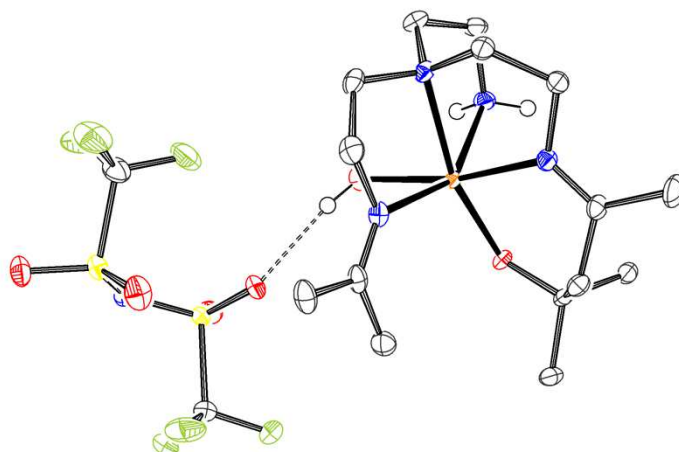


Figure 3.17: Molecular structure of $[\text{Fe}(\text{Imine}_1\text{amine}_1\text{aldol}_1\text{tren})(\text{OH}_2)]\text{NTf}_2$ (7).

The structure was solved in the monoclinic space group $P2_1/n$. The asymmetric unit contains one complex molecule and the anion bonded via hydrogen bond.

CCDC No 1951618

Table 3.18:
Crystal data and structure refinement for $[\text{Fe}(\text{Imine}_1\text{amine}_1\text{aldol}_1\text{tren})(\text{OH}_2)]\text{NTf}_2$ (7).

Empirical formula	$\text{C}_{17} \text{H}_{33} \text{F}_6 \text{Fe} \text{N}_5 \text{O}_6 \text{S}_2$	
Formula weight	637.45	
Temperature	100(2) K	
Wavelength	0.71073 Å	
Crystal system	Monoclinic	
Space group	$P2_1/n$	
Unit cell dimensions	$a = 10.0424(2)$ Å	$\alpha = 90^\circ$.
	$b = 19.1395(5)$ Å	$\beta = 92.0369(12)^\circ$.
	$c = 13.9726(4)$ Å	$\gamma = 90^\circ$.
Volume	$2683.93(12)$ Å ³	
Z	4	
Density (calculated)	1.578 mg/m^3	
Absorption coefficient	0.801 mm^{-1}	
F(000)	1320	
Crystal size	$0.395 \times 0.351 \times 0.180 \text{ mm}^3$	
Theta range for data collection	2.457 to 33.728° .	
Index ranges	$-15 \leq h \leq 15$, $-29 \leq k \leq 29$, $-21 \leq l \leq 21$	

Reflections collected	94684
Independent reflections	10714 [R(int) = 0.0502]
Completeness to theta = 25.242°	99.9 %
Absorption correction	Semi-empirical from equivalents
Refinement method	Full-matrix least-squares on F^2
Data / restraints / parameters	10714 / 4 / 351
Goodness-of-fit on F^2	1.032
Final R indices [$I > 2\sigma(I)$]	R1 = 0.0370, wR2 = 0.0878
R indices (all data)	R1 = 0.0504, wR2 = 0.0933
Largest diff. peak and hole	0.968 and -0.615 e.Å ⁻³

Table 3.19.**Selected bond lengths [Å] and angles [°] for [Fe(Imine₁amine₁aldol₁tren) (OH₂)]NTf₂ (7).**

Fe1-O1	1.9863(9)	Fe1-N4	2.1440(11)	Fe1-N1	2.2563(11)
Fe1-O2	2.1287(10)	Fe1-N3	2.2554(12)	Fe1-N2	2.2991(12)
O1-Fe1-O2	100.12(4)	N4-Fe1-N3	95.70(4)	O1-Fe1-N2	94.12(4)
O1-Fe1-N4	90.22(4)	O1-Fe1-N1	164.65(4)	O2-Fe1-N2	81.29(4)
O2-Fe1-N4	169.15(4)	O2-Fe1-N1	90.44(4)	N4-Fe1-N2	94.79(5)
O1-Fe1-N3	113.51(4)	N4-Fe1-N1	78.79(4)	N3-Fe1-N2	150.31(4)
O2-Fe1-N3	83.26(4)	N3-Fe1-N1	78.57(4)	N1-Fe1-N2	76.37(4)

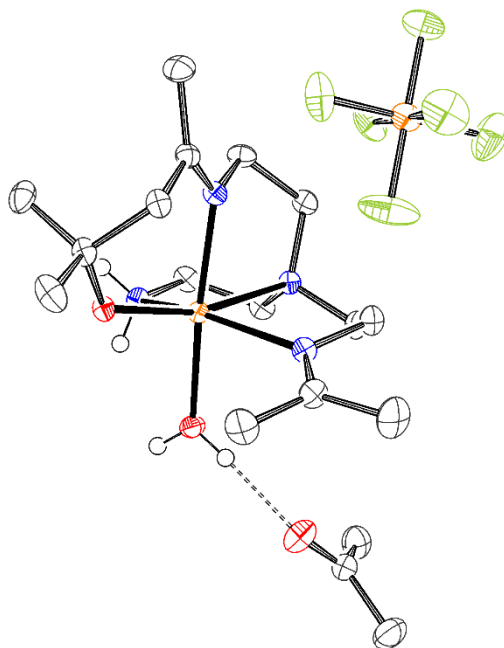


Figure 3.18: Molecular structure of $[\text{Fe}(\text{Imine}_1\text{amine}_1\text{aldol}_1\text{tren})(\text{OH}_2)]\text{PF}_6$ (8).

The crystal structure was solved in the triclinic space group $P\bar{1}$. The asymmetric unit contains one molecule of the complex, connected via hydrogen bond to an acetone molecule and the anion. The anion was found to be disordered over two positions. The disorder was refined with the help of similarity restraints on the anisotropic displacement parameters and same distance restraints on 1,2 and 1,3 distances. Because the phosphor atom positions of the anion disorder were extremely close, their anisotropic displacement parameters were set to the same parameters. The disorder ratio was refined and converged to 0.61(5).

CCDC No 1951620

Table 3.20:
Crystal data and structure refinement for $[\text{Fe}(\text{Imine}_1\text{amine}_1\text{aldol}_1\text{tren})(\text{OH}_2)]\text{PF}_6$ (8).

Empirical formula	$\text{C}_{18} \text{H}_{39} \text{F}_6 \text{Fe} \text{N}_4 \text{O}_3 \text{P}$
Formula weight	560.35
Temperature	100(2) K
Wavelength	0.71073 Å
Crystal system	Triclinic
Space group	$P\bar{1}$

Unit cell dimensions	$a = 10.4679(11) \text{ \AA}$ $b = 11.1596(11) \text{ \AA}$ $c = 12.4051(13) \text{ \AA}$	$\alpha = 110.778(3)^\circ$ $\beta = 101.155(3)^\circ$ $\gamma = 100.229(4)^\circ$
Volume	$1280.5(2) \text{ \AA}^3$	
Z	2	
Density (calculated)	1.453 mg/m^3	
Absorption coefficient	0.721 mm^{-1}	
F(000)	588	
Crystal size	$0.352 \times 0.318 \times 0.115 \text{ mm}^3$	
Theta range for data collection	2.342 to 27.484° .	
Index ranges	$-13 \leq h \leq 13$, $-13 \leq k \leq 14$, $-16 \leq l \leq 16$	
Reflections collected	85933	
Independent reflections	5874 [R(int) = 0.0783]	
Completeness to theta = 25.242°	99.9 %	
Absorption correction	Semi-empirical from equivalents	
Refinement method	Full-matrix least-squares on F^2	
Data / restraints / parameters	5874 / 487 / 375	
Goodness-of-fit on F^2	1.114	
Final R indices [$I > 2\sigma(I)$]	R1 = 0.0509, wR2 = 0.1462	
R indices (all data)	R1 = 0.0602, wR2 = 0.1553	
Largest diff. peak and hole	1.447 and $-1.180 \text{ e.\AA}^{-3}$	

Table 3.21:
Selected bond lengths [\AA] and angles [$^\circ$] for $[\text{Fe}(\text{Imine}_1\text{amine}_1\text{aldol}_1\text{tren})(\text{OH}_2)]\text{PF}_6$ (**8**).

Fe1-O1	1.9920(15)	Fe1-N4	2.1463(18)	Fe1-N1	2.2865(18)
Fe1-O2	2.1333(16)	Fe1-N3	2.2311(19)	Fe1-N2	2.2956(19)
O1-Fe1-O2	98.44(6)	N4-Fe1-N3	95.46(7)	O1-Fe1-N2	95.08(6)
O1-Fe1-N4	89.09(7)	O1-Fe1-N1	162.72(7)	O2-Fe1-N2	80.00(7)
O2-Fe1-N4	171.86(7)	O2-Fe1-N1	94.72(6)	N4-Fe1-N2	96.33(7)
O1-Fe1-N3	114.07(7)	N4-Fe1-N1	77.30(7)	N3-Fe1-N2	148.64(7)
O2-Fe1-N3	84.33(7)	N3-Fe1-N1	78.25(7)	N1-Fe1-N2	76.18(7)

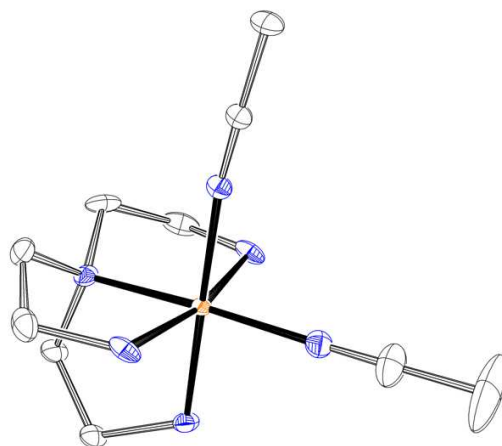


Figure 3.19: Molecular structure of a part of 9, $[\text{Fe}(\text{tren})(\text{MeCN})_2]^+$ (Part 1).

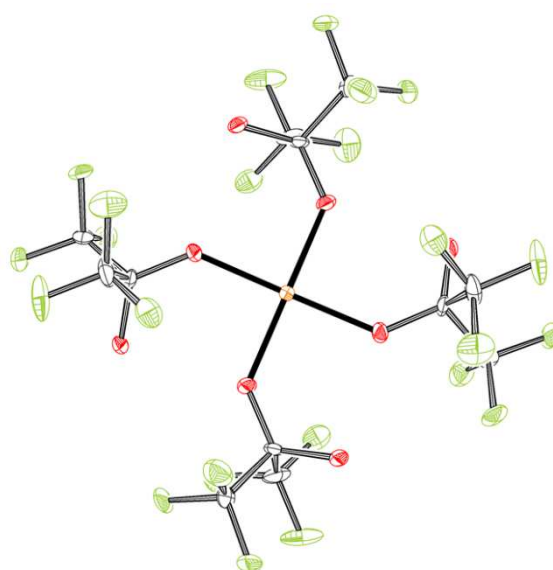


Figure 3.20: Molecular structure of a part of 9, $[\text{Fe}((\text{CF}_3)_2\text{C}(\text{OH})(\text{O}))_4]^{2-}$ (Part 2).

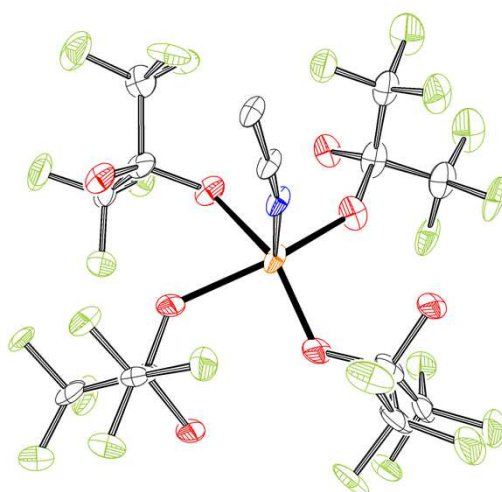


Figure 3.21: Molecular structure of a part of 9, $[\text{Fe}((\text{CF}_3)_2\text{C}(\text{OH})(\text{O}))_4(\text{MeCN})]^{2-}$ (Part 3).

The structure was solved in the tetragonal space group $P4_2/m$. The asymmetric unit contains half of an iron tren complex, where the iron ion is also coordinated by two half occupied acetonitrile molecules. Additionally, two quarter occupied iron $(\text{CF}_3)_2\text{COOH}$ complexes are found, one of them coordinating an additional acetonitrile molecule and another, not coordinated, half-occupied acetonitrile. Beside the described molecules, the asymmetric unit contains further, heavily disordered solvent molecules. As a stable refinement of these was not possible, a bulk solvent model was included into the refinement using SQUEEZE as implemented in PLATON.^[142] SQUEEZE identified two independent solvent voids in the unit cell, located at 0.0 0.5 0.0 and 0.5 0.0 0.5, each containing the equivalent of 82 electrons in 284 \AA^3 . The $(\text{CF}_3)_2\text{COOH}$ molecules were found to be disordered over two or three positions. The disorder was modeled with the help of same distance restraints, similarity restraints on the anisotropic displacement parameters and advanced rigid bond restraints. The disorder ratio was allowed to refine freely and converged to 0.587(1) and 0.482:0.241:0.277. Some anisotropic displacement parameters of the disordered molecules were set to the same parameters using the EADP instruction as implemented in SHELXL. The half-occupied, non-coordinating acetonitrile solvent molecule was restrained to a linear form by defining the sum of the C-N and C-C distance to be the same as the 1,3 C-N distance.

CCDC No 1951611

Table 3.22: Crystal data and structure refinement for $[\text{Fe}(\text{tren})(\text{Cl})_2] (\text{CF}_3)_2\text{C}(\text{OH})(\text{O})$ (9).

Empirical formula	$\text{C}_{50} \text{H}_{65} \text{F}_{48} \text{Fe}_4 \text{N}_{15} \text{O}_{16}$	
Formula weight	2267.57	
Temperature	100(2) K	
Wavelength	0.71073 Å	
Crystal system	Tetragonal	
Space group	$P4_2/m$	
Unit cell dimensions	$a = 17.6043(6) \text{ \AA}$	$\alpha = 90^\circ$.
	$b = 17.6043(6) \text{ \AA}$	$\beta = 90^\circ$.
	$c = 15.2581(6) \text{ \AA}$	$\gamma = 90^\circ$.
Volume	$4728.7(4) \text{ \AA}^3$	
Z	2	
Density (calculated)	1.593 mg/m^3	
Absorption coefficient	0.755 mm^{-1}	

F(000)	2268
Crystal size	0.423 x 0.352 x 0.288 mm ³
Theta range for data collection	2.314 to 28.699°.
Index ranges	-23<=h<=23, -23<=k<=23, -20<=l<=20
Reflections collected	156386
Independent reflections	6338 [R(int) = 0.0627]
Completeness to theta = 25.242°	99.9 %
Absorption correction	Semi-empirical from equivalents
Refinement method	Full-matrix least-squares on F^2
Data / restraints / parameters	6338 / 2235 / 650
Goodness-of-fit on F^2	1.105
Final R indices [$I > 2\sigma(I)$]	R1 = 0.0408, wR2 = 0.0936
R indices (all data)	R1 = 0.0502, wR2 = 0.0977
Largest diff. peak and hole	0.485 and -0.500 e.Å ⁻³

Table 3.23: Selected bond lengths [Å] and angles [°] for [Fe(tren)(Cl)₂](CF₃)₂C(OH)(O) (9).

Fe(1)-N(6)	1.9219(8)	Fe(1)-N(2)	1.9976(8)	Fe(1)-N(4)	2.0282(11)
Fe(1)-N(5)	1.9369(7)	Fe(1)-N(3)	2.0103(7)	Fe(1)-N(1)	2.0308(11)
N6-Fe1-N5	88.44(3)	N2-Fe1-N3	85.37(3)	N6-Fe1-N1	95.57(5)
N6-Fe1-N2	176.87(3)	N6-Fe1-N4	95.10(5)	N5-Fe1-N1	86.34(3)
N5-Fe1-N2	94.67(3)	N5-Fe1-N4	89.45(3)	N2-Fe1-N1	84.23(4)
N6-Fe1-N3	91.52(3)	N2-Fe1-N4	85.35(4)	N3-Fe1-N1	92.11(10)
N5-Fe1-N3	178.44(9)	N3-Fe1-N4	92.11(10)	N4-Fe1-N1	168.41(4)

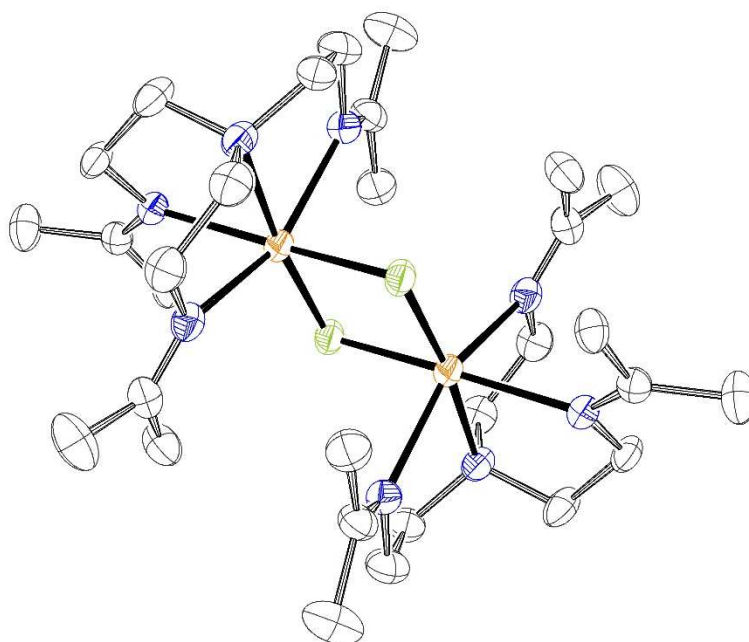


Figure 3.22: Molecular structure of the cation of $[(\text{Fe}(\text{Imine}_3\text{tren}))_2\text{F}_2](\text{BPh}_4)_2$ (10).

The crystal structure was solved in the triclinic space group $P\bar{1}$. The asymmetric unit contains two half complex molecules and two anions. Both complex molecules (except for the iron ion and the bridging fluoride ions) and both anions were found to be disordered over two positions. The disorder was refined with the help of similarity restraints on anisotropic displacement parameters, advanced rigid bond restraints, same distance restraints on 1,2 and 1,3 distances and restraints to a common plane. Some atoms with nearly identical coordinates were constrained to the same anisotropic displacement parameters. All disorder ratios were refined freely and for the complex molecules it refined to 0.883(4) and 0.915(3) and for the anions to 0.71(2) and 0.930(4).

CCDC No 1951618

Table 3.24: Crystal data and structure refinement for $[(\text{Fe}(\text{Imine}_3\text{tren}))_2\text{F}_2](\text{BPh}_4)_2$ (10).

Empirical formula	$\text{C}_{78} \text{H}_{100} \text{B}_2 \text{F}_2 \text{Fe}_2 \text{N}_8$
Formula weight	1320.97
Temperature	100(2) K
Wavelength	0.71073 Å

Crystal system	Triclinic
Space group	$P\bar{1}$
Unit cell dimensions	$a = 14.0831(4) \text{ \AA}$ $\alpha = 83.3186(13)^\circ$. $b = 14.7128(5) \text{ \AA}$ $\beta = 78.4641(12)^\circ$. $c = 17.1650(5) \text{ \AA}$ $\gamma = 84.6412(13)^\circ$.
Volume	$3452.11(18) \text{ \AA}^3$
Z	2
Density (calculated)	1.271 mg/m^3
Absorption coefficient	0.476 mm^{-1}
F(000)	1408
Crystal size	$0.099 \times 0.091 \times 0.021 \text{ mm}^3$
Theta range for data collection	2.361 to 25.682° .
Index ranges	$-17 \leq h \leq 17$, $-17 \leq k \leq 17$, $-20 \leq l \leq 20$
Reflections collected	72372
Independent reflections	13087 [R(int) = 0.0853]
Completeness to theta = 25.242°	99.9 %
Absorption correction	Semi-empirical from equivalents
Refinement method	Full-matrix least-squares on F^2
Data / restraints / parameters	13087 / 4866 / 1529
Goodness-of-fit on F^2	1.018
Final R indices [$I > 2\sigma(I)$]	$R1 = 0.0441$, $wR2 = 0.0921$
R indices (all data)	$R1 = 0.0802$, $wR2 = 0.1054$
Largest diff. peak and hole	0.286 and $-0.415 \text{ e.\AA}^{-3}$

Table 3.25: Selected bond lengths [\AA] and angles [$^\circ$] for $[(\text{Fe}(\text{Imine}_3\text{tren}))_2\text{F}_2](\text{BPh}_4)_2$ (10).

Fe1-F1	1.9533(14)	Fe1-F1#1	2.2023(14)	Fe1-N3	2.192(3)
Fe1-N1	2.229(3)	Fe1-N2	2.223(3)	Fe1-N4	2.215(3)
F1-Fe1-N1	171.0(6)	F1#1-Fe1-N3	82.76(9)	F1-Fe1-N4	102.57(10)
F1-Fe1-F1#	78.35(6)	F1-Fe1-N2	107.81(9)	N1-Fe1-N4	76.87(10)
N1-Fe1- F(1)#1	94.32(8)	N1-Fe1-N2	79.52(10)	F1#1-Fe1-N4	87.86(14)
F1-Fe1-N3	103.67(9)	F1#1-Fe1-N2	173.66(8)	N3-Fe1-N4	149.65(10)
N1-Fe1-N3	75.15(10)	N3-Fe1-N2	94.13(12)	N2-Fe1-N4	92.14(14)
				Fe1-F1-Fe1#1	78.35(6)

4 Additional Procedures

4.1 UV-vis Measurements

UV-vis spectra were measured on an Agilent 8453 spectrometer equipped with a diode array system.

4.2 IR Measurements

IR spectra of solids were measured as KBr pellet on a Bruker IFS 48, collecting data ranging from 400 to 4000 cm^{-1} using a KBr window.

5 Summary

Copper and iron enzymes in nature consist of bulky proteins with either a copper and/or an iron active site which is able to catalyze oxidation processes selectively and under mild conditions. Scientific research has already managed to replicate some of those properties using much simpler structures that are able to achieve similar results, but only under much harsher conditions. From the start, copper and iron complexes have not only been chosen because of their real-life examples, but also because being able to use copper- or iron-based compounds as opposed to their noble metal counterparts also means a more cost-effective approach to finding new catalysts which can potentially be used on an industrial scale. Furthermore, molecular dioxygen, which is preferably used, serves as a sustainable and non-polluting oxidizing agent. Therefore, finding new model compounds which are able to transfer dioxygen reversibly and selectively under as mild conditions as possible is still of great interest for an application in industrial oxidation processes. At the same time, every investigation of such new compounds leads to a better understanding of natural processes and mechanisms, which is just as important as finding new substances with (specific) applications. In recent years, a lot of progress has already been made in this field of research, but many fundamental notions e.g., of exact mechanisms still prove to be elusive. Knowing and understanding more about every single step of these processes will eventually help to find optimized ways for catalytic reactions and help to understand natural processes better.

This thesis focuses on synthetic as well as mechanistic investigations of copper and iron complexes and their reactivity towards dioxygen. Results are therefore divided into two sections: one for copper and one for iron complexes.

5.1 Synthetic and Mechanistic Investigations of Copper Complexes

Many different ligands have been designed in the past to ensure the formation of specific oxygen adduct complexes as reactive intermediates between the low and the high oxidation state of a metal complex. Depending on the steric demands and electronic properties of those ligands, either side-on or end-on oxido species of the metal precursor complex form. Also, dimerization can be enabled or prevented by choosing a specific ligand setup. To further

investigate the influence those features have on the formation of oxygen adduct complexes, a range of ligands based on the parent ligand Tren was prepared and used to investigate their effects on the formation of copper dioxygen adducts. The ligands used to create and investigate copper complexes in this thesis are depicted in Figure 5.1. Me₃tren is a compound which had to be synthesized in the past, but can now be purchased. However, the two other ligands, Isoprop₃tren and Me₃isoprop₃tren, had to be prepared and spectroscopically characterized before using.

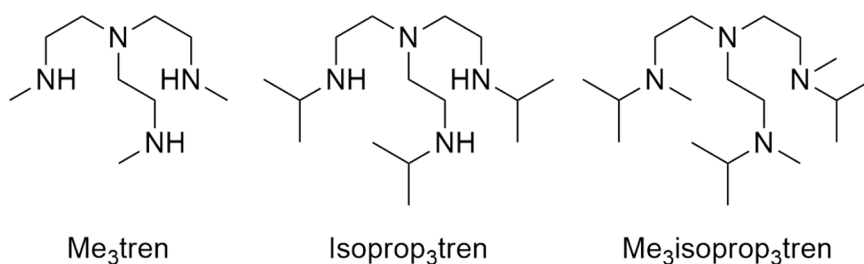


Figure 5.1: Ligands used to prepare copper dioxygen adduct complexes.

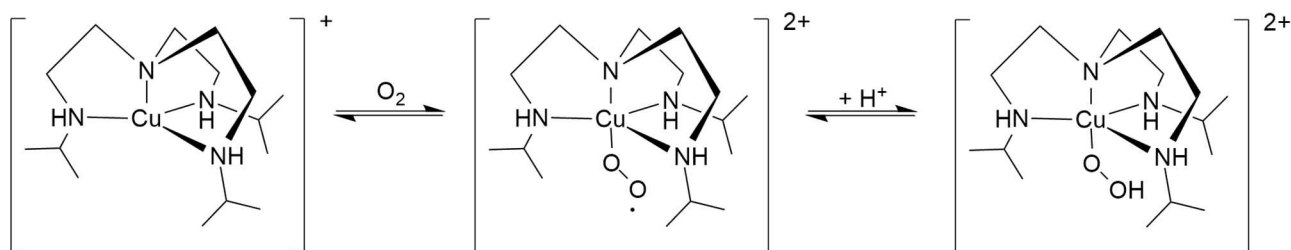
Monomeric copper(I) complexes of the ligands shown in Figure 5.1 were synthesized and structurally characterized. [Cu(Me₃tren)]⁺, [Cu(Isoprop₃tren)]⁺ and [Cu(Me₃isoprop₃tren)]⁺ all revealed a trigonal bipyramidal geometry in solid state. Additionally, copper(II) complexes of the same ligands with chloride or perchlorate as an additional ligand were prepared to predict a possible binding mode for dioxygen. [Cu(Me₃tren)MeCN](ClO₄)₂ formed an almost ideal trigonal bipyramid whereas [Cu(Isoprop₃tren)Cl]Cl displayed a distorted geometry in between a square pyramid and a trigonal bipyramid. Single crystals suitable for X-ray analysis could, unfortunately, not be obtained for [Cu(Me₃isoprop₃tren)]²⁺.

[Cu(Ligand)Cl]Cl complexes in solution were characterized by UV-vis spectroscopy and showed that the solid state geometrical shapes of complexes [Cu(Me₃tren)Cl]Cl and [Cu(Isoprop₃tren)Cl]Cl were retained in solution and [Cu(Me₃isoprop₃tren)Cl]Cl revealed a distortion towards a square pyramidal geometry.

Cyclic voltammetry showed that copper(II) complexes of Me₃tren could be reduced reversibly with a potential of -0.2 V (-0.7 V vs Ferrocene). Copper(II) complexes of the other two ligands however displayed irreversible reduction.

At low temperatures, bench top experiments of all copper(I) complexes showed colors characteristic for different oxygen adduct intermediates upon exposure to pure dioxygen which were mostly very short-lived and which all eventually resulted in dark green decomposition products. One of the complexes however, $[\text{Cu}(\text{Isoprop}_3\text{tren})]^+$ displayed a color change to an intermediate which was of dark turquoise color and was stable for about 60 minutes at -96°C before decomposition. Still, attempts to crystallize the species have not been successful yet.

As bench top experiments of all copper(I) complexes showed colors characteristic for different oxygen adduct intermediates, low temperature stopped flow studies of $[\text{Cu}(\text{Me}_3\text{tren})]\text{ClO}_4$, $[\text{Cu}(\text{Isoprop}_3\text{tren})]\text{SbF}_6$ and $[\text{Cu}(\text{Me}_3\text{isoprop}_3\text{tren})]\text{PF}_6$ in acetone were performed. In all cases, these studies revealed the initial formation of a very short-lived end-on superoxido species prior to further reactions. In case of $[\text{Cu}(\text{Me}_3\text{tren})]\text{ClO}_4$, the formation of a concomitant dinuclear end-on peroxido species could be observed. Using the more sterically shielding ligand $\text{Isoprop}_3\text{tren}$, it was possible to track the formation of the end-on superoxido complex with 0.05s at -90.4°C . However, the data could not be kinetically analyzed because of fast consecutive reactions.



Scheme 5.1: Formation of the end-on superoxido and subsequent hydroperoxido complex of $[\text{Cu}(\text{Isoprop}_3\text{tren})]^+$.

Still, the subsequent formation of another oxygen adduct species could be clearly detected which we assign to a hydroperoxido adduct complex due to the resemblance to other spectra of the same species described in research conducted by Karlin et al., Nam et al., Itoh et al. and Masuda et al. in the past. Scheme 5.1 shows a proposed pathway for the formation of a hydroperoxido intermediate when exposing $[\text{Cu}(\text{Isoprop}_3\text{tren})]\text{SbF}_6$ to pure dioxygen at low temperatures.

Even though it was expected that using Me₃isoprop₃tren (the sterically most demanding ligand of the ones prepared) would stabilize dioxygen adduct species, this goal could not be achieved. Merely the sole formation of a monomeric superoxido complex was detected which was highly unstable, led to fast consecutive reactions and eventually to a fast decay of the complex.

All of the reactions mentioned above were additionally performed in EtCN as a coordinating solvent, expecting the solvent to slow down the formation of the respective superoxido intermediates as well as any subsequent reactions to other adducts. However, low temperature stopped flow showed that this goal could not be achieved. Even though there was an isosbestic point visible in the spectra of [Cu(Me₃tren)]ClO₄, which could not be seen in the spectra when using acetone as a solvent, the species that formed could not be clearly assigned to a different oxygen intermediate due to the reaction's speed.

In case of the complex [Cu(Isoprop₃tren)]⁺, the formation of another oxygen adduct species apart from the monomeric superoxido intermediate could still be seen, but a lot less clearly than in acetone. To further investigate the nature of the forming compound more investigations will be necessary e.g., low temperature IR studies in acetone, EtCN and acetone d₆ or resonance Raman measurements. Also, phenols could be used as an alternative solvent to see whether phenolate adducts instead of a hydroperoxido moiety form during the reaction of the complex with dioxygen or hydrogen peroxide formation could be determined by performing iodometry after quenching the final reaction mixture with HPF₆.^[119]

5.2 Synthetic and Mechanistic Investigations of Iron Complexes

Taking the super-basic but rather complexly built ligand TMG₃tren as a role model for a smaller, but similarly built ligand, Imine₃tren, copper oxygen adduct complexes of that ligand were also supposed to be prepared and further investigated. The desired ligand is depicted in Figure 5.2. Surprisingly, synthesis of this ligand proved to be extremely challenging, as it could not be obtained using a simple condensation reaction even when trying to shift the equilibrium to the product's side in many different ways. Therefore, a template reaction was necessary to obtain the desired ligand. As adding copper(I) salts to a solution of the reaction

mixture merely resulted in immediate decay of the copper mixture, iron was used to substitute copper as a facilitating agent to obtain the desired ligand in its coordinated form.

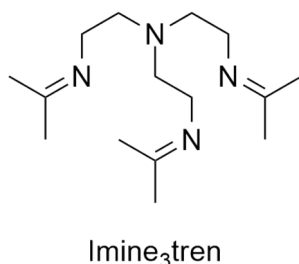


Figure 5.2: The desired ligand synthesized in coordinated form by performing template reactions between tren, acetone, NEt₃ and iron(II) salts.

Iron salts can facilitate the synthesis of template reactions, but using the right type of iron salt is crucial to the process. Many attempts to obtain an [Fe(Imine₃tren)X]⁺ complex resulted in an irreversible decay of the respective compound mixtures. The reversibility of the imine bond formation proved to be the most problematic point in this undertaking. Reversibility leads to the formation of multiple ligand products as well as product mixtures which do not necessarily contain the desired one. In general, the right choice of solvent, metal cation and anion are of paramount importance to succeed in creating a perfect environment for a template reaction. In the given case however, only anions could be interchanged to achieve the desired goal.

It could be found that using iron(II)acetate resulted in the formation of the desired complex, [Fe(Imine₃tren)(OAc)₂] and yielded crystals which could be characterized crystallographically. Interestingly, the complex displayed a six-fold coordination in which one arm of the ligand Imine₃tren was not coordinated by the iron center. Instead, two acetate anions were coordinated, one through single bond formation between an oxygen molecule and the metal center and another through formation of two bonds to the two different oxygen atoms to a second acetate anion. In Figure 5.3, an overview of the two possible coordination modes of the desired compound is shown.

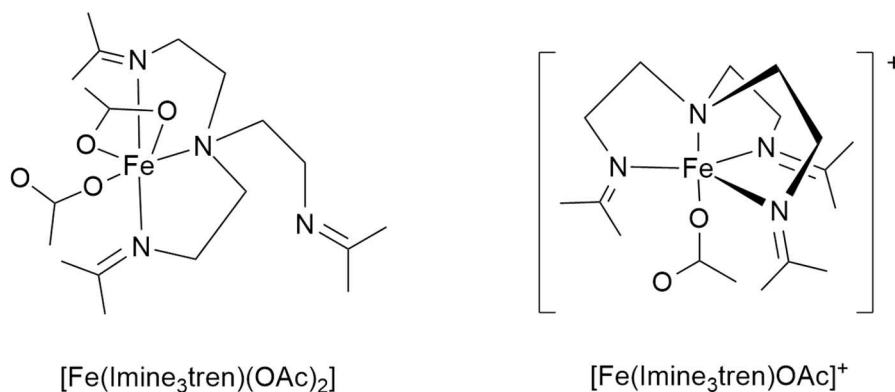


Figure 5.3: Obtained iron(II) complexes containing the desired ligand Imine₃tren.

Full coordination of the ligand Imine₃tren to the respective Fe(II) center could only be achieved by using Fe(II)(OAc)₂ salts and then swapping the anion with OTf⁻ or BPh₄⁻. The second anion prevented the coordination of a second acetate anion leaving enough space for coordination of the third arm of the ligand Imine₃tren. In these cases, coordination of the iron center was five-fold and the observed bond lengths were very similar to those that could be found in the complex [Fe(TMG₃tren)OTf]OTf.

Using NEt₃ as an additional base in the reaction mixture, it was possible to stabilize and facilitate the desired template reaction, but again, concentration of the base needed to be monitored very closely, because when highly concentrated the base initiated the formation of other, macrocyclic varieties of the desired ligand. Again, this is due to the reversible nature of the imine bond formation process.

An interesting result could be achieved using the complex salt [Fe(MeCN)₆](SbF₆)₂ to initiate the template reaction desired. After several months, the formation of a fluoro-bridged di-iron complex formed which reveals a possible binding mode for dioxygen trapping the two “external” fluor atoms in between the two iron cores. Still, as it has not been possible to obtain the desired Fe(II) complex without coordinating anions, it has not been possible to create respective oxygen adduct complexes of [Fe(Imine₃tren)X]⁺ so far either. When [Fe(Imine₃tren)(OAc)₂] was reacted with pure dioxygen at room temperature, only a very sluggish reaction could be detected. Reactions with H₂O₂, iodosobenzene or ozone never produced any detectable intermediates and only resulted in decomposition of the respective compound mixture. Therefore, it is still of great interest to obtain the imine ligand in pure

form, so that it can be used in combination with other metals, such as copper, and to study those complexes and their reactions towards dioxygen.

Curriculum Vitae

Sources & References

- [1] A. Hollemann, N. Wiberg, *Lehrbuch Der Anorganischen Chemie*, De Gruyter, Berlin, **2007**.
- [2] L. H. Gade, *Koordinationschemie*, Weinheim, **1998**.
- [3] E. Riedel, *Anorganische Chemie*, De Gruyter, Berlin, **2004**.
- [4] S. Smith, "50 fascinating things you (probably) didn't know about the Statue of Liberty," **2017** on <https://www.telegraph.co.uk/travel/destinations/north-america/united-states/new-york/articles/statue-of-liberty-fascinating-facts/> [last accessed on 11.06.2020].
- [5] W. Kaim, B. Schwederski, *Bioanorganische Chemie: Zur Funktion Chemischer Elemente in Lebensprozessen*, **2005**.
- [6] R. A. Festa, D. J. Thiele, *Curr. Biol.* **2011**, 21, R877–R883.
- [7] S. Lutsenko, A. Gupta, J. L. Burkhead, V. Zuzel, *Arch Biochem Biophys* **2008**, 476, 22–32.
- [8] B. H. Irving, R. J. P. Williams, *J. Chem. Soc.* **1953**, 3192–3210.
- [9] J. H. Kaplan, E. B. Maryon, *Biophys. J.* **2016**, 110, 7–13.
- [10] S. Lutsenko, N. L. Barnes, M. Y. Bartee, O. Y. Dmitriev, *Physiol. Rev.* **2007**, 87, 1011–1046.
- [11] J. Osredkar, *J. Clin. Toxicol.* **2011**, S3, 1–18.
- [12] P. J. M. W. L. Birker, H. C. Freeman, *J. Am. Chem. Soc.* **1977**, 99, 6890–6899.
- [13] A. Hildebrand, U. Bielefeld, *Chemkon* **1995**, 2, 65–72.
- [14] J. F. Mercer, *Am. J. Clin. Nutr.* **1998**, 67, 1022S–1028S.
- [15] J. H. Menkes, M. Alter, G. K. Steigleder, D. R. Weakley, J. H. Sung, *Pediatrics* **1962**, 29, 764–779.
- [16] D. J. Spira-Solomon, M. D. Allendorf, E. I. Solomon, *J. Am. Chem. Soc.* **1986**, 108, 5318–5328.
- [17] E. I. Solomon, U. M. Sundaram, T. E. Machonkin, *Chem. Rev.* **1996**, 96, 2563–2606.
- [18] M. Pascaly, I. Jolk, B. Krebs, *Chemie unserer Zeit* **1999**, 33, 334–341.
- [19] W. Ternes, *Biochemie Der Elemente - Anorganische Chemie Biologischer Prozesse*, Springer Spektrum, Berlin, Heidelberg, **2013**.
- [20] E. A. Lewis, W. B. Tolman, *Chem. Rev.* **2004**, 104, 1047–1076.
- [21] H. P. Latscha, M. Mutz, *Chemie Der Elemente-Chemie- Basiswissen IV*, Springer Verlag, Berlin, Heidelberg, **2011**.
- [22] A. Chakraborty, S. Ghosh, P. Mukhopadhyay, S. M. Dinara, A. Bag, M. K. Mahata, R. Kumar, S. Das, J. Sanjay, S. Majumdar, D. Biswas, in *MRS Proc.*, **2014**, pp. 81–87.
- [23] C. Janiak, D. Gudat, P. Kurz, H.-J. Meyer, *Moderne Anorganische Chemie*, De Gruyter, Berlin, **2018**.
- [24] J. Williams, *Trends Biochem. Sci.* **1982**, 7, 394–397.
- [25] P. M. H. Kroneck, M. E. S. Torres, *Sustaining Life on Planet Earth : Metalloenzymes Mastering Dioxxygen and Other Chewy Gases*, **2015**.

- [26] S. J. Lippard, J. M. Berg, *Bioanorganische Chemie*, Spektrum Akademischer Verlag, Heidelberg, Berlin, Oxford, **1995**.
- [27] M. Momenteau, C. A. Reed, *Chem. Rev.* **1994**, *94*, 659–698.
- [28] H.-J. Alsfasser, R. Janiak, C. Klapötke, T.M. Meyer, *Moderne Anorganische Chemie*, De Gruyter, Berlin, **2007**.
- [29] S. V Kryatov, E. V Rybak-Akimova, S. Schindler, *Chem. Rev.* **2005**, *105*, 2175–2226.
- [30] A. L. Feig, S. J. Lippard, *Chem. Rev.* **1994**, *94*, 759–805.
- [31] T. L. Poulos, *Chem. Rev.* **2014**, *114*, 3919–3962.
- [32] E. Y. Tshuva, S. J. Lippard, *Chem. Rev.* **2004**, *104*, 987–1012.
- [33] P. L. Holland, *Dalt. Trans.* **2010**, *39*, 5415–5425.
- [34] A. M. Reynolds, B. F. Gherman, C. J. Cramer, W. B. Tolman, *J. Am. Chem. Soc.* **2005**, *44*, 6989–6997.
- [35] C. Würtele, E. Gaoutchenova, K. Harms, M. C. Holthausen, J. Sundermeyer, S. Schindler, *Angew. Chemie* **2006**, *118*, 3951–3954.
- [36] M. T. Kieber-Emmons, J. W. Ginsbach, P. K. Wick, H. R. Lucas, M. E. Helton, B. Lucchese, M. Suzuki, A. D. Zuberbühler, K. D. Karlin, E. I. Solomon, *Angew. Chemie - Int. Ed.* **2014**, *126*, 5035–5039.
- [37] S. Schindler, *Eur. J. Inorg. Chem.* **2000**, 2311–2326.
- [38] R. Jacobson, Z. Tyeklár, A. Farooq, K. D. Karlin, S. Liu, J. Zubieta, *J. Am. Chem. Soc.* **1988**, *110*, 3690–3692.
- [39] K. Fujisawa, M. Tanaka, Y. Moro-oka, N. Kitajima, *J. Am. Chem. Soc.* **1994**, *116*, 12079–12080.
- [40] L. Q. Hatcher, M. A. Vance, A. A. N. Sarjeant, E. I. Solomon, K. D. Karlin, *Inorg. Chem.* **2006**, *45*, 3004–3013.
- [41] T. Fujii, S. Yamaguchi, H. Masuda, *Dalt. Trans.* **2008**, 164–170.
- [42] T. Hoppe, S. Schaub, J. Becker, C. Würtele, S. Schindler, *Angew. Chemie Int. Ed.* **2013**, *52*, 870–873.
- [43] G. M. Yee, W. B. Tolman, in *Sustain. Life Planet Earth Met. Mastering Dioxygen Other Chewy Gases* (Eds.: P.M.H. Kroneck, M.E. Sosa Torres), Springer International Publishing, Cham, **2015**, pp. 131–204.
- [44] T. C. Brunold, E. I. Solomon, *J. Am. Chem. Soc.* **1999**, *121*, 8277–8287.
- [45] A. J. Jasniewski, L. Que, *Chem. Rev.* **2018**, *118*, 2554–2592.
- [46] W. Kaim, *Dalt. Trans.* **2003**, 761–768.
- [47] J. J. Liu, D. E. Diaz, D. A. Quist, K. D. Karlin, *Isr. J. Chem.* **2016**, *56*, 738–755.
- [48] N. W. Aboeella, A. M. Reynolds, W. B. Tolman, *Science* **2004**, *304*, 836–837.
- [49] K. D. Karlin, N. Wei, B. Jung, S. Kaderli, P. Niklaus, A. D. Zuberbühler, *J. Am. Chem. Soc.* **1993**, *115*, 9506–9514.
- [50] M. Schatz, M. Becker, F. Thaler, F. Hampel, S. Schindler, R. R. Jacobson, Z. Tyeklár, N. N.

- Murthy, P. Ghosh, Q. Chen, J. Zubietta, K. D. Karlin, *Inorg. Chem.* **2001**, *40*, 2312–22.
- [51] C. Würtele, E. Gaoutchenova, K. Harms, M. C. Holthausen, J. Sundermeyer, S. Schindler, *Angew. Chemie* **2006**, *45*, 3867–3869.
- [52] J. S. Woertink, L. Tian, D. Maiti, H. R. Lucas, R. A. Himes, K. D. Karlin, F. Neese, C. Würtele, M. C. Holthausen, X. E. Bill, J. Sundermeyer, S. Schindler, E. I. Solomon, *Inorg. Chem.* **2010**, *49*, 9450–9459.
- [53] N. Kitajima, K. Fujisawa, Y. Moro-oka, *J. Am. Chem. Soc.* **1989**, *111*, 8975–8976.
- [54] Y. Zang, J. Kim, Y. Dong, E. C. Wilkinson, E. H. Appelman, L. Que, *J. Am. Chem. Soc.* **1997**, *119*, 4197–4205.
- [55] J. Cho, S. Jeon, S. A. Wilson, L. V. Liu, E. A. Kang, J. J. Braymer, M. H. Lim, B. Hedman, K. O. Hodgson, J. S. Valentine, E. I. Solomon, W. Nam, *Nature* **2011**, *478*, 502–505.
- [56] J. A. R. Hartman, R. L. Rardin, P. Chaudhuri, K. Pohl, K. Wiegardt, B. Nuber, J. Weiss, G. C. Papaefthymiou, R. B. Frankel, S. J. Lippard, *J. Am. Chem. Soc.* **1987**, *109*, 7387–7396.
- [57] P. Chaudhury, K. Wiegardt, B. Nuber, J. Weiss, *Angew. Chemie Int. Ed. English* **1985**, *24*, 778–779.
- [58] K. Kim, S. J. Lippard, *J. Am. Chem. Soc.* **1996**, *118*, 4914–4915.
- [59] C. Jain, E. C. Lingafelter, *J. Am. Chem. Soc.* **1967**, *3*, 724.
- [60] M. Duggan, N. Ray, B. Hathaway, G. Tomlinson, P. Brint, K. Pelin, *Dalt. Trans.* **1980**, 1342–1348.
- [61] M. Ciampolini, N. Nardi, *Inorg. Chem.* **1966**, *5*, 41–44.
- [62] M. Becker, F. W. Heinemann, S. Schindler, *Chem. - A Eur. J.* **1999**, *5*, 3124–3129.
- [63] K. Komiyama, H. Furutachi, S. Nagamoto, A. Hashimoto, H. Hayashi, S. Fujinami, M. Suzuki, T. Kitagawa, *Bull. Chem. Soc. Jpn.* **2004**, *77*, 59–72.
- [64] M. Weitzer, S. Schindler, G. Brehm, S. Schneider, E. Hörmann, B. Jung, S. Kaderli, A. D. Zuberbühler, *Inorg. Chem.* **2003**, *42*, 1800–1806.
- [65] M. Weitzer, M. Schatz, F. Hampel, W. Heinemann, S. Schindler, *Dalt. Trans.* **2002**, 686–694.
- [66] M. Becker, F. W. Heinemann, S. Schindler, *Chem. – A Eur. J.* **1999**, *5*, 3124–3129.
- [67] G. J. P. Britovsek, J. England, A. J. P. White, I. C. London, E. Road, *Inorg. Chem.* **2005**, *44*, 8125–8134.
- [68] S. Kisslinger, H. Kelm, A. Beitat, C. Würtele, H. Krüger, S. Schindler, *Inorganica Chim. Acta* **2011**, *374*, 540–545.
- [69] S. Schäfer, J. Becker, A. Beitat, C. Würtele, *ZAAC* **2013**, 2269–2275.
- [70] C. Würtele, F. W. Heinemann, S. Schindler, *J. Coord. Chem.* **2010**, *63*, 2629–2641.
- [71] M. Sarma, A. Kalita, P. Kumar, A. Singh, B. Mondal, *J. Am. Chem. Soc.* **2010**, *132*, 7846–7847.
- [72] M. Merkel, M. Pascaly, B. Krebs, J. Astner, S. P. Foxon, S. Schindler, *Inorg. Chem.* **2005**, *44*, 7582–7589.
- [73] K.-B. Cho, S. Shaik, W. Nam, *Chem. Commun.* **2010**, *46*, 4511–4513.

- [74] S. V Kryatov, E. V Rybak-Akimova, V. L. MacMurdo, L. Que, *Inorg. Chem.* **2001**, *40*, 2220–2228.
- [75] A. L. Feig, M. Becker, S. Schindler, R. van Eldik, S. J. Lippard, *Inorg. Chem.* **1996**, *35*, 2590–2601.
- [76] C. X. Zhang, S. Kaderli, M. Costas, E. Kim, Y. Neuhold, K. D. Karlin, A. D. Zuberbühler, *Inorg. Chem.* **2003**, *42*, 1807–1824.
- [77] C. Würtele, *End-On “Copper Dioxygen Adduct Complexes,”* JLU Gießen, Gießen, **2008**.
- [78] M. Schatz, M. Becker, O. Walter, *Inorganica Chim. Acta* **2001**, *324*, 173–179.
- [79] F. Thaler, C. D. Hubbard, F. W. Heinemann, R. van Eldik, S. Schindler, I. Fábíán, A. M. Dittler-Klingemann, F. E. Hahn, C. Orvig, *Inorg. Chem.* **1998**, *37*, 4022–4029.
- [80] A. J. Fischmann, A. C. Warden, J. Black, L. Spiccia, *Inorg. Chem.* **2004**, *43*, 6568–78.
- [81] M. Costas, M. P. Mehn, M. P. Jensen, L. Que, *Chem. Rev.* **2004**, *104*, 939–986.
- [82] L. Que, *Acc. Chem. Res.* **2007**, *40*, 493–500.
- [83] L. M. Mirica, X. Ottenwaelde, T. D. P. Stack, *Chem. Rev.* **2004**, *104*, 1013–1045.
- [84] I. P. Y. Shek, T. Lau, W. Wong, J. Zuo, F. June, A. September, *New J. Chem.* **1999**, *23*, 1049–1050.
- [85] V. Raab, J. Kipke, O. Burghaus, J. Sundermeyer, *Inorg. Chem.* **2001**, *40*, 6964–6971.
- [86] J. Will, C. Würtele, J. Becker, O. Walter, S. Schindler, *Polyhedron* **2019**, *171*, 448–454.
- [87] H. Decker, T. Schweikardt, F. Tuczek, *Angew. Chemie Int. Ed.* **2006**, *45*, 4546–4550.
- [88] E. Solem, F. Tuczek, H. Decker, *Angew. Chemie Int. Ed.* **2016**, *55*, 2884–2888.
- [89] S. Itoh, S. Fukuzumi, *Acc. Chem. Res.* **2007**, *40*, 592–600.
- [90] P. Gamez, I. A. Koval, J. Reedijk, *Dalt. Trans.* **2004**, 4079–4088.
- [91] J. A. Drewry, P. T. Gunning, *Coord. Chem. Rev.* **2011**, *255*, 459–472.
- [92] C. E. Elwell, N. L. Gagnon, B. D. Neisen, D. Dhar, A. D. Spaeth, G. M. Yee, W. B. Tolman, *Chem. Rev.* **2017**, *117*, 2059–2107.
- [93] E. I. Solomon, S. S. Stahl, *Chem. Rev.* **2018**, *118*, 2299–2301.
- [94] V. C.-C. Wang, S. Maji, P. P.-Y. Chen, H. K. Lee, S. S.-F. Yu, S. I. Chan, *Chem. Rev.* **2017**, *117*, 8574–8621.
- [95] D. A. Quist, D. E. Diaz, J. J. Liu, K. D. Karlin, *JBIC J. Biol. Inorg. Chem.* **2017**, *22*, 253–288.
- [96] M. Schatz, M. Leibold, S. P. Foxon, M. Weitzer, F. W. Heinemann, F. Hampel, S. Schindler, *Dalt. Trans.* **2003**, 1480–1487.
- [97] K. D. Karlin, S. Kaderli, A. D. Zuberbühler, *Acc. Chem. Res.* **1997**, *30*, 139–147.
- [98] C. Würtele, O. Sander, V. Lutz, T. Waitz, F. Tuczek, S. Schindler, *J. Am. Chem. Soc.* **2009**, *131*, 7544–7545.
- [99] D. Maiti, D.-H. Lee, K. Gaoutchenova, C. Würtele, M. C. Holthausen, A. A. Narducci Sarjeant, J. Sundermeyer, S. Schindler, K. D. Karlin, *Angew. Chemie Int. Ed.* **2008**, *47*, 82–85.
- [100] M. Schatz, V. Raab, S. P. Foxon, G. Brehm, S. Schneider, M. Reiher, M. C. Holthausen, J.

- Sundermeyer, S. Schindler, *Angew. Chemie - Int. Ed.* **2004**, *43*, 4360–4363.
- [101] S. T. Prigge, B. A. Eipper, R. E. Mains, L. M. Amzel, *Science* **2004**, *304*, 864–7.
- [102] W. D. Bailey, D. Dhar, A. C. Cramblitt, W. B. Tolman, *J. Am. Chem. Soc.* **2019**, *141*, 5470–5480.
- [103] T. Abe, Y. Hori, Y. Shiota, T. Ohta, Y. Morimoto, H. Sugimoto, T. Ogura, K. Yoshizawa, S. Itoh, *Commun. Chem.* **2019**, *2*, 12.
- [104] M. Bhadra, J. Y. C. Lee, R. E. Cowley, S. Kim, M. A. Siegler, E. I. Solomon, K. D. Karlin, *J. Am. Chem. Soc.* **2018**, *140*, 9042–9045.
- [105] G. J. Kubas, *Inorg. Synth.* **1979**, *19*, 90–92.
- [106] SHELX-97: G. M. Sheldrick, Universität Göttingen, **1997**.
- [107] H. Gampp, M. Maeder, C. J. Meyer, A. D. Zuberbühler, *Talanta* **1985**, *32*, 95–101.
- [108] F. Thaler, C. D. Hubbard, F. W. Heinemann, R. van Eldik, S. Schindler, I. Fábíán, A. M. Dittler-Klingemann, F. E. Hahn, C. Orvig, *Inorg. Chem.* **1998**, *37*, 4022–4029.
- [109] H. T. Clarke, H. B. Gillespie, S. Z. Weisshaus, *J. Am. Chem. Soc.* **1933**, *55*, 4571–4587.
- [110] W. Eschweiler, *Chem. Ber.* **1905**, *38*, 880–882.
- [111] Z. Tyeklar, R. R. Jacobson, N. Wei, N. N. Murthy, J. Zubieta, K. D. Karlin, *J. Am. Chem. Soc.* **1993**, *115*, 2677–2689.
- [112] A. W. Addison, T. N. Rao, *Dalt. Trans.* **1984**, 1349–1356.
- [113] M. Becker, F. W. Heinemann, F. Knoch, W. Donaubauer, G. Liehr, S. Schindler, G. Golub, H. Cohen, D. Meyerstein, *Eur. J. Inorg. Chem.* **2000**, 719–726.
- [114] Y. J. Choi, K.-B. Cho, M. Kubo, T. Ogura, K. D. Karlin, J. Cho, W. Nam, *Dalt. Trans.* **2011**, *40*, 2234.
- [115] D. V. Yandulov, R. R. Schrock, *Science* **2003**, *301*, 76–78.
- [116] Y. Kobayashi, K. Ohkubo, T. Nomura, M. Kubo, N. Fujieda, H. Sugimoto, S. Fukuzumi, K. Goto, T. Ogura, S. Itoh, *Eur. J. Inorg. Chem.* **2012**, *2012*, 4574–4578.
- [117] A. de la Lande, H. Gérard, V. Moliner, G. Izzet, O. Reinaud, O. Parisel, *JBIC J. Biol. Inorg. Chem.* **2006**, *11*, 593–608.
- [118] R. L. Peterson, J. W. Ginsbach, R. E. Cowley, M. F. Qayyum, R. A. Himes, M. A. Siegler, C. D. Moore, B. Hedman, K. O. Hodgson, S. Fukuzumi, E. I. Solomon, K. D. Karlin, *J. Am. Chem. Soc.* **2013**, *135*, 16454–16467.
- [119] T. Tano, Y. Okubo, A. Kunishita, M. Kubo, H. Sugimoto, N. Fujieda, T. Ogura, S. Itoh, *Inorg. Chem.* **2013**, *52*, 10431–10437.
- [120] L. Q. Hatcher, K. D. Karlin, *JBIC J. Biol. Inorg. Chem.* **2004**, *9*, 669–683.
- [121] S. Yamaguchi, S. Nagatomo, T. Kitagawa, Y. Funahashi, T. Ozawa, K. Jitsukawa, H. Masuda, *Inorg. Chem.* **2003**, *42*, 6968–6970.
- [122] G. J. Karahalís, A. Thangavel, B. Chica, J. Bacsá, R. B. Dyer, C. C. Scarborough, *Inorg. Chem.* **2016**, *55*, 1102–1107.
- [123] C. Citek, B.-L. Lin, T. E. Phelps, E. C. Wasinger, T. D. P. Stack, *J. Am. Chem. Soc.* **2014**, *136*, 14405–14408.

- [124] J. Will, L. Schneider, J. Becker, S. Becker, A. Miska, C. Gawlig, S. Schindler, *Isr. J. Chem.* **2020**, *60*, 999–1003.
- [125] A. Trehoux, J. P. Mahy, F. Avenier, *Coord. Chem. Rev.* **2016**, *322*, 142–158.
- [126] Y. Lee, S. Hong, Y. Morimoto, W. Shin, S. Fukuzumi, W. Nam, *J. Am. Chem. Soc.* **2010**, *132*, 10668–10670.
- [127] L. Que, Y. Dong, *Acc. Chem. Res.* **1996**, *29*, 190–196.
- [128] C. J. Reed, T. Agapie, *J. Am. Chem. Soc.* **2019**, *141*, 9479–9484.
- [129] A. S. Borovik, C. E. MacBeth, A. P. Golombek, V. G. Young, C. Yang, K. Kuczera, M. P. Hendrich, *Science* **2000**, *289*, 938–941.
- [130] J. England, M. Martinho, E. R. Farquhar, J. R. Frisch, E. L. Bominaar, E. Münck, L. Que, *Angew. Chemie - Int. Ed.* **2009**, *48*, 3622–3626.
- [131] A. R. McDonald, L. Que, *Coord. Chem. Rev.* **2013**, *257*, 414–428.
- [132] S. Schaub, A. Miska, J. Becker, S. Zahn, D. Mollenhauer, S. Sakshath, V. Schünemann, S. Schindler, *Angew. Chemie - Int. Ed.* **2018**, *57*, 5355–5358.
- [133] S. P. de Visser, J. U. Rohde, Y. M. Lee, J. Cho, W. Nam, *Coord. Chem. Rev.* **2013**, *257*, 381–393.
- [134] K. I. Alexopoulou, L. Schneider, A. Miska, C. Würtele, S. Schindler, *ZAAC* **2018**, *644*, 759–762.
- [135] S. Kisslinger, H. Kelm, S. Zheng, A. Beitat, C. Würtele, R. Wortmann, S. Bonnet, S. Herres-Pawlis, H. J. Krüger, S. Schindler, *ZAAC* **2012**, *638*, 2069–2077.
- [136] T. P. Zimmermann, S. Dammers, A. Stammler, H. Bögge, T. Glaser, *Eur. J. Inorg. Chem.* **2018**, 5229–5237.
- [137] L. Krause, R. Herbst-Irmer, G. M. Sheldrick, D. Stalke, *J. Appl. Crystallogr.* **2015**, *48*, 3–10.
- [138] G. M. Sheldrick, *Acta Crystallogr. Sect. A* **2015**, *71*, 3–8.
- [139] “<https://www.ccdc.cam.ac.uk/structures/>”
- [140] P. Müller, *Crystallogr. Rev.* **2009**, *15*, 57–83.
- [141] A. Thorn, B. Dittrich, G. M. Sheldrick, *Acta Crystallogr. Sect. A* **2012**, *68*, 448–451.
- [142] A. L. Spek, *Acta Crystallogr. Sect. C* **2015**, *71*, 9–18.
- [143] M. R. Bukowski, S. Zhu, K. D. Koehntop, W. W. Brennessel, L. Que, *J. Biol. Inorg. Chem.* **2004**, *9*, 39–48.

List of Figures

Figure 1.1: The copper scavenging amino acid D-Pen depicted in its ionic form as a zwitterion.....	3
Figure 1.2: Deferoxamine B.....	11
Figure 1.3: The porphyrin sub-unit in its protonated, deprotonated and coordinated form.....	12
Figure 1.4: The three heme protein categories; heme a, b and c.....	13
Figure 1.5: The active site of the iron proteins hemoglobin and myoglobin	14
Figure 1.6: Proposed structure for ‘activated bleomycin’.....	15
Figure 1.7: Copper-oxygen cores characterized in synthetic complexes so far	20
Figure 1.8: The active site of sMMO in its reduced and its oxidized state.....	21
Figure 1.9: Ligands used to synthesize the respective copper(II) oxygen adduct complexes.....	23
Figure 1.10: Ligands used to synthesize the respective copper(II) oxygen adduct complexes.....	24
Figure 1.11: The first synthetic complex to model the active site of hemerythrin using the ligand Me ₃ TACN and one of the few non-heme iron oxygen adduct complexes determined by X- ray crystallography and the ligand used	26
Figure 1.12: An array of tripodal, tetradentate ligands based on the tren unit used in copper and iron bioinorganic chemistry.....	28
Figure 1.13: Aliphatic derivatives of the parent ligand tren. Left, already successfully investigated ligand systems elsewhere	34
Figure 2.1: List of ligands.....	37
Figure 2.2: Molecular structures of the cations of [Cu(Me ₃ tren)]ClO ₄ , [Cu(Isoprop ₃ tren)]SO ₃ CF ₃ and [Cu(Me ₃ isoprop ₃ tren)]BPh ₄	44
Figure 2.3: Molecular structure of [Cu(Isoprop ₃ tren)Cl]Cl.....	46
Figure 2.4: Reacting 1 with dioxygen in acetone in a bench top experiment at –80 °C	48
Figure 2.5: Reaction of [Cu(Me ₃ tren)] ⁺ with dioxygen in acetone at -76°C	50
Figure 2.6: Reaction of [Cu(Isoprop ₃ tren)] ⁺ with dioxygen in acetone at -90.4°C	51
Figure 2.7: Reaction of [Cu(Isoprop ₃ tren)] ⁺ with dioxygen in acetone at -95°C	52
Figure 2.8: Reaction of [Cu(Me ₃ isoprop ₃ tren)] ⁺ with dioxygen in acetone at -86°C.....	53

Figure 2.9: Time-resolved spectra of the reaction of $[\text{Cu}(\text{Me}_3\text{tren})\text{ClO}_4]$ with dioxygen using low temperature stopped flow techniques	62
Figure 2.10: Time-resolved spectra of the reaction of $[\text{Cu}(\text{Isoprop}_3\text{tren})]\text{SbF}_6$ with dioxygen using low temperature stopped flow techniques	63
Figure 2.11: UV-vis data of the copper(II) complexes $[\text{Cu}(\text{Me}_3\text{tren})\text{Cl}]\text{Cl}$, $[\text{Cu}(\text{Isoprop}_3\text{tren})\text{Cl}]\text{Cl}$ and $[\text{Cu}(\text{Me}_3\text{isoprop}_3\text{tren})\text{Cl}]\text{Cl}$	64
Figure 3.1: Tripodal ligands a) tmpa, b) tren ($R_1 = R_2 = \text{H}$), c) protonated $[\text{H}_3\text{1}]^{3+}$, d) TMG_3tren and e) $\text{Imine}_3\text{tren}$	66
Figure 3.2: Different ligands obtained from the template reaction of iron(II) salts with tren and acetone	67
Figure 3.3: Molecular structure of $[\text{Fe}(\text{Imine}_3\text{tren})(\text{OAc})_2]$	70
Figure 3.4: Molecular structure of $[(\text{Fe}(\text{Imine}_3\text{tren})(\text{OAc}))\text{OTf}]$	70
Figure 3.5: Molecular structure of the cation of the cation of $[(\text{Fe}(\text{Imine}_3\text{tren}))_2(\text{F}_2)](\text{SbF}_6)_2$	72
Figure 3.6: Cyclic voltammogram of $[\text{Fe}(\text{Imine}_3\text{tren})(\text{OAc})_2]$	77
Figure 3.7: IR spectrum of $[\text{Fe}(\text{Imine}_3\text{tren})(\text{OAc})_2]$	78
Figure 3.8: UV-vis spectra of $[\text{Fe}(\text{Imine}_3\text{tren})(\text{OAc})_2]$ before and after the reaction with O_2 in EtCN ..	79
Figure 3.9: Stopped-flow measurements of the reaction of $[\text{Fe}(\text{Imine}_3\text{tren})(\text{OAc})_2]$ with O_2 in acetone at 25 °C	80
Figure 3.10: Stopped-flow measurements of the reaction of $[\text{Fe}(\text{Imine}_3\text{tren})(\text{OAc})_2]$ with H_2O_2 in methanol at -40 °C	81
Figure 3.11: Molecular structure of $[\text{Fe}(\text{Imine}_3\text{tren})(\text{OAc})_2]$	82
Figure 3.12: Molecular structure of the cation of $[\text{Fe}(\text{Imine}_3\text{tren})\text{OAc}]\text{OTf}$	84
Figure 3.13: Molecular structure of the cation of $[\text{Fe}(\text{Imine}_3\text{tren})\text{OAc}]\text{BPh}_4$	86
Figure 3.14: Molecular structure of $[(\text{Fe}(\text{Imine}_3\text{tren}))_2(\text{F}_2)](\text{SbF}_6)_2$	88
Figure 3.15: Molecular structure of $[(\text{Fe}(\text{tren}))_2\text{O}](\text{OTf})_2$	90
Figure 3.16: Molecular structure of $[\text{Fe}(\text{ClEI})(\text{H}_2\text{O})(\text{OAc})]\text{OAc}$	92
Figure 3.17: Molecular structure of $[\text{Fe}(\text{Imine}_1\text{amine}_1\text{aldol}_1\text{tren})(\text{OH}_2)]\text{NTf}_2$	94
Figure 3.18: Molecular structure of $[\text{Fe}(\text{Imine}_1\text{amine}_1\text{aldol}_1\text{tren})(\text{OH}_2)]\text{PF}_6$	96

Figure 3.19: Molecular structure of a part of 9, $[\text{Fe}(\text{tren})(\text{MeCN})_2]^+$ (Part 1)	98
Figure 3.20: Molecular structure of a part of 9, $[\text{Fe}((\text{CF}_3)_2\text{C}(\text{OH})(\text{O}))_4]^{2-}$ (Part 2)	98
Figure 3.21: Molecular structure of a part of 9, $[\text{Fe}((\text{CF}_3)_2\text{C}(\text{OH})(\text{O}))_4(\text{MeCN})]^{2-}$ (Part 3).....	98
Figure 3.22: Molecular structure of the cation of $[(\text{Fe}(\text{Imine}_3\text{tren}))_2\text{F}_2](\text{BPh}_4)_2$	101
Figure 5.1: Ligands used to prepare copper dioxygen adduct complexes	105
Figure 5.2: The desired ligand synthesized in coordinated form by performing template reactions between tren, acetone, NEt_3 and iron(II) salts.....	108
Figure 5.3: Obtained iron(II) complexes containing the desired ligand $\text{Imine}_3\text{tren}$	109

List of Schemes

Scheme 1.1: Reversible binding of dioxygen by hemocyanin.....	17
Scheme 1.2: Proposed reaction mechanism for the activation of phenol by tyrosinase	17
Scheme 1.3: Proposed reaction mechanism of copper, zinc superoxide dismutase (SOD).....	19
Scheme 1.4: Reversible binding of dioxygen by hemerythrin via a yet unobserved iron(II)/iron(III) superoxido intermediate	20
Scheme 1.5: Possible intermediates in the activation of dioxygen by non-heme diiron enzymes primarily based on the canonical mechanism for sMMOH.....	21
Scheme 1.6: Reaction of $[\text{Cu}(\text{L})(\text{EtCN})]^+$ with O_2 in EtCN (L = tmpa, $\text{Me}_2\text{uns-penp}$, Me_4apme , Me_6tren)	29
Scheme 2.1: Visual reaction pathway of the syntheses of the ligands prepared	58
Scheme 5.1: Formation of the end-on superoxido and subsequent hydroperoxido complex of $[\text{Cu}(\text{Isoprop}_3\text{tren})]^+$	106

List of Tables

Table 1.1: Some general, physical and chemical properties of elemental copper	1
Table 1.2: Selected copper proteins and their biological functions.....	6
Table 1.3: Some general, physical and chemical properties of elemental iron	8
Table 1.4: A small selection of iron proteins and their biological functions	15
Table 1.5: UV-vis spectroscopic data for superoxido and peroxido complexes of tripodal tetra-dentate ligands discussed	30
Table 2.1: Crystal data and structure refinement for $[\text{Cu}(\text{Me}_3\text{tren})]\text{ClO}_4$	54
Table 2.2: Selected bond lengths [\AA] and angles [$^\circ$] for $[\text{Cu}(\text{Me}_3\text{tren})]\text{ClO}_4$	55
Table 2.3: Crystal data and structure refinement for $[\text{Cu}(\text{Isoprop}_3\text{tren})]\text{SO}_3\text{CF}_3$	55
Table 2.4: Selected bond lengths [\AA] and angles [$^\circ$] for $[\text{Cu}(\text{Isoprop}_3\text{tren})]\text{SO}_3\text{CF}_3$	56
Table 2.5: Crystal data and structure refinement for $[\text{Cu}(\text{Me}_3\text{isoprop}_3\text{tren})]\text{BPh}_4$	56
Table 2.6: Selected bond lengths [\AA] and angles [$^\circ$] for $[\text{Cu}(\text{Me}_3\text{isoprop}_3\text{tren})]\text{BPh}_4$	57
Table 2.7: Crystal data and structure refinement for $[\text{Cu}(\text{Isoprop}_3\text{tren})\text{Cl}]\text{Cl}$	57
Table 2.8: Selected bond lengths [\AA] and angles [$^\circ$] for $[\text{Cu}(\text{Isoprop}_3\text{tren})\text{Cl}]\text{Cl}$	58
Table 2.9: Photographs of copper(I) complexes reacting with pure dioxygen at low temperatures in acetone and in EtCN.....	60
Table 3.1: Crystal data and structure refinement for $[\text{Fe}(\text{Imine}_3\text{tren})(\text{OAc})_2]$, $[\text{Fe}(\text{Imine}_3\text{tren})(\text{OAc})\text{OTf}]$ and $[(\text{Fe}(\text{Imine}_3\text{tren}))_2\text{F}_2](\text{SbF}_6)_2$	68
Table 3.2: Selected interatomic distances [\AA] and angles [$^\circ$] for $[\text{Fe}(\text{Imine}_3\text{tren})(\text{OAc})_2]$	71
Table 3.3: Selected interatomic distances [\AA] and angles [$^\circ$] for $[(\text{Fe}(\text{Imine}_3\text{tren})(\text{OAc}))\text{OTf}]$	72
Table 3.4: Selected interatomic distances [\AA] and angles [$^\circ$] for $[(\text{Fe}(\text{Imine}_3\text{tren}))_2(\text{F})_2](\text{SbF}_6)_2$	73
Table 3.5: Theoretic and measured IR data of $[\text{Fe}(\text{Imine}_3\text{tren})(\text{OAc})_2]$	78
Table 3.6: Crystal data and structure refinement for $[\text{Fe}(\text{Imine}_3\text{tren})(\text{OAc})_2]$	82
Table 3.7: Selected bond lengths [\AA] and angles [$^\circ$]for $[\text{Fe}(\text{Imine}_3\text{tren})(\text{OAc})_2]$	83
Table 3.8: Crystal data and structure refinement for $[\text{Fe}(\text{Imine}_3\text{tren})\text{OAc}]\text{OTf}$	84
Table 3.9: Selected bond lengths [\AA] and angles [$^\circ$] for $[\text{Fe}(\text{Imine}_3\text{tren})\text{OAc}]\text{OTf}$	85

Table 3.10: Crystal data and structure refinement for $[\text{Fe}(\text{Imine}_3\text{tren})\text{OAc}]\text{BPh}_4$	86
Table 3.11: Selected bond lengths [\AA] and angles [$^\circ$] for $[\text{Fe}(\text{Imine}_3\text{tren})(\text{OAc})]\text{BPh}_4$	87
Table 3.12: Crystal data and structure refinement for $[(\text{Fe}(\text{Imine}_3\text{tren}))_2\text{F}_2](\text{SbF}_6)$	88
Table 3.13: Selected bond lengths [\AA] and angles [$^\circ$] for $[(\text{Fe}(\text{Imine}_3\text{tren}))_2\text{F}_2](\text{SbF}_6)$	89
Table 3.14: Crystal data and structure refinement for $[(\text{Fe}(\text{tren}))_2\text{O}](\text{OTf})_2$	90
Table 3.15: Selected bond lengths [\AA] and angles [$^\circ$] for $[(\text{Fe}(\text{tren}))_2\text{O}](\text{OTf})_2$	91
Table 3.16: Crystal data and structure refinement for $[\text{Fe}(\text{ClEI})(\text{H}_2\text{O})(\text{OAc})]\text{OAc}$	92
Table 3.17: Selected bond lengths [\AA] and angles [$^\circ$] for $[\text{Fe}(\text{ClEI})(\text{H}_2\text{O})(\text{OAc})]\text{OAc}$	93
Table 3.18: Crystal data and structure refinement for $[\text{Fe}(\text{Imine}_1\text{amine}_1\text{aldol}_1\text{tren})(\text{OH}_2)]\text{NTf}_2$	94
Table 3.19: Selected bond lengths [\AA] and angles [$^\circ$] for $[\text{Fe}(\text{Imine}_1\text{amine}_1\text{aldol}_1\text{tren})(\text{OH}_2)]\text{NTf}_2$	95
Table 3.20: Crystal data and structure refinement for $[\text{Fe}(\text{Imine}_1\text{amine}_1\text{aldol}_1\text{tren})(\text{OH}_2)]\text{PF}_6$	96
Table 3.21: Selected bond lengths [\AA] and angles [$^\circ$] for $[\text{Fe}(\text{Imine}_1\text{amine}_1\text{aldol}_1\text{tren})(\text{OH}_2)]\text{PF}_6$	97
Table 3.22: Crystal data and structure refinement for $[\text{Fe}(\text{tren})(\text{Cl})_2](\text{CF}_3)_2\text{C}(\text{OH})(\text{O})$	99
Table 3.23: Selected bond lengths [\AA] and angles [$^\circ$] for $[\text{Fe}(\text{tren})(\text{Cl})_2](\text{CF}_3)_2\text{C}(\text{OH})(\text{O})$	100
Table 3.24: Crystal data and structure refinement for $[(\text{Fe}(\text{Imine}_3\text{tren}))_2\text{F}_2](\text{BPh}_4)_2$	101
Table 3.25: Selected bond lengths [\AA] and angles [$^\circ$] for $[(\text{Fe}(\text{Imine}_3\text{tren}))_2\text{F}_2](\text{BPh}_4)_2$	102

Erklärung

Ich habe die vorgelegte Dissertation selbständig und ohne unerlaubte fremde Hilfe und nur mit den Hilfen angefertigt, die ich in der Dissertation angegeben habe. Alle Textstellen, die wörtlich oder sinngemäß aus veröffentlichten Schriften entnommen sind, und alle Angaben, die auf mündlichen Auskünften beruhen, sind als solche kenntlich gemacht. Bei den von mir durchgeführten und in der Dissertation erwähnten Untersuchungen habe ich die Grundsätze guter wissenschaftlicher Praxis, wie sie in der „Satzung der Justus-Liebig-Universität Gießen zur Sicherung guter wissenschaftlicher Praxis“ niedergelegt sind, eingehalten.

Gießen, 15. März 2021

Janine Will

